An innovative framework for structural health monitoring of long-span bridges

Dissertation

submitted to the

Department of Architecture, Civil Engineering and Environmental Sciences
University of Braunschweig – Institute of Technology

and the

Department of Civil and Environmental Engineering
University of Florence

in candidacy for the degree of a
Doktor-Ingenieur (Dr.-Ing.) /
Dottore di Ricerca in processes, materials and constructions in civil and environmental engineering and for the protection of the historic-monumental heritage[*)]

by
Gabriele Comanducci
Born 15.04.1985
from Sansepolcro (AR), Italy

2016

*) Either the German or the Italian form of the title may be used.

An innovative framework for structural health monitoring of long-span bridges

Short abstract:

Structural Health Monitoring of structures has received a wide diffusion and development in the last decade. Steps forward have been made in many fields as, for instance, in sensing technologies, data migration facilities and data pre/post processing algorithms. Many of these advancements have found their first application on monitoring of bridges which are considered among the most crucial structures to be monitored because of both their importance in the economic activities of a country and the relevance of the economic effort necessary for their construction and maintenance.

Within this context the structural health monitoring of bridges aimed at the continuous condition assessment of such structures not only seems to be very promising for increasing the cost-effectiveness of the maintenance procedures but can be still considered a challenge. To this purpose tools based on multivariate statistical analysis are becoming very popular for automatically revealing the existence of damage in structures using vibration data under changing environmental and operational conditions (typically temperature, humidity and traffic intensity).

In the present PhD Thesis, considering natural frequencies as damage-sensitive features, multivariate statistical analysis are newly applied for monitoring the structural health state of bridges, accounting for the linear and non-linear correlations between such dynamic features and the environmental and operational conditions. A procedure based on the continuous modal frequencies tracking, Principal Component Analysis and Novelty Detection is proposed. The effectiveness and the capability in damage detection of such technique is previously tested on the pseudo-experimental response data of an analytical parametric model of suspension bridge with damage in one main cable and subjected to wind loading and changing temperature. Thereafter, in order to have an absolutely realistic representation of the operational and environmental conditions, the same technique is tested on long-term real bridge data.

The obtained results demonstrate in both cases the feasibility of permanent monitoring systems for the real-time condition assessment of bridges and the robustness of the proposed procedure in revealing the existence of damage. In fact, even if the effects induced on frequencies by damage are very small, of the

order of few per mil, in any case smaller than those induced by environmental and operational conditions, the adopted statistical technique allows to reveal its occurrence in a reliable and prompt manner. Moreover, the absolute general nature of the proposed approach may reveal, in perspective, its extension to any other structure equipped with a permanent monitoring system.

Keywords: Structural Health Monitoring, Multivariate Statistical Analysis, damage detection, suspension bridges.

Contents

1 INTRODUCTION **1**

1.1 Introduction to SHM 2

1.2 Aim of the thesis 5

2 MULTIVARIATE STATISTICAL ANALYSIS TECHNIQUES FOR SHM **7**

2.1 The problem of vibration-based damage detection 9

2.1.1 Introduction to vibration-based techniques for SHM . . 9

2.1.2 Damage detection through change in natural frequencies 13

2.1.3 Statistical process control for damage detection 19

2.2 Multiple linear regression 22

2.3 Principal Component Analysis (PCA) 24

2.3.1 Introduction to PCA 24

2.3.2 Principal Components: derivation and definition 26

2.3.3 Classical PCA 29

2.3.4 Local PCA 30

2.4 Novelty detection 31

3 A NEW INTEGRATED TECHNIQUE FOR OMA AND SHM OF BRIDGES **35**

3.1 Operational Modal Analysis for civil structures 37

3.1.1 Introduction 37

3.1.2 Sample experimental and field application 39

3.2 Proposed integrated technique for SHM 53

3.2.1 Continuous modal identification and frequency tracking 53

3.2.2 Removal of environmental effects 56

3.2.3 Damage detection 58

4 APPLICATION TO SHM OF SUSPENSION BRIDGES WITH MAIN CABLE DAMAGE **59**

4.1 Continuum model of damaged suspension bridge 61

4.1.1 Static response 62

4.1.2 Equations of motion under wind loading 65

4.2 Wind effects on eigenfrequencies 67

4.2.1 New Carquinez Bridge 68

4.2.2 Akashi Kaikyo Bridge 70

4.3 Temperature effects on eigenfrequencies 72

4.4 Damage effects on eigenfrequencies 74

4.5 Damage detection 76

4.5.1 Continuous response simulation and analysis 77

4.5.2 Regressive models 91
4.5.3 PCA-based techniques 92
4.5.4 Application with measurements noise 103
4.6 Discussion of results 110

5 APPLICATION TO SHM OF A REAL LONG-SPAN ARCH BRIDGE 113
5.1 Introduction 115
5.2 Infante Dom Enrique arch bridge 116
5.2.1 Description of the structure 116
5.2.2 Monitoring system 120
5.3 Damage detection 122
5.3.1 Permanent monitoring data analysis 122
5.3.2 Regressive model 131
5.3.3 PCA-based techniques 134
5.4 Discussion of results 144

6 CONCLUSION AND RECOMMENDATION 147

Bibliography 153

A APPENDIX 165
A.1 Wind loads 165
A.1.1 Buffeting loads 166
A.1.2 Self-excited loads 166
A.2 Structural eigenmodes 168
A.3 System matrices 170
A.4 Effect of t_{trn} on Linear PCA effectiveness 172

Dedicated to my daughter

"Ognuno vede quel che tu pari, pochi sentono quel che tu sei."

"Everyone sees what you appear, few ones feel what you are."

(Niccolò Machiavelli)

1

INTRODUCTION

This chapter introduces the concept of Structural Health Monitoring of bridges, the research field in which the present work of thesis is contextualized. After some very synthetic hints concerning the historical evolution of this practice, the main issue of the thesis is focused and the global organization of the manuscript is drawn.

Contents

1.1 Introduction to SHM 2
1.2 Aim of the thesis 5

1.1 Introduction to SHM

Since the origins of the modern civil engineering the monitoring of structural conditions aimed at the evaluation of the structural health state was a common practice and a challenge. However, only in the last decades this activity has been univocally recognized as a multidisciplinary engineering practice which goes by the name of Structural Health Monitoring.

Because of its complexity and importance, both in terms of required knowledge in many different fields of engineering and of the economical effort one has to bear, the structural health monitoring in the course of time was always more and more specifically applied to *major structures* that is structures with a big economical and/or cultural impact on people. For both these reasons many bridges (but not each), all over the word belong to the category of major structures: their importance has been steadily growing as critical nodes by which not only highways but also railroads, airports, waterways and ports are linked and where not only traffic but also communication, water and gas systems are carried.

All that has produced the necessity to have available objective nondestructive tools, in support of the classical subjective visual inspections, able to describe in real-time the performance and the current condition of use of such fundamental infrastructures. Within this context the definition of structural health can be given as the manner by which engineers represent the state and the performance of an in-service bridge in qualitative and quantitative (by using indexes) way; therefore structural heath monitoring is the system of devices, and analytical tools by using which this representation can be obtained.

Historically many bridge collapses have driven engineers to find innovative solutions aimed at structural health assessment. Many of these cases could be cited but one of the most famous was the failure in 1967 of the eye-bar chain suspension Silver Bridge (Fig. 1.1), in which 46 people lost their lives. After this failure, systematic inspections of bridges (National Bridge Inspection Program, NBIP), started in the United States aimed at damage identification in order to avoid future collapses [1]. The first rudimental techniques, based essentially on periodical visual inspections of the structure had to wait the coming of some technological innovations both in the monitoring instrumentation field and informatics field and in the data communication tools.

The early setups of health monitoring in an automated fashion resorting digital techniques, came during the 80's when the modal parameters of the structure started to be used as tools for damage-presence identification. Over the years

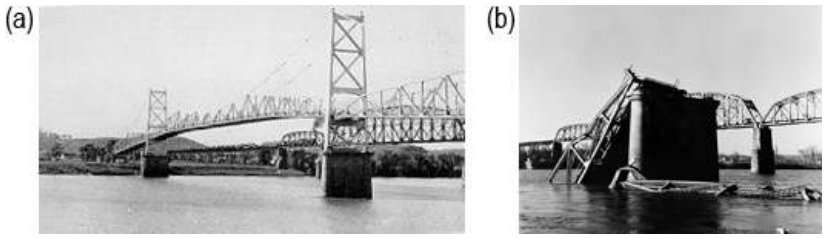

Figure 1.1: Sylver Bridge, Ohio (USA), before (a) and after (b) its collapse on december 15^{th} 1967.

new technologies and new algorithms involving data acquired with monitoring systems temporarily placed on bridges were developed motivated not only by damage detection purpose but also by the need of scheduling the maintenance activities of such structures and by a change towards a performance-based design approach.

Today's SHM is still an active research field even though has reached its adulthood: national and federal programs for bridge health assessment and maintenance by using SHM are widespread in the U.S., Canada, many European countries and in Asia, and big economical sources are devoted to this purposes in many cases. Many health monitoring techniques (classified in the most generic manner, in local and global ones) are well established and new complex systems continue to be installed all over the word, sometimes with slightly different purposes. In Tab. 1.1 some big bridges in the word equipped with permanent monitoring systems are listed.

The duration of the monitoring campaign in conjunction with the complexity of the realized monitoring system, allows to characterize the damage in different ways, or levels [2], of growing complexity, as shown later on in Fig. 2.1. The mentioned figure resumes in a very simple manner the complexity of health assessment problem and holds in itsself all the future objectives both from the technical and economical point of view that in many cases have to be solved still today.

The currently successfully implemented applications have allowed to extend the goals of SHM systems for (i) validating design assumptions and parameters with the potential benefit of improving design specification and guidelines giving the *know how* for future similar structures (ii) detecting anomalies both in loading and in response, and possible damage/deterioration at an early stage to ensure structural and operational safety; (iii) real time information for safety assessment immediately after disaster and extreme events; (iv) evidence and instruction for planning and prioritizing bridge inspection, rehabilitation, maintenance and repair; (v) monitoring repairs and reconstruction with the

Table 1.1: Examples of long-span bridges equipped with permanent monitoring systems; (bridge complex, b.c.).

Bridge	Type	Country	Year	Total length [m]	span [m]
Jianngyin Bridge	suspension	China (Jangsu)	1997	3000	1385
2nd Nanjing Yangtze River Bridge	cable stayed	China (Jangsu)	2001	2938	628
Runyang South Bridge	suspension	China (Jangsu)	2005	35 km b.c.	1940
Tsing Ma Bridge	suspension	China (Hong Kong)	1997	2160	1377
Stonecutters Bridge	cable-stayed	China (Hong Kong)	2004	1596	1018
Humen Bridge	suspension	China(Guangdong)	1997	3618	888
Xupu Bridge	cable-stayed	China (Shanghai)	1997	8354 b.c.	590
4th Qianjiang Bridge	arch	China(Zhejiang)	2002	1376	580
I35W St.Anthony Falls Bridge	box girder (pre-tens.)	US(Minnesota)	2008	371	154
Great Belt Bridge	suspension	Denmark	1998	6790 b.c.	1624
Confederation Bridge	box girder (post-tens.)	Canada	1997	12.9 km b.c.	250
Commodore Barry bridge	steel cantilever US(Pennsykvania)	1974	4240	502	
Akashi Kaikyo Bridge	suspension	Japan	1998	3911	1991
Seohae Bridge	suspension	Korea	2000	7310	470
Vasco da Gama Bridge	cable stayed	Portugal	1998	7.2 km b.c.	420
Ponte di San Michele	arch	Italy	1889	266	150
Øresund Bridge	cable-stayed	Sweden-Denmark	2000	7845	490
Infante Dom Enrique Bridge	arch	Potugal	2002	371	280

view of evaluating the effectiveness of maintenance, retrofit and repair works; and (v) obtaining massive amounts of in situ data for leading-edge research in bridge engineering, such as wind- and earthquake-resistant designs, new structural types and smart material applications (fiber optic for instance) finalized to realize monitoring systems structure integrated.

1.2 Aim of the thesis

Despite SHM has reached its adulthood and many breakthrough have been made in different fields such as that of computational techniques or data processing and management systems, rather than of sensing technologies, still today many other aspects concerning SHM still require further developments especially toward a clear definition of the cost-effectiveness of a SHM system. Many works in recent years try to focus the attention on this aspect showing detailed costs-benefits analysis in the short and long term of SHM systems [3].

In the matter of the optimization of the cost-effectiveness in SHM systems installations, the chance to realize very effective tools capable to reliably assess the health state of the considered structure, which are in addiction characterized by low costs both in terms of necessary installed devices and data management, represents a great challenge, potentially allowing SHM not only in major structures.

Within this context, the present work of thesis introduces and describes a closed loop procedure which can allow to gain the aforementioned target. Actually, the presented methodology is based on the continuous evaluation of the modal properties of a bridge through the permanent monitoring of its dynamic response under common environmental and operational conditions. Being modal frequencies the adopted damage sensitive features, thanks to the high sensitivity of the measurement devices available in the market, the procedure can address the condition assessment of the bridge with very restrained costs: a limited number of devices generally suffices for the identification of resonant frequencies, and the automated nature of the proposed procedure require a minimum intervention of the users.

The adopted SHM strategy starts from the automated identification of bridge resonant frequencies. Being the structures not inserted in controlled environment, the modal properties obtained from continuous monitoring of the structure are affected by changing in both environment and operational conditions. This circumstance may impede the identification of damage whose

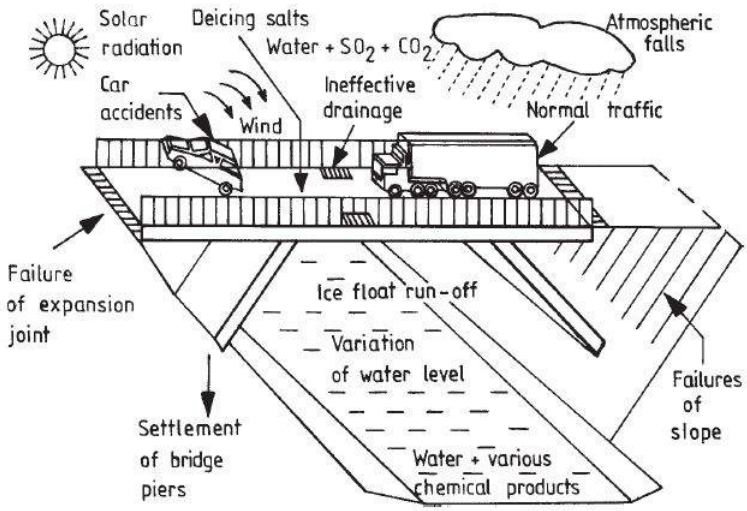

Figure 1.2: Sketch representing the external factors, both operational and anvironmental, which act on bridges.

effects on the same dynamic characteristics are usually remarkably smaller than those induce by external factors (Fig. 1.2)

In the present work of thesis different statistical techniques (namely Regressive Models and Principal Component Analysis) for removing the environmental and operational effects on modal properties are considered, enabling in such a way damage detection. More specifically, their effectiveness is tested on artificially generated response data of a long span suspension bridge with main cable damage, where damage detection is addressed also in the case of pretty small damage conditions. Moreover to gain in completeness the implemented techniques are applied on the data of a real long span arch bridge. Different realistic damage conditions are artificially considered and efficiently detected by the proposed procedures. A comprehensive study has finally allowed to compare the effectiveness of classical linear Regressive Models techniques with that of Principal Component Analysis based ones whose main advantage resides in the fact that they do not require the measurements of the environmental conditions further limiting the number of needed installed sensors, and reducing the costs.

2

MULTIVARIATE STATISTICAL ANALYSIS TECHNIQUES FOR SHM

This chapter briefly introduces the problem of damage identification through vibration-based methods. A synthetic overview is drawn at the beginning, underlining the basic idea behind these techniques. Later on, the attention is focused on the more detailed explanation about the methodologies adopted in the present thesis for obtaining damage sensitive features, specifically Multiple Linear Regression, Classical Principal Component Analysis and Local Principal Component Analysis. Finally the application of such features in statistical process control for damage detection is illustrated.

Contents

2.1 The problem of vibration-based damage detection . 9
2.1.1 Introduction to vibration-based techniques for SHM . 9
2.1.2 Damage detection through change in natural frequencies 13
2.1.3 Statistical process control for damage detection 19
2.2 Multiple linear regression 22
2.3 Principal Component Analysis (PCA) 24
2.3.1 Introduction to PCA 24
2.3.2 Principal Components: derivation and definition . . . 26
2.3.3 Classical PCA 29
2.3.4 Local PCA 30
2.4 Novelty detection 31

2.1 The problem of vibration-based damage detection

This section provides a general overview concerning vibration-based methods for structural health monitoring with particular reference to its application on bridge structures. After an introduction which drafts the principal motivations of the recent worldwide acceptance of such an approach to major structures health assessment, the attention is focused on vibration-based methods which make direct or indirect use of resonance frequencies as damage sensitive features, and on their use in statistical process control for damage detection purpose.

2.1.1 Introduction to vibration-based techniques for SHM

Damage is a common condition in structures and, depending on many factors, may not produce any significant consequence in their common use, or conversely may be the cause of a structural failure. For these reasons the capability of monitoring a structure and of detecting a damage at the earliest possible stage is one of the most intensively explored fields among all engineering branches, from mechanical, to civil and aerospace engineering.

In the past decades, a special interest has arisen in regard to the prevention against the sudden failure of structural components. The most proper way to achieve this purpose seemed to develop suitable tools able to detect damage in structures at the early state and more specifically, structural health monitoring based on the vibration of structures revealed, since the beginning of its application, to potentially become a very promising diagnostic instrument of great importance for the civil, aeronautical and mechanical engineering communities. This is why various developments of non-destructive techniques based on changes in the structural vibration signatures have been extensively studied and published not only for the purpose of detecting damage occurrence but also of identifying its location and severity.

At this point a proper definition of damage it is mandatory. In the most general possible meaning, a damage can be defined as a change introduced in a system, either intentional or unintentional, which adversely affects the current or future performance of that system [4]. Depending on the conditions of exposure, the damaged system may reveal its unfavorable state both immediately after damage occurrence or even after a long time. The just stated definition of damage implicitly assumes and requires the comparison between two different conditions

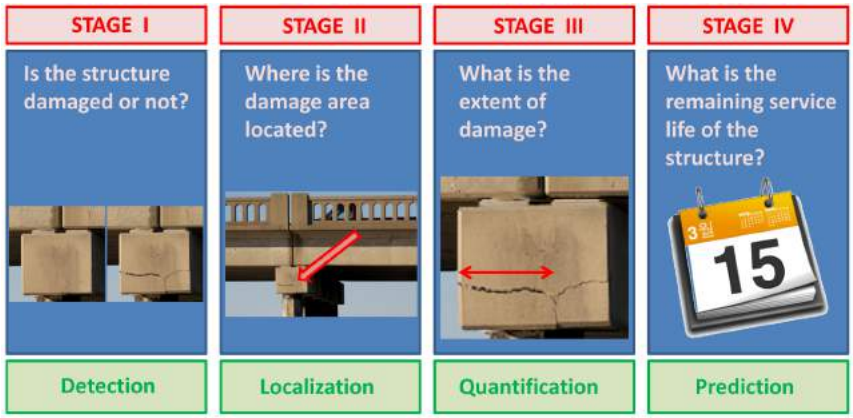

Figure 2.1: Key phases in damage diagnosis by Rytter, [2].

of the system under investigation: an initial one which has to be considered as reference and generally undamaged, and a second one, representing the current state of the system, which has to be checked, being potentially subjected to damage. Then, it is generally admitted the original division by Rytter [2] of damage diagnosis in four different stages 2.1:

1 determination of the **presence** of damage in the structure;

2 determination of damage **location** in the structure;

3 quantification of damage **severity**;

4 prognosis of the **remaining service life** of the damaged structure.

The first two levels can be performed by the so called data driven method alone (methods essentially based on field measurements only) and do not require structural model. On the contrary, the fourth and, partially, the third levels make use of numerical models. Moreover, these last two stages may also require local non-destructive testing, visual inspection, human skills and further theoretical concepts such as fracture mechanics ar fatigue analysis, [5]. The present thesis will focus on the first stage of damage diagnosis which can still be considered a challenge today.

Regarding damage occurrence in bridge structures, there can be many different scenarios (see Chap. 1) depending on a large amount of factors inherent to the bridge itself and its installation such as, structural system, constituent materials, kind of underneath obstacle (river rather than sea or canyon), quality of preservation measures, adequacy of maintenance activities as well as sort of loading traffic (common vehicle, heavy transport, trains or crowd simply) and climatic conditions at the construction site. In any case, the common factor between all the different damage conditions in bridges lies in the changes

of the physical properties in the damaged component. The principal idea of vibration-based SHM is exactly founded on this joint condition indeed. Intuitively the basic concepts consists in the fact that commonly measured modal parameters (particularly frequencies, mode shapes, and modal damping) depend upon structural physical properties (mass, damping, and stiffness). Therefore, variations of these properties, such as reductions in stiffness resulting from the onset of cracks or loosening of a connection, will cause changes in these modal properties that can be more or less easily detected. Using changes in modal properties or features derived from these quantities, as damage sensitive tools indicators, may lead the process of vibration-based damage detection to eventually reduce to some form of a pattern recognition problem [4].

For several years various and different explanations have been provided for the limited application of SHM based on the vibration of infrastructures. Among them, the misleading idea that the local nature of damage could not be revealed by method based on the use of global quantities (as modal properties are), and that, in any case, such local phenomenon could be captured only by the response of higher modes, generally the most difficult to be excited in modal testing of structures. However spectacular failures resulting in loss of lives, the aging state of infrastructures and the peer successes of modal testing [6] especially in aeronautic [7] and mechanical engineering [8] have led towards an always more marked increase in research activities for developing mathematical and physical foundation for this particular SHM approach. Nowadays vibration-based techniques are well-established and many literature comprehensive surveys can be found on this topic, (see for instance [4, 9, 10]). Despite that, there is still a lack of proofs on the actual effectiveness on full-scale systems of many of proposed methods and the capability in damage detection has been rigorously verified in few cases only. The aim of the present thesis, in this sense, is to consider some recently more widely adopted techniques and systematically verify their effectiveness in damage detection with real and artificially generated bridge response data.

Based on the available scientific literature, many different classification can be promoted concerning vibration based SHM techniques. A first common subdivision of damage assessment techniques can be fulfilled identifying the following three categories [11]:

- **modal testing**;
- **vibration based** methods;
- **non-traditional** methods.

The first category is probably the most popular being widely applied especially in mechanical and aerospace application [12]: variation of modal parameters (frequencies, mode shapes and response to ad hoc excitation), are adopted

as damage indicators. Non-traditional methods more specifically deal with genetic algorithms, neural networks, signal processing techniques such as the wavelet analysis or Wigner-Ville transforms. Focusing the attention on the second listed category, which is the main interest of the present dissertation and of the following applications, two further relevant subcategories should be distinguished: **model-based** and **data-driven** methods. The former typically aim at identifying damage through numerical or analytical models previously tuned to real data, generally using optimization techniques. The latter, on the contrary, are based on the analysis of vibrational monitoring data only, without relying on a priori models. The proper choice of the damage detection approach is crucial since the acquired data alone are generally not informative about the presence of anomalies.

Another common classification is made in regard to the effect of damage on the structure and consequently on the types of data available in the measurements of structural vibrations: linear and non-linear approaches can be distinguished in this way [4, 10]. More specifically:

- **linear approaches** are adopted when the structure can be modeled as a linear-elastic system before and after damage occurrence. Variations of modal properties are due to changes in geometrical and/or physical properties of the structure which however continues to allow the use of linear equations of motion;

- **non-linear approaches** should be used to guarantee a more performing damage identification, whenever a structural anomaly occurrence entails non-linear effects on system behavior. For instance, this is the common condition induced by fatigue crack formation.

In the field of linear analysis methods, a significant and central role is fulfilled by those which make a more or less direct use of structural modal properties. Among them, with the exception of those based on modal frequencies, illustrated aside later on in this chapter, it is worth mentioning, for instance, those grounded on mode shapes, changes in node position, MAC [13] or other assurance criteria [14]. The use of mode shapes has been always very attractive being these last not only unique characteristics of the considered structure but also the only capable ones to give a spatial description of the resonance and so to potentially determine damage position. Literature works also show how mode shapes are more sensitive to damage when compared to frequencies,(see for instance [15]). Unfortunately, some penalizing aspects, such as the need of a large number of measurement points and the duration itself of each measurement for achieving a detailed mode estimates, have limited in fact their use. Nevertheless many literature works, both dated and more recent, show very

interesting results in damage detection through mode shapes with particular reference to bridge structures [16, 17, 18].

Other research works propose the use of structural damping [19] or specific damping capacity [20] to detect damage, producing the friction between cracks surfaces dissipative effects. Many studies have revealed how damping could be a structural parameter more sensitive to damage than frequencies [21] being, in addition, less susceptible to boundary conditions. However the limited accuracy in damping estimation has limited its actual use as structural integrity assessment tool.

Finally other methods are worth mentioning which make use of dynamically or statically measured flexibility [22]. Defined as the inverse of the static stiffness matrix, the flexibility matrix is related to damage occurrence being variations in stiffness related to damage presence. Different works available in literature, make use of flexibility matrix (see for instance [23, 24, 25]) but its actual application in structural health monitoring still remains rather restricted.

2.1.2 Damage detection through change in natural frequencies

Natural frequencies can be considered the most popular class of modal parameters for damage detection purpose and an amount of literature in structural assessment proposes methodologies where shifts in structural resonant frequencies are directly or indirectly used as indicator of the anomalous behavior of the system under investigation. Furthermore, as reported in [4], it is notable reminding how the observation that changes in structural properties entail variations in vibration frequencies constituted the original encouragement for using modal methods for structural health assessment.

When a damage occurs and extends in a structure, the stiffness reduces consequently implying a variation, generally a decrease, in the natural frequencies of the system. Starting from this statement of fact, the evaluation of such shift not only may potentially allow to recognize damage occurrence but also may enable damage localization through a proper identification of the most affected mode. Unfortunately, this diagnostic procedure is seldom a linear process and involves somewhat not negligible difficulties among which the most relevant are represented by the generic low sensitivity of frequencies to damage (see Sec.4.4) especially in complex and/or big structures and, on the contrary, a high susceptibility in regard to the boundary conditions (environmental and operational conditions). These reasons made researchers skeptical in the past decades on the use of frequencies for health assessment purpose [26, 27] with the exception of situations where their estimates could be very accurate, that

is in a controlled environment, typical of quality control in manufacturing. In addiction, the exclusive adoption of such parameters seemed to allow the accomplishment of the stage 1 only in damage identification procedure. Nevertheless the use of natural frequencies implies many other advantages such as, for instance, quick and easy measurements necessary for the extraction of this dynamic properties. Moreover, experimental techniques for the determination of resonant frequencies are classical vibrational measurement techniques; thus allowing the vibrational measurements to be extensive with a great number of measurement points and a very cheap experimental procedure [10]. As a consequence, a relative confident accuracy can be achieved in frequency estimation and the uncertainties in their measure can be easily evaluated. Moreover dealing with global dynamic characteristics of the system, their interpretation with analytical or finite elements models can help towards a proper choice of the measurement points for optimizing frequency evaluation and potentially enabling not only damage localization but also the assessment of its severity. Actually, following the inverse process, natural frequencies are the best candidates among structural dynamic properties to be used for the optimal tuning of the aforementioned FE models and to potentially enable stages 2 and 3 in damage diagnosis procedure.

2.1.2.1 Methods overview

It is generally admitted that the first academic work dealing with damage detection through changes in frequencies was [28], where vibration tests were performed to determine the onset of reinforcement unbonding in composite materials. After that, several papers proposed other applications in different engineering fields especially making efforts towards the definition of proper damage indicators based on resonant frequencies estimation. The common factor of all these approaches remains, however, the comparison between two different monitored states: an initial undamaged reference one a second damaged one which has to be checked. For instance in [29] the frequency variation $\Delta\omega_i^2$ of the i^{th} generic mode is calculated by using both mass matrix and mode shapes and estimating variations in stiffness $\Delta\mathbf{k_n}$ matrix only. Further works, preparing the ground for applications of statistical pattern recognition techniques in health monitoring of infrastructures, propose Normalized Natural Frequencies (NNF) built by differently defined ratios between undamaged and damaged estimated modal frequency as for example

$$NNF_i = \frac{\omega_i^{dm}}{\omega_i^{und}} \tag{2.1}$$

being ω_i^{dm} and ω_i^{und} resonant frequency of the i_{th} mode in damaged and undamaged state respectively. An analogue notation will be adopted later on in Chap.4. Alternatively, the variation of frequency between the two different states $\%C$ can be underlined by adopting the following defined ratio

$$C_i(\%) = 100 \times \frac{\omega_i^{und} - \omega_i^{dm}}{\omega_i^{und}} \tag{2.2}$$

Exploiting the just defined ratios and even more if a direct use of frequencies is chosen, implicitly require an extremely reliable and accurate evaluation of the considered properties in order to reduce as much as possible the uncertainties in their estimate. Another interesting indicator of damage defined through the ratio between frequencies in damaged and undamaged state can be find in [30].

Some other methods in literature, not so different from the just described ones, do not require the comparison between damaged and undamaged state indeed, but they are based only on an accurate estimation of the frequency in the damaged state and of materials properties of the structure.
Finally in this short overview on the most diffused methodologies for damage detection based on resonant frequencies, it is worth mentioning the Damage Location Assurance Criterion (DLAC) and its evolution for the case of multiple damage, the Multiple Damage Location Assurance Criterion (MDLAC), introduced by Messina et al. in [31] and [32] respectively, and reported also in many other works, as for instance recently in [33, 34]. Both coefficients are based on experimental and theoretical calculation of the frequency shifts induced by damage occurrence while damage position is estimated by predicting different damage configurations and calculating the coefficients for each configuration. Damage scenario which furnishes the highest value of the coefficient (which ranges from 0 to 1) allows to predict in a reasonably manner the position or somehow the area in which damage could be located.

From this brief survey it arises quite clearly how the use of frequencies for damage identification is substantially limited to the first stage of damage diagnosis described in 2.1.1. Actually, the main problem especially in damage localization, consists in the not uniqueness of the solution. Anyway, due to the advantages previously exposed, frequencies can be considered to this day as the most widely adopted tool for health assessment in many engineering fields, and accordingly to this frequencies will be adopted also in the present work of thesis for the purpose of enabling damage detection in bridges.

2.1.2.2 Environmental and operational effects on modal frequencies

The main problem one has to face with in the case of measurements on structures which are not placed in a controlled environment, concerns the reliability of the evaluated dynamic characteristics of the structure being these lasts deeply affected by environmental and operational conditions indeed, and being, on the contrary, the effects induced by damage very low (usually smaller than 1% on frequencies) depending on crack size and location. Then, it can be generally stated that in the case of monitoring of infrastructures, external factors alway produce effects that overtake those induced by damage occurrence; for this reason the current trend in the structural health monitoring field is to look for features which are insensitive to changing environment allowing in such a way to potentially detect anomalies (see for instance [35, 36, 37]).

There are many external factors which may produce relevant effects non only on the dynamic response of the structure but also on the static one. Among them one of the most relevant is certainly temperature whose effect on structural behavior is therefore one of the most investigated in literature, as for instance in [38, 39]. The relevance of a correct estimation and a proper interpretation of the effects that changing temperature produces on the dynamic properties of the investigated structure, has arisen in the last decades since structural modal properties have been revalued as an optimal tool enabling damage detection.

Many researchers pointed out the leading position of temperature in influencing the dynamic response of bridges in comparison with damaged one ([40, 41]), observing, in most of cases, an essentially linear correlation among frequencies and temperature. Actually, this is generally true but is also deeply influenced by the characteristics of the considered structure, as for instance in the case of bridges, by its structural scheme, its restraint conditions as well as deck configuration and constituent materials. For example, in the case of suspension bridges it is well known that temperature increase produces the reduction of steel's Young's modulus and simultaneously the elongation and slackening of the cables leading to lower tensions and hence reduced geometric stiffness. This entails effects in such kind of bridges that are predictably different from those that similar conditions may produce for example in a prestressed girder bridges. For the purpose of underlining this aspect, in Fig. 2.2 some examples from literature works are shown representing the relationships among in situ measured temperature and identified modal frequencies of bridges characterized by different structural schemes.

Strictly related to temperature, there are some other environmental factors that, combined with temperature indeed, may differently affect the behavior

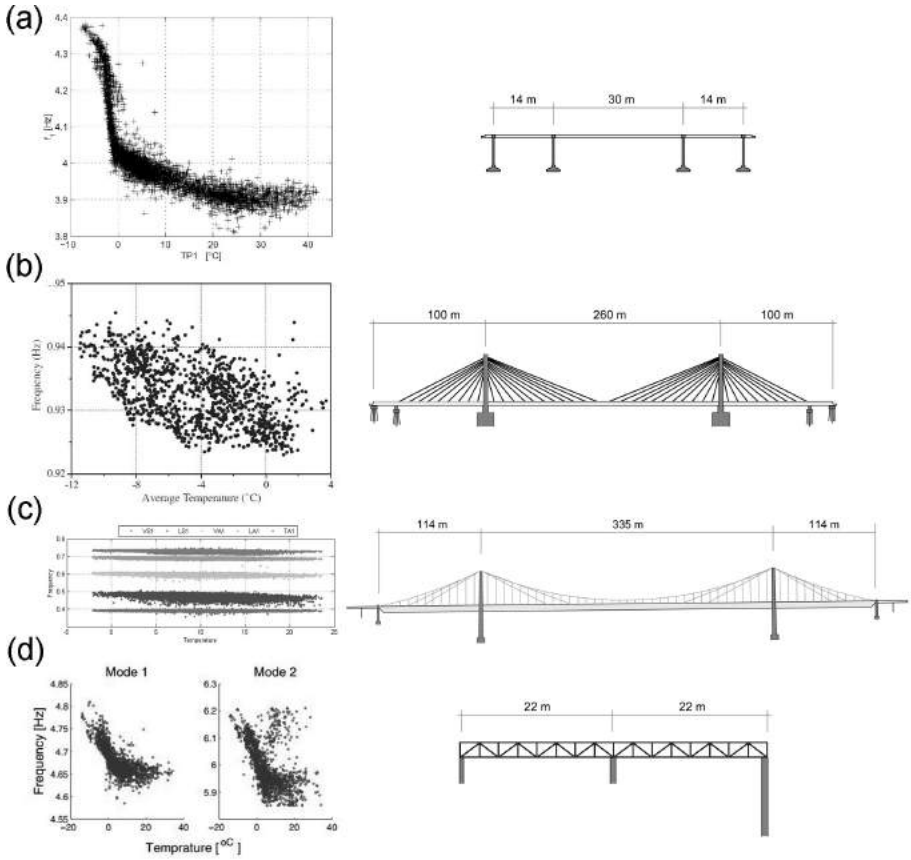

Figure 2.2: Identified modal frequency versus measured temperature for different bridge structures: (a) Z-24 post-tensioned concrete box girder bridge [41]; (b) Tianjin Yonghe cable stayed bridge [42]; (c) Tamar suspension bridge [43]; (d) Dowling Hall footbridge (steel frame with reinforced concrete deck) [44]

of the materials constituting the structure and, as a consequence, the global behavior of the overall structure somehow. These factors are solar heating and cloud cover. Anyway, their effects are generally small and very difficult to be separately estimated, and for these reasons, in most cases, they can be incorporated among those induced by temperature in some way.

In the field of bridge health monitoring through structural dynamic properties, with particular reference to slender cable-supported bridges, one of the most relevant environmental factor one have to take into account is wind. Actually wind conditions are also acknowledged to affect the behavior of cable supported bridges, since the deck structure is more flexible in comparison with other bridge structural systems. After the Tacoma Narrow Bridge failure in 1940, an higher attention has been paid to bridge-wind interaction, especially focusing on vortex shedding, buffeting, but also on the conditions of instability such as galloping or flutter, conditions these last that may lead to bridge closure and even collapse. When the bridge stiffness is inadequate, the wind actions are modified or even generated by the structural response itself which gives rise to aero-elastic effects that can be interpreted as aerodynamic damping and stiffness. Analytical approaches, for example using flutter derivatives, may reveal in a more accurate way this effect and quantify both terms, aerodynamic damping and stiffness, which lead to apparent variations of the natural frequencies of bridges [45].

Wind-induced changes in frequency also appear in the results of modal identification in operational conditions, where increments and decrements of identified natural frequencies with increasing wind speed may be observed depending on the aerodynamic properties of the considered bridge. As reported in literature, as for instance in [46], these variations, generally more marked in torsional modes, are in the order of the per cent, so comparable with those produced by other environmental factors. Unfortunately, the FE models largely used to study and understand bridges behavior, not always correctly catch this phenomenon. Frequency changes due to variations in the geometry of the cables as they deflect under steady wind action, can also be important. Moreover, or additionally, reductions of effective stiffness from movements of joints for larger displacements at higher wind speeds may be crucial.

All these aspects related to wind action on bridges could not be easily considered separately but, on the other hand, produce global effects on the dynamic response of the structure which necessarily reflect in terms of apparent variations of the dynamic properties. Despite from Tacoma Narrow Bridge failure, a deeply higher attention to the aerodynamic design especially of bridge deck section has been paid and a large amount of papers have been devoted to the characterization of the aerodynamic behavior of bridges through wind-tunnel tests, few works only can be found concerning the estimation of wind effects on modal properties identified by in situ measurements and in this sense there is

a lack of knowledge in the field of structural health monitoring. The renewed interest towards the optimal estimation of modal properties for application to permanent monitoring of infrastructures, has led to bridge this gap [42, 47, 48], especially because wind effects on structural dynamic characteristic are generally of non linear nature and can nullify or at the very least reduce the effectiveness of most commonly used techniques for damage detection.

In addiction to what has been exposed till now, a particular attention should be devoted in regard to the operational factors which may also play a certain role in the evaluation of bridge frequencies producing a further dispersion of their value under a statistical point of view. In bridge engineering traffic is considered as the main operational factor [49, 50]. It produces relevant effects both on the static (in terms of additional masses) and dynamic response of the bridge due to its dynamic loading on the deck. Anyway the estimation of its effects on frequencies, or modal properties more in general, is anything but trivial being traffic effects depending on many factors as for instance, the nature of the traffic (common vehicle, heavy trucks rather than crowd, trains or extreme vehicle), its dynamic acting properties (velocity with which it moves on the bridge) as well as its statistical distribution (that is how in general different traffic load sources combine themselves and their action on the bridge).

Such effects due to operational conditions, superimposed to those associated with previously described environmental factors, make practically impossible to detect damage through a straight usage of frequencies or derived quantities as damage-sensitive features. For these reasons the currently adopted trend is to exploit the quantities obtained from vibration-based techniques in statistical approaches in order to evaluate and consequently keep out the effects associated to external factors enhancing in such a way the sensitivity to anomalous occurrences.

2.1.3 Statistical process control for damage detection

There is a wide literature which makes use of the previously described techniques, parameters and quantities for damage detection purpose. Anyway most of these works do not apply such tools in statistical analysis procedures. In the last decade the steadily growing interest towards structural health monitoring of large infrastructures and the simultaneous admission of the limits in many cases of the techniques applied until then, moved the researches towards the application of well established but limited methods following a statistical approach in order to improve the reliability of the features chosen for damage detection purpose by limiting the uncertainties in their estimation and increasing, on the

other hand, their sensitivity to structural anomalies [37]. This trend has posed the process of structural health monitoring in the context of statical pattern recognition paradigm.

As referred in [51], this paradigm can be divided in four different steps (Fig. 2.3), namely

- **operational evaluation**, that is the complex of the preliminary procedures aimed at defining the components in the investigated system which may potentially be susceptible to damage, the operational and environmental conditions in which the system to be monitored functions, and the limitations on acquiring data in such conditions;

- **data acquisition and cleansing** involves the proper choice of types and locations of the sensors for monitoring activity. The variability of environmental and operational conditions, and the simultaneous potential time growth of cracks suggest the collection of data almost continuously in order to define a statistical characterization of external sources effects on measurements. Data cleansing is the part of the process that implies the choice of reliable data for the extraction of effective damage sensitive features;

- **feature extraction and data reduction** consist in the stage during which features being used for establishing if a structure is damaged or not, are extracted from the acquired data. The most proper features depend upon the specific considered study case but, as underlined in Subsecs. 2.1.1 and 2.1.2, the most widely adopted ones in monitoring of infrastructures are resonant frequencies and mode shapes. Numerous features are often identified for a structure and assembled into the so called feature vector. Anyway it is generally desirable to reduce the dimension of the problem without significant loss of information, in the perspective of enlarging the samples number for building the statistical model;

- **statistical model development**, concerns the adoption of algorithms and strategies by which features are finally employed for damage detection. Apart short discussion is devoted to these stage in a row.

The development of statistical methods for addressing the goal of damage detection, represents the stage in SHM process that has received the greatest attention in the technical literature during the last years. As just mentioned it essentially consists in the implementation of algorithms that operate on the extracted features to identify damage occurrence on the structure [52]. The adopted algorithms belong to three main categories, *group classification*, *regression analysis* and *outlier detection*, respectively. The first two types of algorithms generally belong to a general classification referred to as *supervised*

Figure 2.3: Stages in the process of the statistical pattern recognition paradigm.

learning that is the situation when data from damaged and undamaged states are available. Conversely *outlier detection*-based algorithms generally belong to the so called *unsupervised learning*. These latter are the most diffusely investigated in the latest applications of structural health monitoring of infrastructures [35], [53]. Following the current trend also the present work the of thesis focuses on these ones, and in the specific case, control charts analysis will be carried out, being one of the most commonly adopted method in this class.

In the following sections the considered procedures for features extraction and condensation, and for building the statistical model of control charts analysis are described more in details.

2.2 Multiple linear regression

Multiple Linear Regression (MLR) is one of the first adopted and the simplest available statistical tool enabling the evaluation of environmental and operational condition effects on estimated modal properties aimed at the extraction of damage sensitive features for structural SHM. MLR is a statistical technique that can be used for predicting values of one or more *response* (dependent) variables from a collection of *predictors* (independent) variables. It can also be used for assessing the effects of the predictor variables (input of the model) on the responses (dependent variables) [54].

Despite its knowledge as statistical tool is quite old its application in the field of health assessment of infrastructures is relatively recent. In [40, 41] MLR are performed to remove temperature effects on Z-24 modal frequencies identified over one year of continuous monitoring. In the mentioned references it is demonstrated that different behavior of the asphalt layer above and below freezing temperature (see Fig. 2.2(a))induced a bilinear correlation between frequencies and temperature and for this reason MLR are applied only in the case of temperature higher than 0^oC. Anyway the results in damage detection seem to be quite promising. In [55], a similar study is conducted on the vibration measurements of the Alamosa Kanyon Bridge in New Mexico (USA) whose modal frequencies are subjected to daily variations around 5%. Starting from these former applications classical MLR models have been developed and enhanced in more advanced ARX, ARMA and ARMAV models which are to this day widely investigated in literature [56, 57, 58].

In the field of Structural Health Monitoring the established linear regressive model is adopted to predict future values of the dependent variable when only

the predictors are known. By defining a *residual error* as the difference between the value predicted by the model and the measured one, once this quantity exceeds a previously fixed threshold it is likely that the bridge undergoes abnormal conditions that it had not experienced during the training period in which the model has been built. In order to gain this target it is therefore mandatory to use a first set of data of the undamaged structure in operational conditions and under changing environment to properly build the model.

The baseline equations for classical Linear Regressive Model are expressed as follow [54]

$$\begin{aligned} y_1 &= \beta_0 + \beta_1 z_{11} + \beta_2 z_{12} + \cdots + \beta_p z_{1p} + \varepsilon_1 \\ y_2 &= \beta_0 + \beta_1 z_{21} + \beta_2 z_{22} + \cdots + \beta_p z_{2p} + \varepsilon_2 \\ &\cdots \\ y_N &= \beta_0 + \beta_1 z_{N1} + \beta_2 z_{N2} + \cdots + \beta_p z_{Np} + \varepsilon_N \end{aligned} \tag{2.3}$$

that is, in compact notation

$$\mathbf{y} = \mathbf{Z} \cdot \boldsymbol{\beta} + \boldsymbol{\varepsilon} \tag{2.4}$$

where $\mathbf{y}$ is a N-by-1 column vector with N observations of the dependent variable y, $\mathbf{Z}$ is a N-by-p matrix with the corresponding N values of p selected independent variables, $\boldsymbol{\beta}$ is a p-by-1 vector with the parameters to be determined that weight the contribution of each independent variable, and $\boldsymbol{\varepsilon}$ is a N-by-1 column vector that contains the values of the random error ε , which accounts for measurement errors of the elements of $\mathbf{y}$ and for the effects of other variables not explicitly considered in the model. This last term is assumed to have zero mean, constant variance and to be constituted by independent events, that is mathematically

$$\begin{aligned} \mathrm{E}[\boldsymbol{\varepsilon}] &= 0 \\ \mathrm{Cov}[\boldsymbol{\varepsilon}] &= \mathrm{E}\left[\boldsymbol{\varepsilon} \cdot \boldsymbol{\varepsilon}^T\right] = \sigma_\varepsilon^2 \cdot \mathbf{I} \end{aligned} \tag{2.5}$$

where E is the " statistical expectation " operator, ^{T} denotes the transpose and $\mathbf{I}$ represents an identity matrix with N-by-N dimension. The first column of $\mathbf{Z}$ is usually composed by ones and the remaining columns contain the independent variables, which are often normalized (subtracting the variable mean from each observation and then dividing the difference by the variable standard deviation). In this way, the mean of the independent variable is given by the first element of vector $\boldsymbol{\beta}$.

The first step of a regression analysis is the selection of independent variables that can contribute to explain the variations observed on the dependent variables. In the context of analysis of the time evolution of modal parameters,

the first candidates are generally measured temperatures but also wind speed and humidity, (generally the easiest to be measured). Then, the parameters contained in $\boldsymbol{\beta}$ matrix should be estimated in order to provide the best possible fit between the observations and the values of the independent variable provided by the model. One of the most common way to gain this target consists in the use of the least squares method, which minimizes the sum of the squared errors [54]. Anyway in the following application a different approach is followed, that is the one based on QR decomposition of $\mathbf{Z}$ matrix, being more efficient under a numerical point of view.
Once also this step is accomplished the *residual error* matrix can be defined as follow

$$\mathbf{e} = \mathbf{y} - \hat{\mathbf{y}} \tag{2.6}$$

where $\mathbf{y}$ is the value of the considered modal property directly calculated from field measurements while $\hat{\mathbf{y}}$ is its estimate by means of MLR. $\mathbf{e}$ is successively adopted as damage sensitive feature in the definition of the statistical model enabling the condition assessment of the structure as will be successively illustrated.

2.3 Principal Component Analysis (PCA)

In the present section the statistical tool which takes the name of Principal Component Analysis, currently referred to as PCA, is introduced as direct method capable to supply damage sensitive features which can be exploited for building the statistical model as described in the process of the statistical pattern recognition paradigm. After the introduction which briefly draws the historical steps of PCA, the common approach adopted for introducing the concept of Principal Component (PC) is described at first. Then the considered methodologies, that is Classical PCA, and Local PCA, implemented in the proposed damage detection approach (see Chap. 3), are properly described.

2.3.1 Introduction to PCA

PCA is an old method and despite in many cases the roots of mathematical techniques are difficult to be traced, the origin of PCA methodology is almost univocally attributed to Pearson [59] and Hotelling [60] that in 1901 and 1933 respectively, independently gave the earliest descriptions of the technique.

Pearson obtained the definition of Principal Components in the optimization problem of finding lines and planes that best fit a set of points in n-dimensional spaces. He predicted the huge potentialities of the method under the computational point of view.

Hotelling's approach started from the ideas of factor analysis but at the end, PCA, which Hotelling formally defines, is rather different in character from factor analysis. Hotelling affirms that there is a limited, smaller $fundamental\ set\ of\ variables$ which determine the original N variables in the considered problem. He calls these variables " $PrincipalComponents$ " in order to avoid confusion with the terms "$factor$" which has different uses in mathematics. In the original ideas, such components are chosen to maximize their contributions to the total of the variances of the original variables.

After the original contributions few works only can be found concerning PCA and its application has been limited since computational methods and available tools were not adequate. Anyway after the sixties a renewed interest in PCA has arisen especially thanks to the contribution of Rao [61], and Jeffers [62, 63]. Nowadays, PCA is one of the most widely adopted technique for dimensionality reduction, which transforms data in the high-dimensional space to space of lower dimensions. It represents a very useful tool in data analysis in many fields as for instance energy, multi-sensor data fusion, materials science, gas chromatographic analysis, ecology, video and image processing, agriculture, color coating, climate and automatic target recognition.

As underlined in [64] many are the advantages of PCA application and consequently of working in a subspace (reduced dimension problem), advantages that can be synthetically summarized as follows:

- the reduced dimension has the effect of retaining the most of the useful information while reducing noise and other undesirable effects;
- PCA is the optimal (in terms of mean squared error) linear scheme for compressing a set of high dimensional vectors;
- model parameters can be estimated directly from the data;
- once these parameters are available, data compression and decompression are easy operations to be carried out;
- PCA provides a way to understand and visualize the structure of complex data sets;
- time and memory that are used in data processing are relatively small;

PCA technique anyway entails also some shortcomings that on the other hand can be summarized in:

- some methods for finding the principal components directions can meet some troubles in the case of high dimension problems (many n variables) or of cases with a huge number of samples N;

- it is not clear how standard PCA approach can deal with data sets which contain a non-negligible number of missing values;

Moreover it is worth noting that the standalone tool of PCA does not produce any dimension reduction: it only rotates the axes of the original data along the directions of maximum variance. Dimension reduction is subsequently performed by retaining only some (the ones with maximum variance) of these directions. In this sense some drawbacks may be find in the proper choice of the direction one have to account for this purpose.

The original formulation of PCA is the orthogonal transformation which can deal with linear data. However, the real-world data is usually nonlinear and some of it, especially multimedia data, is multilinear. For these reasons in the recent years a great deal of effort has been put for extending PCA via manifolds based, kernel-based and tensor-based techniques also to non linear and multilinear transformations. This generalization has made PCA relevant in a wider range of application.

Lastly, in the last decade, PCA has revealed to be a very promising tool even in the field of of structural health monitoring. Nowadays many applications of PCA can be found in literature, especially in combination with other techniques with the purpose of dimensionality reduction of the considered problem [58, 65] but also in more direct applications for damage detection [66, 67, 68].

2.3.2 Principal Components: derivation and definition

Suppose to be interested in defining the structure of covariances and correlations of n random variables. If n is not small enough, a simple observation of the n variances and $n(n-1)/2$ correlations or covariances would not be useful. In the light of this fact, it could be better to look for a few ($\ll n$) derived variables that preserve most of the information given by these variances and correlations or covariances.

In this sense PCA concentrates on variances even if covariances and correlations are not ignored. Once a vector $\mathbf{y}$ of n random variables is defined, the first step consists in looking for a linear function $\boldsymbol{\alpha}_1^T\mathbf{y}$ of the elements of $\mathbf{y}$ which

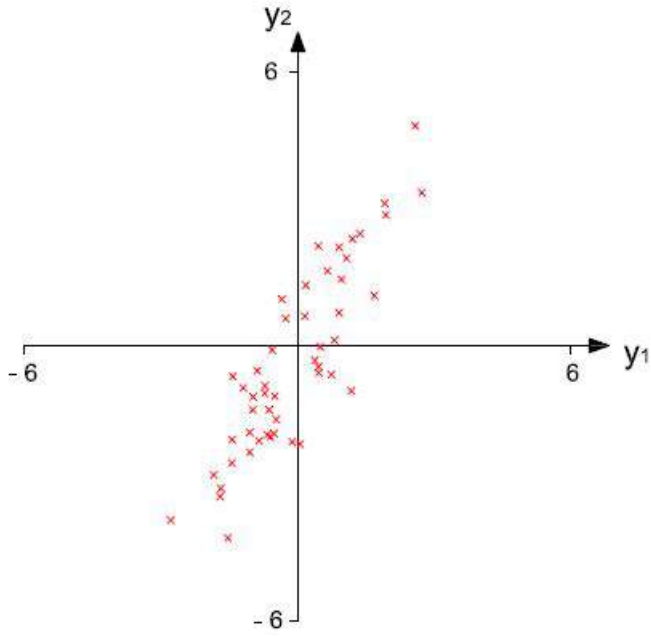

Figure 2.4: Plot of 50 observations on two variables y_1, y_2.

explain maximum variance, where $\boldsymbol{\alpha_1}$ is a vector of n constants α_{11},α_{12}, ..., α_{1n}. Such a function is defined so that

$$\boldsymbol{\alpha_1^T}\mathbf{y} = \alpha_{11}y_1 + \alpha_{12}y_2 + \cdots + \alpha_{1n}y_n = \sum_{j=1}^{n} \alpha_{1j}y_j \tag{2.7}$$

The second step consists in looking for another linear function $\boldsymbol{\alpha_2^T}\mathbf{y}$ uncorrelated with the previous one and again having maximum variance. In such a way at the k^{th} step a linear function $\boldsymbol{\alpha_k^T}\mathbf{y}$ is defined that has maximum variance and is uncorrelated with the previously defined $\boldsymbol{\alpha_1^T}\mathbf{y}$, $\boldsymbol{\alpha_2^T}\mathbf{y}$, $\cdots$,$\boldsymbol{\alpha_{k-1}^T}\mathbf{y}$. The k^{th} derived variable, $\boldsymbol{\alpha_k^T}\mathbf{y}$ is the k_{th} *PrincipalComponent* (PC). Being n the number of random variables of the problem, up to n PCs could be found, but it is hoped, in general, that most of the variance in the original data $\mathbf{y}$ will be expressed by l PCs only, where $l < n$.

The simple case where $n = 2$ is unrealistic but very useful to demonstrate the reduction in complexity that can be achieved by transforming the original variables to PCs. Actually in this simple situation the data can be plotted exactly in two dimensions. Fig. 2.4 gives a plot of 50 observations on two highly correlated variables y_1, y_2. Looking at the the data plot it is deducible that their variation is more marked in y_1 rather than in y_2 direction. If we transform

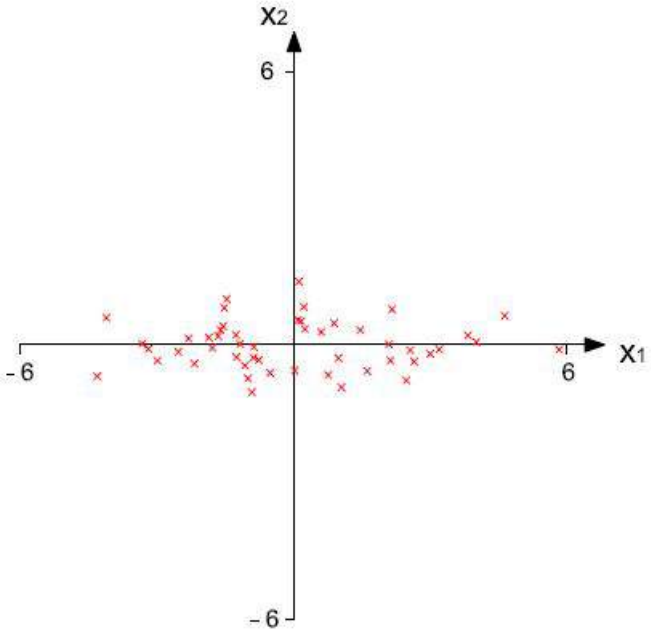

Figure 2.5: Plot of the 50 observations from Fig. 2.4 with respect to their PCs x_1, x_2.

to PCs x_1, x_2, we obtain the plot given in Fig. 2.5 where now it is irrefutable that there is greater variation in the direction of x_1, but very little variation in the direction of x_2. A very intuitive and useful geometrical interpretation of PCs for damage detection purpose in the just considered simple case with $n = 2$, can be also found in [67]. More generally, if a set of n (>2) variables has substantial correlations among them, then the first few PCs will account for most of the variation in the original variables. On the contrary, the last few PCs identify directions in which there is very little variation that means that they identify almost constant linear relationships among the original variables.

Once the PCs are defined, it is mandatory determining how to find them. Let us define a vector of random variables $\mathbf{y}$ and its known covariance matrix $\mathbf{\Sigma}$, that is a matrix whose $(i,j)th$ element is the covariance between the i^{th} and j^{th} elements of $\mathbf{y}$ when $i \neq j$ and the variance of the j^{th} element of $\mathbf{y}$ when $i = j$. The generic k^{th} PC given by $\mathbf{x_k} = \boldsymbol{\alpha}_{\boldsymbol{k}}^{\boldsymbol{T}}\mathbf{y}$ for $k = 1, 2, \cdots, n$ is the eigenvector of $\mathbf{\Sigma}$ corresponding to its k^{th} largest value λ_k. Moreover if unity vector length condition is imposed (that is $\boldsymbol{\alpha}_{\boldsymbol{k}}^{\boldsymbol{T}}\boldsymbol{\alpha}_{\boldsymbol{k}} = 1$), it easy to demonstrate that λ_k represents the variance of $\mathbf{x_k}$ (λ_k= var(x_k)).

The form of the PCs is obtained considering the function $\boldsymbol{\alpha}_{\mathbf{1}}^{\boldsymbol{T}}\mathbf{y}$, and maximizing

$\text{var}[\boldsymbol{\alpha_1^T}\mathbf{y}] = \boldsymbol{\alpha_1^T}\boldsymbol{\Sigma}\boldsymbol{\alpha_1}$ with the constraint $\boldsymbol{\alpha_1^T}\alpha_1 = 1$. This target is generally addressed through the standard approach of Lagrange multipliers, that is maximize

$$\boldsymbol{\alpha_1^T}\boldsymbol{\Sigma}\boldsymbol{\alpha_1} - \lambda(\boldsymbol{\alpha_1^T}\boldsymbol{\alpha_1} - 1) \tag{2.8}$$

where λ is a Lagrange multiplier. Differentiation with respect to $\boldsymbol{\alpha_1}$ gives

$$\boldsymbol{\Sigma}\boldsymbol{\alpha_1} - \lambda\boldsymbol{\alpha_1} = 0 \tag{2.9}$$

or

$$(\boldsymbol{\Sigma} - \lambda\mathbf{I_p})\boldsymbol{\alpha_1} = 0 \tag{2.10}$$

being $\mathbf{I_p}$ the $n \times n$ identity matrix. Thus λ is an eigenvalue of $\boldsymbol{\Sigma}$ and $\boldsymbol{\alpha_1}$ the corresponding eigenvector. To decide which of the n eigenvectors gives $\boldsymbol{\alpha_1^T}\mathbf{y}$ with maximum variance, note that the quantity to be maximized is

$$\boldsymbol{\alpha_1^T}\boldsymbol{\Sigma}\boldsymbol{\alpha_1} = \boldsymbol{\alpha_1^T}\boldsymbol{\lambda}\boldsymbol{\alpha_1} = \boldsymbol{\lambda}\boldsymbol{\alpha_1^T}\boldsymbol{\alpha_1} = \lambda \tag{2.11}$$

so λ must be as large as possible. Thus, $\boldsymbol{\alpha_1}$ is the eigenvector corresponding to the largest eigenvalue of $\boldsymbol{\Sigma}$, and $\text{var}[\boldsymbol{\alpha_1^T}\mathbf{y}] = \boldsymbol{\alpha_1^T}\boldsymbol{\Sigma}\boldsymbol{\alpha_1} = \lambda_1$ the largest eigenvalue.
Similarly, in order to define the second PC $\boldsymbol{\alpha_2^T}\mathbf{y}$, $\boldsymbol{\alpha_2^T}\boldsymbol{\Sigma}\boldsymbol{\alpha_2}$ must be maximized with the constraints conditions to be uncorrelated with $\boldsymbol{\alpha_1^T}\mathbf{y}$, that is $\text{cov}[\boldsymbol{\alpha_1^T}\mathbf{y}\boldsymbol{\alpha_2^T}\mathbf{y}] = 0$, and that $\boldsymbol{\alpha_1^T}\boldsymbol{\alpha_1} = 1$ again. Following the same approach it can be demonstrated that for third, fourth, $\cdots$, nth PCs the vectors of coefficients $\boldsymbol{\alpha_3}$, $\boldsymbol{\alpha_4}$, $\cdots$, $\boldsymbol{\alpha_n}$ are the eigenvectors of $\boldsymbol{\Sigma}$, corresponding to λ_3, λ_4, $\cdots$, λ_n, the third, fourth largest, $\cdots$, and the smallest eigenvalue respectively. Moreover, due to the imposed constraint conditions, it results that

$$\text{var}\left[\boldsymbol{\alpha_1^T}\mathbf{y}\right] = \lambda_k \quad \text{for } k = 1, 2, \cdots, n \tag{2.12}$$

.

2.3.3 Classical PCA

As already mentioned, in the present work of thesis, natural frequencies are considered as the basic dynamic quantities enabling condition assessment of long-span bridges and Classical PCA approach is the first adopted among PCA-based ones for extracting damage sensitive features. More specifically

The theoretical dissertation concerning the definition and the extraction of PCs is explicitly based on [69]

PCA is exploited to reduce the variability of natural frequency estimates caused by changes environmental factors (see the following Chap. 3).

Let us denote with $\mathbf{Y} \in \mathbb{R}^{n \times N}$ the observation matrix containing N samples of the frequency estimates of n vibration modes of the structure. These data can be remapped into the vectorial space generated by the Principal Components (PCs) that constitute an orthogonal basis. The remapped matrix, $\mathbf{X} \in \mathbb{R}^{n \times N}$, called the *score matrix*, is written as

$$\mathbf{X} = \mathbf{T}\mathbf{Y} \tag{2.13}$$

where $\mathbf{T} \in \mathbb{R}^{n \times n}$ is the *loading matrix*, obtained by performing the Singular Value Decomposition (SVD) of the covariance matrix of the original data as follows

$$\mathbf{Y}\mathbf{Y}^{\mathbf{T}} = \mathbf{U}\mathbf{S}^2\mathbf{U}^{\mathbf{T}} \tag{2.14}$$

and setting

$$\mathbf{T} = \mathbf{U}^{\mathbf{T}} \tag{2.15}$$

By definition, each row of the loading matrix contains the coefficients of a singular PC, while $\mathbf{S}^2$ is a diagonal matrix containing the singular values of the covariance matrix, which represent the variance contribution of each PC.

2.3.4 Local PCA

Lower-dimensional representation without significant loss of information performed through classical Principal Components Analysis approach presents many limitations whose recognition has driven the scientific community towards the development of nonlinear extensions of PCA by using different tools as for instance neural networks. Differently to the most commonly followed approach Kambhatla and Leen in [70] introduce non-linearity using a piecewise-linear or *local* approach, obtained by a proper partition of the original n-dimensional space defined by the possible values of y into q regions. Linear PCs are then found separately for each defined region. The obtained algorithm is comparatively computationally faster than other non linear methods as well as being equally accurate.

Loca PCA process can be divided in two different fundamental stages, listed in a row. Again, if $\mathbf{Y} \in \mathbb{R}^{n \times N}$ denotes the observation matrix containing N samples of the frequency estimates of n vibration modes of the structure, Local PCA

- first performs the partition of the space defined by the n y variables of $\mathbf{Y}$ into q disjoint regions $(\mathbf{Y_1}, \mathbf{Y_2}, \cdots, \mathbf{Y_q})$ each one o them characterized by its *centroid* $\widetilde{\mathbf{Y}} = \left(\widetilde{\mathbf{Y}}_1, \widetilde{\mathbf{Y}}_2, \cdots, \widetilde{\mathbf{Y}}_q\right)$
- then applies the Classical PCA in each region by calculating the local covariance matrices $\mathbf{\Sigma_i}$ for $i = 1, 2, \cdots, q$

In the following application the first step is accomplished in the simplest way through the use $k - means$ algorithm, also referred to as *Lloyd's algorithm*. The obtained partition is an *Eucliedan Partition* being each $\mathbf{Y_i}$ region defined by the following condition

$$\mathbf{Y}_i = \left\{\mathbf{y} | d_E(\mathbf{y}, \widetilde{\mathbf{Y}}_i) < d_E(\mathbf{y}, \widetilde{\mathbf{Y}}_j), \forall i \neq j\right\} \tag{2.16}$$

where i=1,2,$\cdots$,q while d_E denotes the Euclidean norm between the generic sample $\mathbf{y}$ and the centroid $\widetilde{\mathbf{Y}}_i$ of the i^{th} region to which it belongs. Once the clustering analysis has been performed and the data partition accomplished, the Classical PCA is applied in each region to the covariance matrix of the data normalized to the centroid $\widetilde{\mathbf{Y}}_\mathbf{i}$ as follows

$$(\mathbf{Y_i} - \widetilde{\mathbf{Y}}_\mathbf{i})(\mathbf{Y_i} - \widetilde{\mathbf{Y}}_\mathbf{i})^T = \mathbf{U}_i \mathbf{S}_i^2 \mathbf{U}_i^T \tag{2.17}$$

where for every i^{th} region, $\mathbf{U}_i$ is an orthonormal matrix whose columns form an hyperplane of principal components and $\mathbf{S}_i$ is a diagonal matrix of singular values indicating the variances associated to the corresponding PCs in $\mathbf{U}_i$.

Once also this step has been, performed the original data contained in $\mathbf{Y}$ matrix can be projected, in each region, into the PCs-defined space by using the relation

$$\mathbf{X_i} = \mathbf{T_i} \cdot (\mathbf{Y_i} - \widetilde{\mathbf{Y}}_\mathbf{i}) \tag{2.18}$$

being

$$\mathbf{T_i} = \mathbf{U_i^T} \tag{2.19}$$

the *loading matrix* in the generic i^{th} region.

2.4 Novelty detection

As already mentioned the last step in the process of the statistical pattern recognition paradigm consists in the construction of a statistical model which can be used as benchmark for damage detection purpose, accomplished through the so-called *novelty detection* (NDT).

NDT is based on the concept of *outlier* which is formally defined in [71] as follow:
"*An outlier is an observation which deviates so much from the other observations as to arouse suspicions that it was generated by a different mechanism.*"
It is now clear as the first step in NDT consists in a proper definition of a normal, or reference condition characterizing the system so that any new observation can be compared with this state: any significant deviations from the reference are considered to signal novelty or damage [72].

Now the main issue reside in defining what is normal or not, being the properties of the investigated systems susceptible to variation in environmental and operational conditions. The most common way to address this purpose is to collect data over a long enough time period t_{trn} (called *trainig period*) to span all the normal conditions. Actually as described in [54], "*to improve the quality of goods and services, data need to be examined for causes of variation. When a manufacturing process is continuously producing items or when we are monitoring activities of a service, data should be collected to evaluate the capabilities and stability of the process. When a process is stable, the variation is produced by common causes that are always present, and no one cause is a major source of variation*".

Similarly, also in SHM, if the system, that is the monitored structure, is stable, it is possible to define quantities related to the system itself whose variance is stable over time, being produced by common conditions one is able to evaluate. Such quantities are the features extracted from the operations of data normalization and cleansing previously described, that is, in the specific application of the this thesis, the *resudual error* between the estimations of modal frequencies through MLR or PCA-based methods and their corresponding values identified from the structural response.

In the case of multivariate problems NDT can be performed by using probabilistic or statistical methods. Following the latter ones, damage detection is pursued through the calculation of statistical distances and the successive construction of *control charts* which typically consist of data plotted in time order and horizontal lines, called control limits, that indicate the amount of variation due to common causes. Many statistical distances or *novelty indexes* can be defined. Among the most commonly used there are, the *Mahalanobis squared distance*, Q-statistic and T^2-statistic.

In the present work of thesis novelty detection is pursued by computing the latter listed distance, T^2-statistic, which has revealed to be a particularly sensitive tool [73]. It is defined as:

$$T^2 = gr \cdot (\overline{\mathbf{e}} - \overline{\overline{\mathbf{e}}})^T \cdot \mathbf{\Sigma}^{-1} \cdot (\overline{\mathbf{e}} - \overline{\overline{\mathbf{e}}}) \tag{2.20}$$

where gr is an integer parameter, referred to as *group averaging size*, $\overline{\mathbf{E}}$ is the mean of the residuals in the subgroup of gr observations, while $\overline{\overline{\mathbf{E}}}$ and $\mathbf{\Sigma}$ are the mean of the residuals and the covariance matrix of the original data, respectively, computed in the training period t_{trn}.

Once the statistical distance has been chosen the control limits, Upper Control Limit (UCL) and Lower Control Limit (LCL) respectively, should be defined. In most of cases their calculation is generally based on the assumption of gaussian distribution of the statistical distance and consequently by fixing a proper confidence interval through the standard deviation of the statistical distance itself. Anyway different definitions of the control limits could be given as for instance by adopting a different hypothesis for the statistical distribution of the adopted distance. Finally, in a very practical manner, it can be stated that an outlier is a value of the novelty index which lies outside the fixed control limits.

3

A NEW INTEGRATED TECHNIQUE FOR OMA AND SHM OF BRIDGES

This chapter is devoted to describe the implemented automated tool for structural condition assessment of bridges. At first a brief overview on automated techniques for modal parameters identification is drawn. Within this context some modal identification analysis experienced during the PhD period on different structures are described. Finally the methodology for SHM of bridges adopted in the following study cases in Chap. 4 and 5 is fully described, from the considered technique for the removal of the environmental effects to the construction of the control charts for damage detection.

Contents

3.1 Operational Modal Analysis for civil structures . . . 37
3.1.1 Introduction 37
3.1.2 Sample experimental and field application 39
3.2 Proposed integrated technique for SHM 53
3.2.1 Continuous modal identification and frequency tracking 53
3.2.2 Removal of environmental effects 56
3.2.3 Damage detection 58

3.1 Operational Modal Analysis for civil structures

3.1.1 Introduction

The complete knowledge of the dynamical properties of the investigated structure is the basis for the application of vibration-based techniques aimed at identifying anomalies in the behavior of the system, as underlined in the previous Chap. 2. In the same chapter, it has been mentioned that the problem of the identification of the modal properties is an old problem widely and deeply investigated at least since the last sixty years starting from applications to laboratory mock-up in the field of mechanical and aeronautical engineering.

The earlier applications were based on the measurements of the system response under the loading of known and measured external input. The comparison between input and output with proper techniques allowed to extract the modal properties of the considered structure. This approach, currently referred to as Experimental Modal Analysis (EMA), is nowadays well established and many reliable algorithms [74], permit to gain very good estimate of the dynamical features. Despite the usage of this approach still remain today the most widely adopted in mechanical engineering or, anyway, in the case of controlled environment tests, its successful application to full scale civil structures like bridges, dams or buildings, is also documented in many cases [75]. However some challenges, difficult to be overcome (above all the necessity heavy and expensive devices for applying controlled and measurable dynamic excitations), have in fact limited the use of such approach in the most of situations.

The most commonly followed approach for testing civil engineering structures is that of Ambient Vibration Tests (AVT) which have revealed to be much more practical and economical being the external loading sources constituted by freely available ambient forces, like wind or traffic circulating over or nearby the structure. This entails, as a consequence, that AVT can be performed without suspending the common usage of the considered structure and that all the measured or evaluated quantities are in effect representative of the real conditions of the structure, not being the loading source artificially generated.

On the other hand, AVT also imply some disadvantages as for instance the lower signal to noise ratio due to the lower excitation level. For this reason high sensitivity sensors are generally required in performing such kind of tests. Moreover the modal mass is not estimated and the frequency content of the

excitation may not cover all the frequency band of interest, especially when very stiff structures with high natural frequencies are investigated.

The verification of all these limitations, has lead to the development of more powerful algorithms for modal parameter identification, even if, most of them are based on techniques previously established for EMA. As modal information is derived from structural responses only (outputs), when the system is in operational conditions, this process is usually called Operational Modal Analysis (OMA) or Output-only Modal Analysis. Given that the knowledge of the input is replaced by the assumption that the input is a realization of a stochastic process (white noise), the determination of a model that fits the measured data is also named Stochastic System Identification. In the present work of thesis only OMA techniques will be considered. Actually, the application of statistical methods for damage detection purpose requires the availability of a bulk of data which can be provided only by the installation of permanent monitoring systems which should not interfere with the common activity and use of the structure.

The methods available to perform the identification of modal parameters of dynamic systems based on their response to ambient excitation are usually classified as frequency domain or time domain methods.

Frequency domain methods start from output spectrum or half-spectrum matrices previously estimated from the measured outputs. Even if they are not based on the assumption of "natural modal decomposition" these techniques still take advantage of the fact that simply considering a smaller frequency band, the influence of modes outside of this band has a reduced relevance on the results. The drawback of frequency domain is that the spectral density estimates always suffer from some kind of bias, and thus it is not as easy as in the time domain to base the modal extraction on information that is bias free or nearby bias free.

These methods can be either non-parametric or parametric. Among non-parametric methods the first to be applied was the so-called Peak-Picking [76] whose main idea is that any structural modes reasonably lightly damped is only influencing the response of the structure in a narrow frequency band around the natural frequency of the considered mode. The violation of the conditions of low damping and well separated modes leads less effective the extraction of modal properties especially for what concerns mode shapes.

Frequency Domain Decomposition (FDD) presented in [77] is a slightly more sophisticated non-parametric frequency domain method. Based on the singular value decomposition (SVD) of the spectral density matrix this method overcomes some of the limitations of the Peak-Picking method.

Among parametric method working in the frequency domain one of the most commonly adopted in civil engineering applications is the poly-Least Squares Complex Frequency domain method (p-LSCF), also known with the name of PolyMAX.

Nowadays, the available time domain methods for operational modal analysis, extensively explored in [78], are essentially based on two types of models: discrete-time stochastic state-space models and ARMA (Auto-Regressive Moving Average) or just AR (Auto-Regressive) models.

The formulations that use state-space models, designated stochastic subspace identification (SSI) methods, constitute the parametric approach that is more commonly adopted for civil engineering applications. The model can be identified either from correlations (or covariances) of the outputs (Covariance driven Stochastic Subspace Identification, SSI-cov) or directly from time series [79] (Data driven Stochastic Subspace Identification SSI-data). These two methods are very closely related. Still, the SSI-cov has the advantage of being faster and based on simpler principles, whereas the SSI-data permits to obtain some further information with a convenient post-processing, as for instance, the decomposition of the measured response in modal contributions. In the present work, the algorithm of the SSI-DATA method will be adopted.

3.1.2 Sample experimental and field application

Since the beginning of the PhD experience, many practical applications of modal identification techniques have been carried out for different purposes and on different types of structures. In the following subsections a brief overview on the experienced in field activities is drawn and the main outcomes concerning the modal identification only are presented. These practices have allowed to gain a satisfactory capability in the design process of AVT especially improving the understanding on the optimal choice of sensors type, sensors layout and measurement acquisition settings.

3.1.2.1 Application to a simple multistory frame

In the Laboratory of Structural Dynamics of the Department of Civil and Environmental Engineering of the University of Perugia an experimental set up for developing and testing innovative solutions for the active control of structural vibration is built up. The structure consists in a steel frame with an

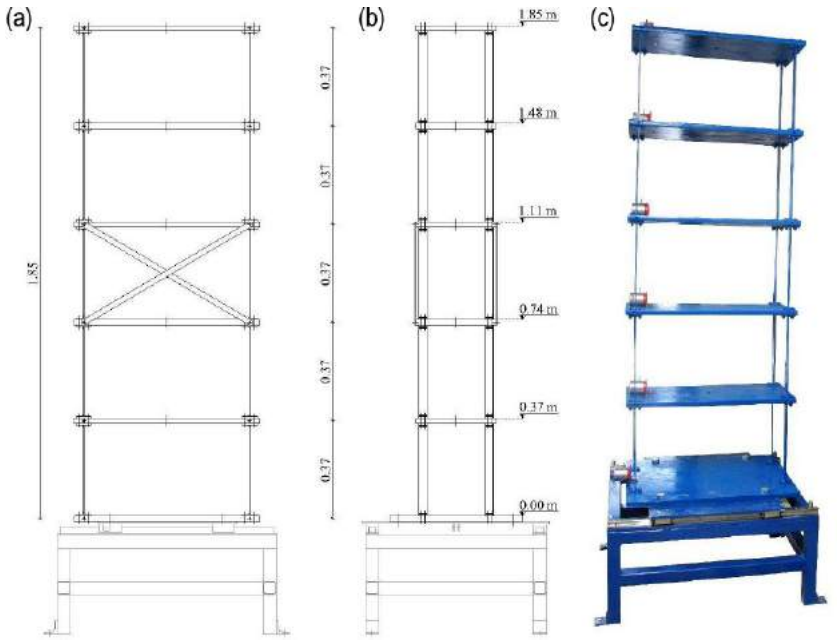

Figure 3.1: Test structure: elevation (front)(a), elevation (lateral) (b), 3D image (c).

inertial actuator on the top floor. In order to test the effectiveness of the control strategy the dynamic features of the overall system must be fully described and known. This purpose is reached by performing Ambient Vibration Test (AVT) and then extracting the modal properties of the structure through Operational Modal Analysis (OMA).

The physical model of the system, comprehensive of the devices necessary for active control purpose, is made of the following components: (i) shaking system; (ii) frame structure; (iii) AMD; (iv) monitoring sensors; (v) controller. AVT and numerical modeling involve only components (ii) whose view and geometrical details are presented in Fig. 3.1. The test structure is a five-story single-bay $S235$ steel frame having a total height of about 1.9 m. Each floor is made of 70x30x2cm steel plates of about 32.8 Kg weight. The flexural rigidity of each story can be varied using either 0.5x3x34cm or 0.4x3x34 cm steel columns. The number of degrees of freedom can be changed by means of removable bracing steel elements having cross sections with dimensions 0.3x2cm. The structural configuration considered for AVT consists of the use 0.5x3x34cm columns for the lowest two stories and 0.4x3x34cm in the remaining ones, with no bracings.

The frame structure has been modeled with SAP 2000 commercial software

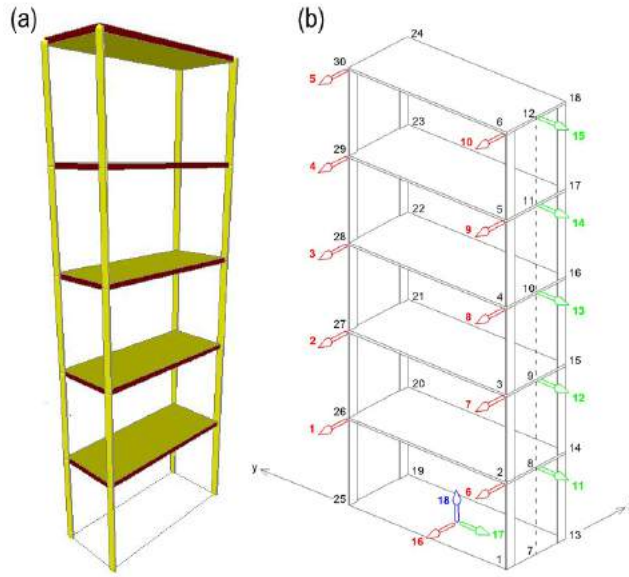

Figure 3.2: View of the 3D FEM in SAP 2000 (a) and sensors layout fro the AVT (b).

(Fig. 3.2(a)) in order to have also a numerical benchmark for the modal analysis which are performed by using an overall system of 16 accelerometers, 15 single axis MEMs DC 3711B112G and 1 triaxial MEMs DC 3713112G placed at the base, whose layout for the AVT is reported in Fig. 3.2(b).

Once the set-up has been prepared and properly configured, AVT are performed. During the tests three persons load the structure as randomly as possible in all the directions by slightly hitting the stories with sharp objects and paying attention not to hit the accelerometers or their cables. The sample rate for the acquisition is fixed in 1 ms for time series length of $9 - 10$ minutes. After data acquisition, techniques working in frequency domain, namely FDD and EFDD, and SSI-PC in the time domain, are applied to deduce the modal properties of the structure. The resonant frequencies of the first 10 modes identified by using the different mentioned techniques are summarized in Tab. 3.1 while the modal shape of the first three in-plane, out-of-plane and torsional mode are reported in Fig. 3.3. The current notation is adopted for nominate the modes: LY, LX and LZ stand for in-plane, out-of-plane and torsional mode, while the number denotes the order of the model. The results of the research on active control strategies applied to the illustrated mock-up as study case, can be found in [80].

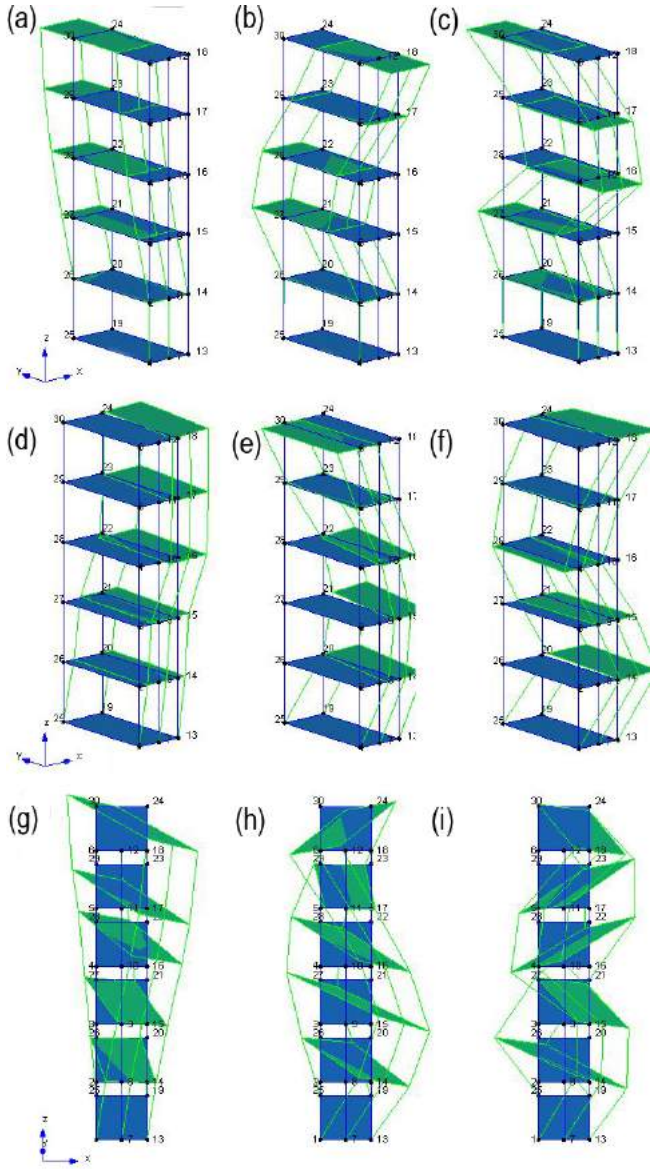

Figure 3.3: Plot of the modal shapes identified through FDD method of the first three in-plane bendin modes (a)-(c), three out-of-plane bending modes (d)-(f) and three torsional modes (g)-(i).

Table 3.1: Modal frequencies of the five-story frame structure identified through FDD, EFDD and SSI-PL techniques.

$n^o mode$	$type$	FDD [Hz]	$EFDD$ [Hz]	$SSI-PL$ [Hz]
1	$LY1$	1.8015	1.803	/
2	$LY2$	5.008	5.016	5.014
3	$LX1$	6.323	6.334	6.395
4	$LY3$	7.512	7.481	7.486
5	$LZ1$	9.770	9.810	9.204
6	$LY4$	12.330	12.30	12.340
7	$LX2$	22.220	22.220	22.230
8	$LZ2$	30.74	30.73	30.72
9	$LX3$	36.500	36.560	7
10	$LZ3$	51.710	51.700	51.72

Acknowledgment The research group of Structural Design of the University of Perugia gratefully acknowledge the financial support of the "Cassa di Risparmio di Perugia" Foundation that funded this study through the project "Development of active control systems for the response mitigation under seismic excitation" (Grant Number 2010.011.0490).

3.1.2.2 Application to a RC arch bridge

In February 2012 the modal properties of Montecastelli Bridge have been investigated by AVT. The structure is a reinforced concrete arch road bridge, about 70 m long, owned by the Province of Perugia. It crosses the Tiber river along the SR3bis secondary road that connects the towns of Città di Castello and Umbertide in central Italy.

The bridge, located very close to the village of Montecastelli, was built as a replacement of a multi-span masonry arch bridge that was partially destroyed during the second world war. Unfortunately, no precise information is available on this former bridge but, according to the memories of the people leaving in the neighborhood of the structure, it was composed by three consecutive arches with one pylon permanently in the water and another one in the flood plain. The two arches over the river were destroyed during the war, while the one in the flood plain still exists and hosts the SR3bis road. The new bridge was constructed as a replacement of the two destroyed spans. The choice of reinforced concrete was presumably dictated by the requirement of avoiding any pylon in water. The views of the Montecastelli bridge is shown in the

picture of Fig. 3.4(a). The structure under study includes: (a) two twin arches, providing the main structural system; (b) vertical struts supporting the deck; (c) the deck structure made by a slab supported by two longitudinal members connected by transverse girders in correspondence of each vertical strut; (d) a support system consisting of a reinforced concrete side wall on fill embankment on the south side and (e) a concrete wall contrasting against the historical masonry arch bridge on the north side.

The two twin arches, of 68.7 m span and about 13 m rise, consist of two variable height members, with fixed width, connected by transverse girders and supporting the concrete deck through vertical struts. In the 20 m central segment, arches and deck join together. The planar distance between the twin arches is equal to the width of the masonry arch on the north side. For this reason the longitudinal girders of the deck are about 1 m external with respect to the vertical struts supported by the two arches and are resting over cantilever ends of the transverse girders. The geometrical characteristics of the bridge are not known precisely as a geometrical survey and the original drawings are not available. A few approximate geometrical characteristics are shown in the plan and elevation of Fig. 3.4(b) and (c) where the sensors layout adopted for AVT is also underlined.
To the purpose of investigating the vertical modal behaviour of the deck, 9 cross section of the bridge (Fig. 3.4(c)) are equipped with 12 uni-axial WR 731A piezoelectric accelerometers capable to measure accelerations of ± 0.50 g with a sensitivity of 10 V/g. In the 3 cross sections located in the middle of the bridge, sensors are placed on both sides of the deck in order to properly catch the torsional modes of the bridge.

AVT are performed by acquiring the vertical accelerations of the bridge under wind and traffic loading. During the tests ambient temperature remained approximately constant around $6 - 7^o$C. A total of 8 consecutive time windows of 1800 s are collected with a sampling frequency of 200 Hz, which is fairly larger than that required for the considered bridge, whose dominant natural frequencies are below 15 Hz. Fig. 3.5 presents the mode shapes and the mean frequencies of the first six modes identified from the 8 data sets through automated SSI procedure developed in [81] and successively adopted in the proposed integrated procedure for bridge SHM.

3.1.2.3 Application to a rural curch bell tower in Umbria

The considered study case is the bell-tower of the old church of Ponte Pattoli a small rural town few Km far away from the city of Perugia (Fig. 3.1). The

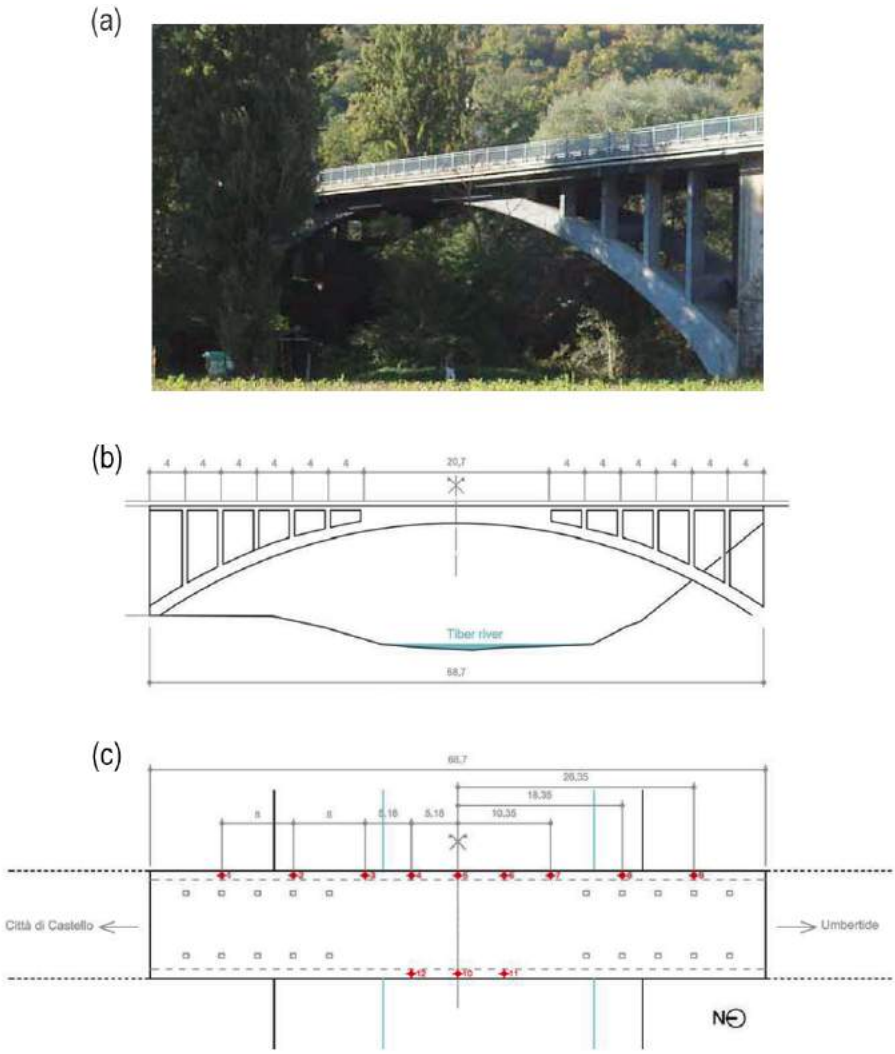

Figure 3.4: Montecastelli bridge over Tiber river: view (a), elevation (b), plan and sensors layout (c).

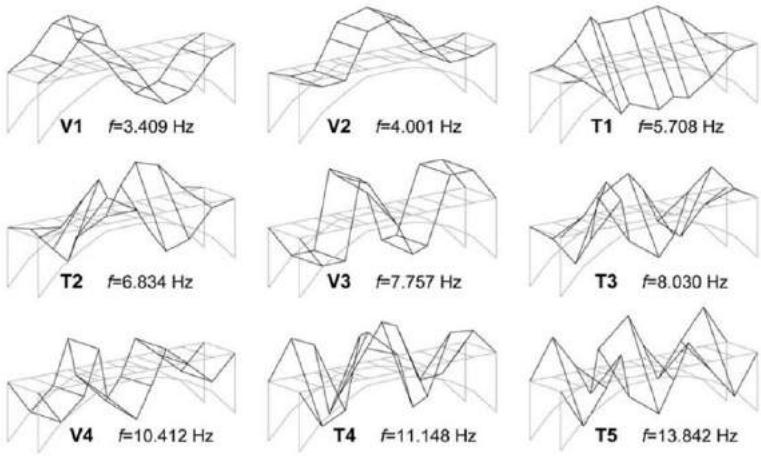

Figure 3.5: Identified mode shapes and corresponding natural frequencies of the Montecastelli Bridge.

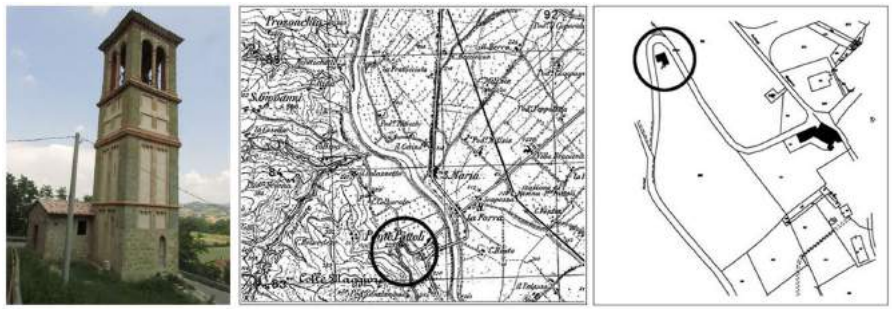

Figure 3.6: View of the bell tower of the Ponte Pattoli's "Old" church and cadastral maps maps (Ponte Pattoli, Perugia, Italy).

bell-tower was erected in 1867, neighboring to the structure of the old small church of Ponte Pattoli which dates back to the 1750 along the way linking the small town to the city of Perugia. Despite small-sized, the investigated structure presents many interesting architectural features as well as a great relevance for the local community.

Its shaft has a squared section of 5.40 m and an overall height of 21.8 m. There are three floors at the height of 11.6 m, 14.95 m and 19.9 m respectively: the first two are constituted by clay vaults while the latter, directly under the ceiling of the tower, is made of wood beams and bricks. The thickness of the walls which are made of classical brick masonry, decreases from 1.30 m at the base to 0.60 at the top.

The investigations performed on the tower are aimed at verifying the accelera-

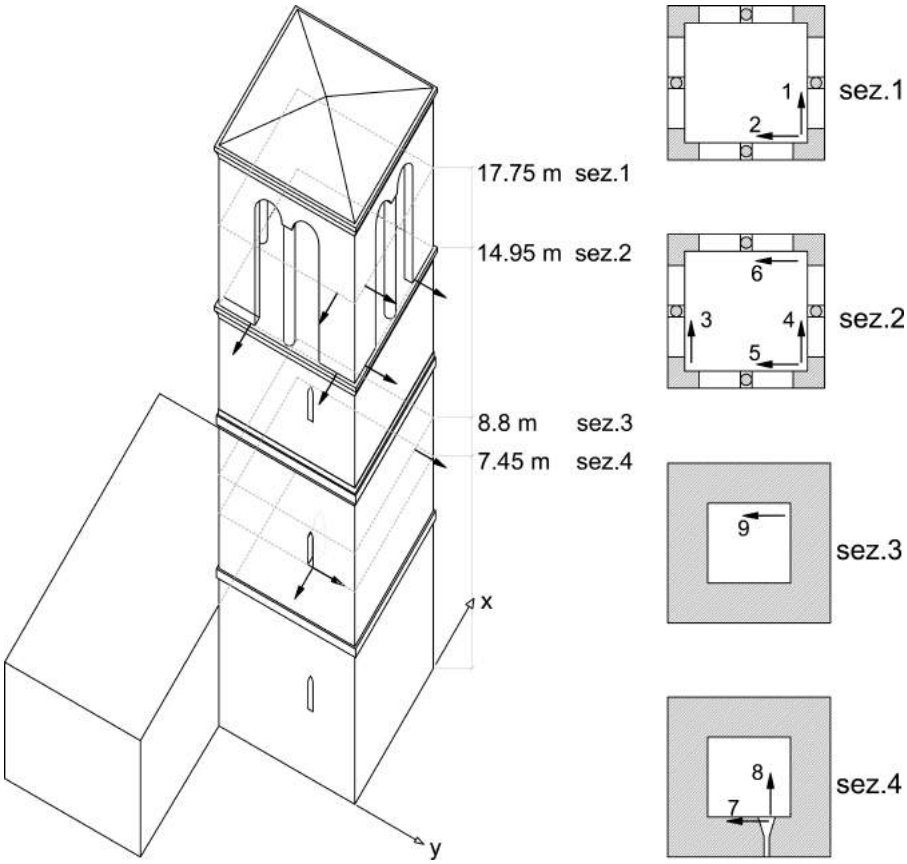

Figure 3.7: Sensors layout for the AVT.

tion levels under the action of the three bronzed bells installed on the belfry and to compare the measurements with those acquired before the restoration and consolidation operations which have been ultimated in 2012. During these acceleration tests also AVT are carried out in order to obtain a dynamical characterization of the restored tower. 9 PCB293C accelerometers with nominal sensitivity of 1 V/g are installed on the structure following the layout depicted in Fig. 3.8.

Time histories of 30 are acquired at the sample frequency of 1000 Hz. After been properly post-processed, the registered accelerations are exploited by mean of identification techniques in the frequency domain, namely FDD and EFDD, and the modal parameters of the structure are estimated. Some results obtained by the conducted dynamical investigations are resumed in Fig. 3.8 where the first four identified mode shapes are represented together with the corresponding frequencies.

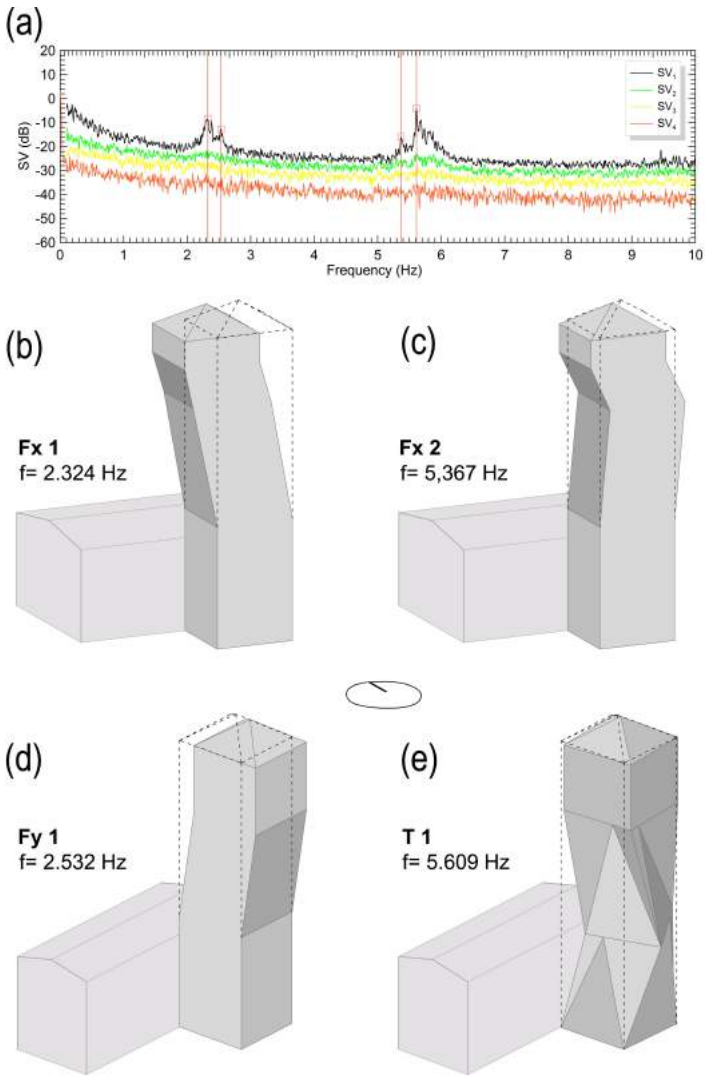

Figure 3.8: Identified modal frequencies through FDD application (a). Modal shapes of the first four identified modes (b)-(e).

3.1.2.4 Application to a monumental bell tower in Perugia

The Basilica of San Pietro in Perugia belongs to an historical monumental Benedictine abbey located in the southern part of the city. The abbey was erected in 996 while the first erection of the bell-tower dates back to the 13^{th} century. Throughout the centuries the bell-tower has been subjected to several structural and architectural interventions, both for consolidation and for changing its intended use. The actual configuration is dated back to the 15^{th} century and the design is attributed to the architect Bernardo Rossellino. Various structural interventions were necessary to repair damages caused by lightning shocks that several times threatened the stability of the structure. In the last years, the restoration and consolidation measures for the damage occurred after the strong Umbria-Marche earthquake of 1997 have been concluded.

The bell tower stands out between the basilica and other branches of the abbey, with a total height of about 61.45 m. In the first 17 m the structure is restrained by the bordering buildings, so that the tower is free to move only in the last 45 m (Fig. 3.9). The bell tower is constituted by a dodecagonal shaft in the first 26 m, a belfry with hexagonal cross section reaching an height of about 41 m and a cusp at the top. The constituent material is not homogeneous. The shaft is made by stone masonry, with large external portions realized in brick masonry as structural rehabilitation measures due to the occurrence of several damages. Some details on this aspect are given in Fig. 3.10(a) where the numerical modeling of the structure is also depicted. In order to fully characterize the dynamic behavior of the bell-tower and to successively gain an optimal tuning of the FEM, AVT and OMA have been performed in two different periods from December 2013 to February 2015. The tests are also aimed at defining the most appropriate hardware setup for the SHM system to be installed. For this reason AVT have been also carried out by using different types of accelerometers located in one or two sections of the bell-tower, as shown in Fig. 3.10(b)(c) where Section 1 is at the base of the cusp (40.8 m), while Section 2 at the base of the belfry (29.1 m). More details concerning the adopted instrumentation and the setting for the measurements can be found in [82]. In Tab. 3.2 the identified modal frequencies of the bell-tower of the Basilica of San Pietro are reported, while in Fig. 3.11 the mode shapes of the first three modes are depicted. The modal propertied are obtained by means of the SSI data driven technique adopted in the integrated SHM procedure described in the following Sec. 3.2.

Since October 2014 a continuous dynamic monitoring system has been installed onto the bell-tower with the purpose of investigating the evolution of the

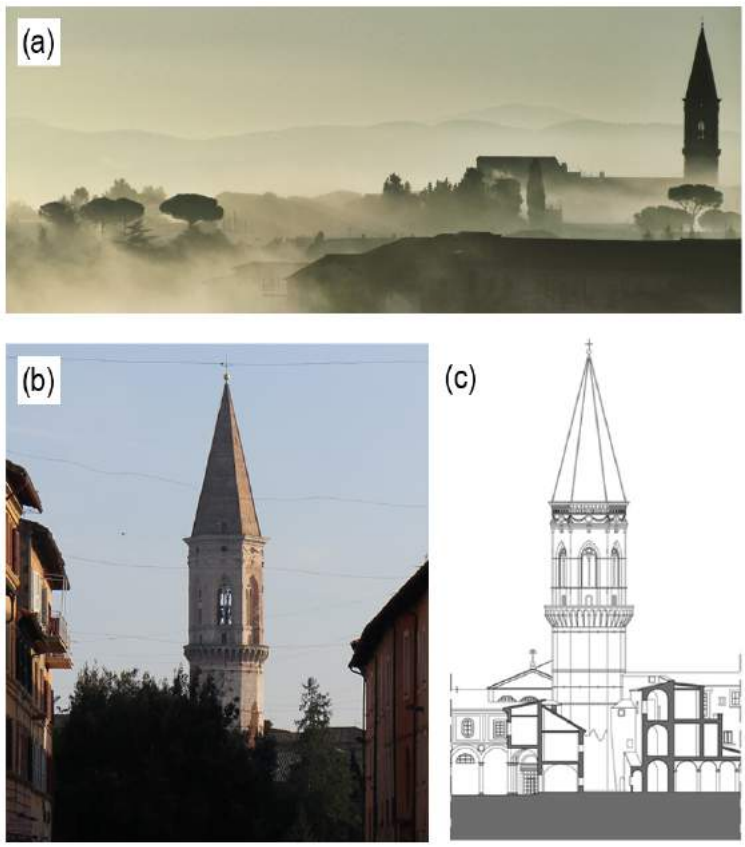

Figure 3.9: View of the bell-tower of the Basilica of San Pietro in Perugia, Italy (a)-(b). Geometrical survey of the bell-tower (c)

Table 3.2: Identified modal frequencies bell-tower of the Basilica of San Pietro.

$n^o mode$	$type$	SSI [Hz]
1	$LX1$	1.449
2	$LY1$	1.518
3	$LT1$	4.345
4	$LX2$	4.586
5	$LY2$	4.861

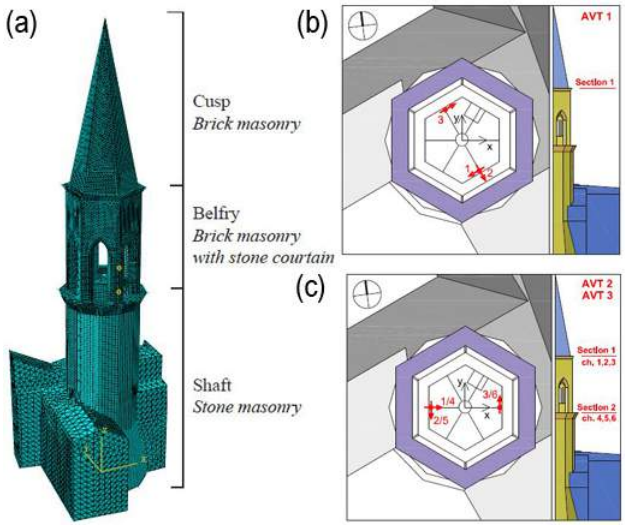

Figure 3.10: Finite Element Model of the bell-tower (a). Sensors layouts during AVT1 (b) and AVT2 (c).

natural frequencies of the bell-tower and to use such information for early damage detection. The monitoring system comprises three high-sensitivity accelerometers, fixed at the base of the cusp, as described in Fig. 3.10(b)(c), for AVT 3. Monitoring data can be accessed at any time via the internet and are transmitted to the server of the Laboratory of Structural Dynamics of University of Perugia were they are automatically processed to extract modal parameters and other synthetic information. Fig. 3.12(a) shows the time

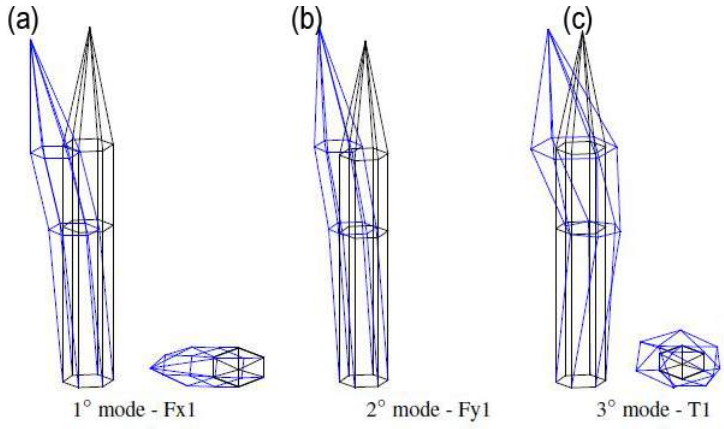

Figure 3.11: Mode shapes relative to the first three modes of the bell-towe, identified through AVT.

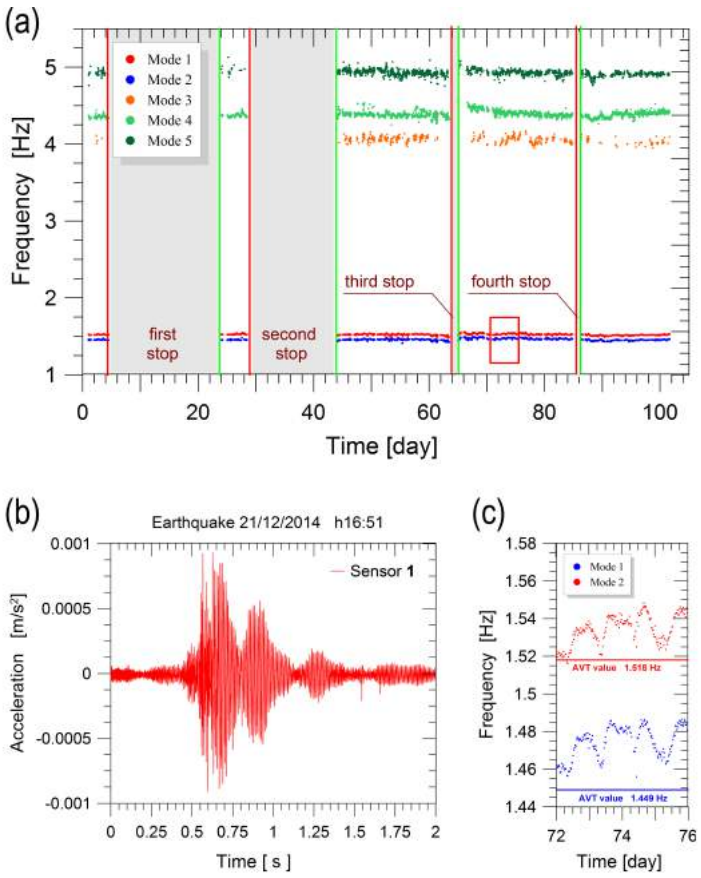

Figure 3.12: Preliminary results of the permanent monitoring system: frequency time histories of the first 5 identified modes (a), acceleration measurements of one sensor during a small earthquake on the 21^{th}/12/2014 and detailed view of the daily oscillation of the identified frequency time histories for the first two modes (c).

evolution of the first natural frequencies, while in Fig. 3.12(c) a detailed view of the daily fluctuations due to changes in ambient conditions of the first two modal frequencies is represented. In addiction, the installation of the permanent monitoring system has allowed to register the seismic response of the tower to many earthquake events. In Fig. 3.12(b) the acceleration registered by sensor 1 during the seismic event of December 21^{th} 2014 is reported. The earthquake had a magnitude of 3.6 on the Richter scale and its epicenter was located in Citerna (Perugia), about 75 Km far from the bell tower.

Acknowledgment The research group of Structural Design of the University of Perugia gratefully acknowledge the financial support of the "Cassa di Risparmio di Perugia" Foundation that funded this study through the project "Structural

Monitoring for the protection of the Cultural Heritage: the bell-tower of the Basilica of San Pietro in Perugia and the dome of the Basilica of Santa Maria degli Angeli in Assisi" (Project Code 2014.0266.021).

3.2 Proposed integrated technique for SHM

In the present section the proposed integrated technique for Operational Modal Analysis and Structural Health Monitoring is described. The procedure combines different established tools which work together automatically for the purpose of enabling the structural condition assessment of the investigated system. More specifically, in the present work of thesis, the case of bridge structures is considered but the absolutely general nature of all the single procedures involved in the proposed close loop method leads this last suitable in a wide range of applications in the monitoring of civil structures. As an example, the following proposed procedure is currently applied for the condition assessment of historical buildings (see Subsec. 3.1.2.4) which is a pretty new field of interest in vibration-based SHM.

The method, whose working scheme is presented in Fig. 3.13, cover all the steps of the process of the statistical pattern recognition paradigm from data acquisition and cleansing, to feature extraction and statistical model construction for structural condition assessment. Each of this stage is described in its crucial aspects in the following Subsections of the present Chapter, while the effectiveness of the procedure will be globally verified in the following Chap. 4 and 5 where it will be applied to a numerical model of a long span suspension bridge with main cable damage and to a real concrete arch bridge, respectively.

3.2.1 Continuous modal identification and frequency tracking

Modal properties of the bridge are identified by means of a Stochastic Subspace Identification procedure [83] which is the branch of modal identification techniques more widely investigated in the recent years being particularly apt to be automated and being very effective in the identification also of closely spaced and/or weakly excited modes. The adopted technique which belongs to the classic form of data driven (SSI-data) procedures, is automated through the use of clustering analysis which is adopted for interpreting the results of

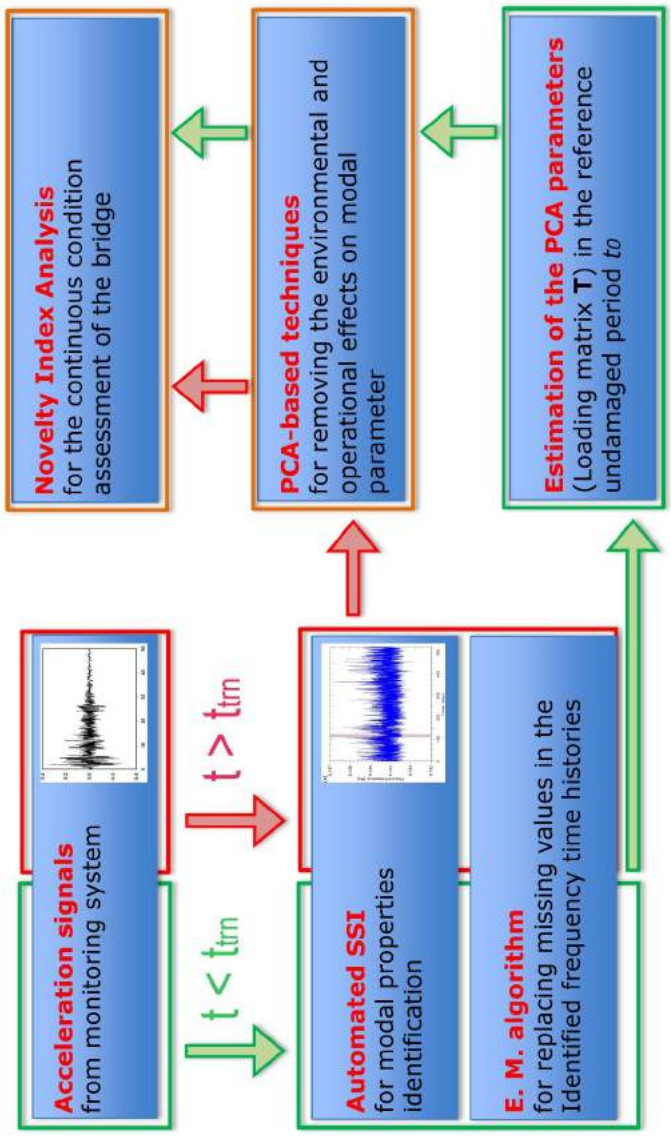

Figure 3.13: Structure of the proposed method for SHM of bridges.

SSI output for varying the two main parameters affecting the results which are the order n_o of the model and half the number i_r of output block rows adopted to build the block Hankel matrix.

The SSI-data technique integrated in the proposed SHM procedure consists in the following steps:

- run of SSI-data analysis for different values of n_o and i_r;
- elimination of noise modes;
- clustering of remaining modes;
- merging of clusters from different setups;
- extraction of mean values of modal parameters estimates with 95% confidence intervals under variation of n_o and i_r.

All the details concerning the just listed steps of the considered SSI identification technique are reported in [81].

Once the modal properties of the bridge are extracted from the single setup of acceleration measurement, those which are chosen as damage sensitive quantities must be properly collected in the so-called *observation marix* $\mathbf{Y}$. As already underlined, in the present work of thesis frequencies are considered as quantities enabling damage detection. The tracking of the identified modal frequencies is automatically performed by means of a double similarity check on both frequency value and mode shape (MAC value), assuming as reference solution the modal frequencies and the related mode shapes obtained from AVT. These lasts must precede in any case the installation of a permanent monitoring system with the purpose of fully characterize the dynamic behavior of the investigated structure. The following results in the next chapters are obtained by imposing a tolerance of 5% on frequency estimates and a MAC value bigger than 0.50 being the evaluation of mode shapes generally less reliable. Moreover it is worth specifying that in the former study case, the one concerning the numerical model of a suspension bridge (Chap. 4), the exact eigenproblem solution is assumed as the reference. This first step of modal properties tracking, if properly set, can allow to avoid the problem of multiple identified modes.

One of the main problem one have to face with in the field of Operational Modal Analysis is that low or particular excitation conditions may not allow a complete identification of the dynamic properties in the range of interest, especially for what concerns the higher modes, always more difficult to be excited. These incomplete identification determine the presence of missing values in the observation matrix. In order to tackle the issues of such missing identified modes, another automated procedure is applied once $\mathbf{Y}$ has been

built or new observations are added to it. More specifically missing data are replaced by application of the probabilistic procedure based on the *Expectation Maximization* (EM) *algorithm* [84], which is effective if the percentage of missing data is not too large. In the following applications, always less than 2% of modal frequencies are missing, which can be considered a satisfactory percentage to apply the mentioned algorithm. Such missing data are effectively replaced by the adopted technique which is based on a generalized *e-step* of the EM algorithm properly adapted for learning the principal components of a data set (concept of the Probabilistic model of PCA). During this step, for each incomplete observation vector, $\mathbf{y}_i$, representing the i-th column of the observation matrix, $\mathbf{Y}$, two vectors $\widetilde{\mathbf{x}}_i$ and $\widetilde{\mathbf{y}}_i$ are computed such that the norm $\parallel \mathbf{T}^T\widetilde{\mathbf{x}}_i - \widetilde{\mathbf{y}}_i \parallel$ is minimized. Afterwards, the i-th column of $\mathbf{Y}$ is replaced by $\widetilde{\mathbf{y}}_i$ and the i-th column of $\mathbf{X} = \mathbf{TY}$ is replaced by $\widetilde{\mathbf{x}}_i$. For the sake of brevity, the minimization algorithm necessary to compute $\widetilde{\mathbf{x}}_i$ and $\widetilde{\mathbf{y}}_i$ is not described here and the reader is referred to [85] for the details.

3.2.2 Removal of environmental effects

Once the observation matrix has been completely built, the environmental and operational effects that affect the identified frequency time histories (overlapped to the residual random errors in output-only frequency identification), must be removed through the multivariate statistical techniques illustrated in the previous Chap. 2 in order to obtain features only sensitive to damage.

As mentioned in advance, the damage-sensitive features are the residual error, collected in the *residual error matrix* $\mathbf{e}$, and calculated as the difference between the value of the frequency directly estimated through the modal identification technique and its calculation by means of MLR or PCA-based techniques. While the application in this sense has been pretty much completely described in the case of MLR (see Sec. 2.2), some more details should be given in the case of PCA-based techniques.

First of all it is necessary to remark how both in the case of MLR and Classical and Local PCA the parameters involved in the feature extraction must be estimated in a statistical manner, during a period, referred to as *training period* t_{trn}, during which the structure is in the reference healthy state and experiences all the "normal condition" (Sec. 2.4). Literature results [86] referring to bridges subjected to changes in temperature and operational conditions (traffic) suggest that t_{trn} should be at least equal to one year, so that a nearly complete record of environmental and operational conditions is considered during the training period. In the application to the study case in Chap. 4 where the main

issue concerns the elimination of wind effects, considering the daily, micro-meteorological and seasonal periodicity of wind speed, it is very likely that a one year-long training period is needed for removing wind effects, as well. On the contrary, in the case of PCA-based techniques applied to real bridge data (Chap. 5), it will be shown in that maybe using t_{trn} longer that one year could allow to obtain better results.

Now to the purpose of removing the aforementioned effects from identified frequency time histories, the common approach to both Linear and Local PCA consists in the base idea that a limited number, l, of PCs usually suffice to reconstruct the major part of the variance of the original data. Consequently, a rectangular reduced loading matrix, $\hat{\mathbf{T}} \in \mathbb{R}^{l \times n}$, is obtained by considering only the first l columns of matrix $\mathbf{U}$ in Eq. 2.15 for the Classical PCA and in Eq. 2.19 for the Local PCA. In such a way only the PCs that are responsible for the majority of the variance are accounted for and the environmental and operational effects can be properly removed. Actually the reduced loading matrix is used for model dimension reduction and for re-mapping the reduced-order data into the original space, yielding a modified observation matrix $\hat{\mathbf{Y}}$ as

$$\hat{\mathbf{Y}} = \hat{\mathbf{T}}^T \hat{\mathbf{T}} \mathbf{Y} \tag{3.1}$$

for the Linear PCA and

$$\hat{\mathbf{Y}}_\mathbf{i} = \hat{\mathbf{T}}_\mathbf{i}^\mathbf{T} \mathbf{X}_\mathbf{i} = \hat{\mathbf{T}}_\mathbf{i}^\mathbf{T} \hat{\mathbf{T}}_\mathbf{i} (\mathbf{Y}_\mathbf{i} - \widetilde{\mathbf{Y}}_\mathbf{i}) + \widetilde{\mathbf{Y}}_\mathbf{i} \tag{3.2}$$

for each i_{th} cluster of the Local PCA. In such way $\hat{\mathbf{Y}}$ and $\hat{\mathbf{Y}}_\mathbf{i}$ matrices only contain the part of the variance that is associated to changes environmental and operational conditions. On the other hand, the so-called *cleaned frequencies*, that is the frequencies where the environmental factors are removed, can be defined as follows

$$\mathbf{Y}^* = \overline{\mathbf{Y}} + \mathbf{e} \tag{3.3}$$

where $\overline{\mathbf{Y}} \in \mathbb{R}^{n \times 1}$ is a vector containing the mean values of the original frequency data, while $\mathbf{e}$ is the residual error matrix.

The just defined procedure allows to determine for each new observation vector, $\mathbf{y}_j$, the corresponding residual error calculated with different techniques on the base of parameters estimated over one or more year long training period. The only note which is mandatory to me mentioned is that in the case of Local PCA the calculation of the residual error for each new observation require preventively to establish to which cluster the new observation belongs. This target is accomplished by calculating its Euclidean distance with each centroid $\widetilde{\mathbf{Y}}_\mathbf{i}$ and choosing the cluster with whom centroid such distance is minimal.

3.2.3 Damage detection

Independently to adopted techniques, the residual error matrix, $\mathbf{e}$, given by

$$\mathbf{e} = \mathbf{Y} - \hat{\mathbf{Y}} \tag{3.4}$$

defined in the training period t_{trn} allows to estimate the Control Limits introduced in Sec. 2.4. These limits which allow to determine if a new observation is an outlier or not, that is if the structure is damaged or not can be defined in many different ways. In the present work of thesis, as already mentioned T^2-statistic is the adopted statistical distance (Eq. 2.20). Its Lower Control Limit is 0 while its Upper Control Limit is statistically computed as the value corresponding to a cumulative frequency of 95% in the training period. According to the proposed SHM procedure, the novelty index is updated after a group of gr new observations acquired and the probability of having a false alarm is equal to 5%.

4

APPLICATION TO SHM OF SUSPENSION BRIDGES WITH MAIN CABLE DAMAGE

This chapter is devoted to show the results of the application of the previously described PCA-based tecniques to the first case of study which consists in an analytical model of a long-span suspension bridge under wind action, changing temperature and characterized by main cable damage. The continuum model adopted in the analysis is described at first alongside with the mathematical formulation used for simulating wind action and changing temperature and their effects over identified modal parameters. A deterministic analysis is then conducted in order to separately evaluate effects induced on modal frequencies by wind, temperature and damage. Finally the proposed damage detection procedure is tested on the continuously simulated response of the bridge model and the results are properly illustrated and explained.

Contents

4.1 Continuum model of damaged suspension bridge . . 61
4.1.1 Static response 62
4.1.2 Equations of motion under wind loading 65
4.2 Wind effects on eigenfrequencies 67
4.2.1 New Carquinez Bridge 68
4.2.2 Akashi Kaikyo Bridge 70
4.3 Temperature effects on eigenfrequencies 72
4.4 Damage effects on eigenfrequencies 74
4.5 Damage detection 76
4.5.1 Continuous response simulation and analysis 77
4.5.2 Regressive models 91
4.5.3 PCA-based techniques 92
4.5.4 Application with measurements noise 103
4.6 Discussion of results 110

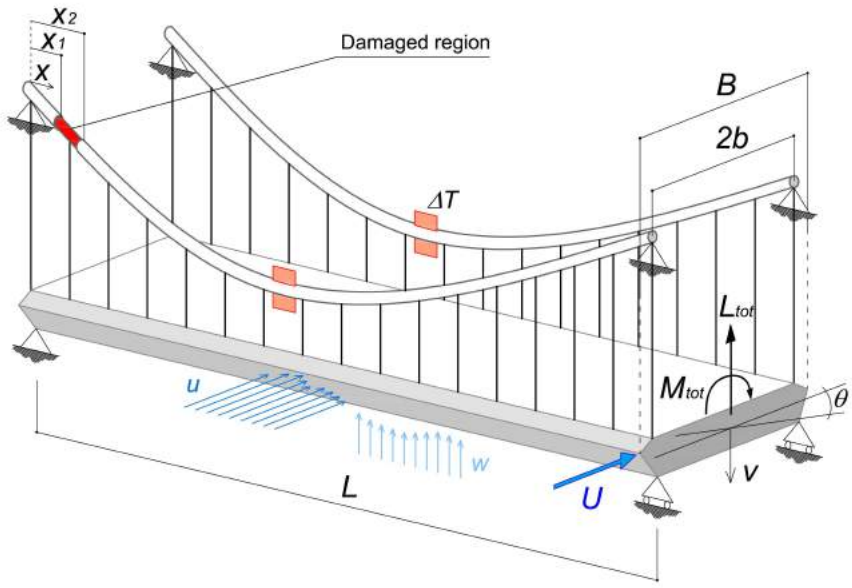

Figure 4.1: Continuum model of suspension bridge with damaged main cable, subject to wind loading and changing temperature

4.1 Continuum model of damaged suspension bridge

The coupled vertical-torsional motion of a single-span, damaged, suspension bridge subjected to the excitation of a turbulent wind is studied (Fig. 4.1 (a)) following previous work [87, 88]. The bridge is composed by two shallow main cables, a stiffening girder and a uniform distribution of vertical hangers. The main cables, placed at a distance $2b$, are hinged at fixed anchors placed at the same vertical elevation and are modeled as mono-dimensional linearly elastic continua with negligible flexural and shear rigidities and weight per unit length w_c. The deck is modeled as a uniform, linearly elastic beam with Euler-Bernoulli flexural behavior and classic St. Venant torsional behavior; its weight per unit length is detoted with w_g. The hangers are uniformly distributed, massless and inextensible. The total span of the bridge is equal to L. The Young moduli of the materials constituting the cable and the girder are denoted by E_c and E_g, respectively, while the shear modulus of the material constituting the girder is denoted by G_g. The inertial momentum and the torsional constant of the girder are denoted by J_g and J_t, respectively.

One of the two main cables is supposed to be subjected to a diffused damage in the region $x_1 < x < x_2$ consisting of a reduced cross section equal to $A_c(1-\eta)$, A_c being the undamaged cross-section. The considered damage is completely described by the damage *intensity factor*, $\eta \in [0,\ 1]$, the *extension factor*, δ, and the *position factor*, γ. The last two factors are defined as

$$\begin{aligned} \delta &= \tfrac{x_2 - x_1}{L} \\ \gamma &= \tfrac{x_1 + x_2}{2L} \end{aligned} \tag{4.1}$$

4.1.1 Static response

In the hypothesis of parabolic static profile of the cable, the static response of the bridge under dead loads w_g and w_c, is fully described by means of the following two parameters, the *sag augmentationfactor*:

$$\kappa^2 = \frac{f_{d,\Delta T}}{f_{u,0}} \tag{4.2}$$

and the *tension lossfactor*:

$$\chi^2 = \frac{H_{d,\Delta T}}{H_{u,0}} \tag{4.3}$$

where $f_{u,0}$ and $H_{u,0}$ represent the sag of the cable and the horizontal component of tension obtained in a "reference state", (that is undamaged and corresponds to $\Delta T = 0$), while $f_{d,\Delta T}$ and $H_{d,\Delta T}$ are the same quantities evaluated in an state representative of "operational" conditions, that is, for nonzero ΔT and a potential damage in one main cable. The mathematical formulation needed behind this synthetic dissertation can be found in [89] and [88].
The dependence of κ^2 and χ^2 upon damage characteristics and temperature variation allows some remarks. First of all it is worth to observe that the presence of damage in a cable generally induces a sag augmentation, namely $f_d \geq f_u$. Such occurrence in one main cable only produces in the present model a static rotation $\theta_0(x)$ of the deck cross-section which can be quantified throughout the *sag augmentationfactor* as follow:

$$\theta_0(x) = \frac{\kappa^2 - 1}{2b} y_u(x) \tag{4.4}$$

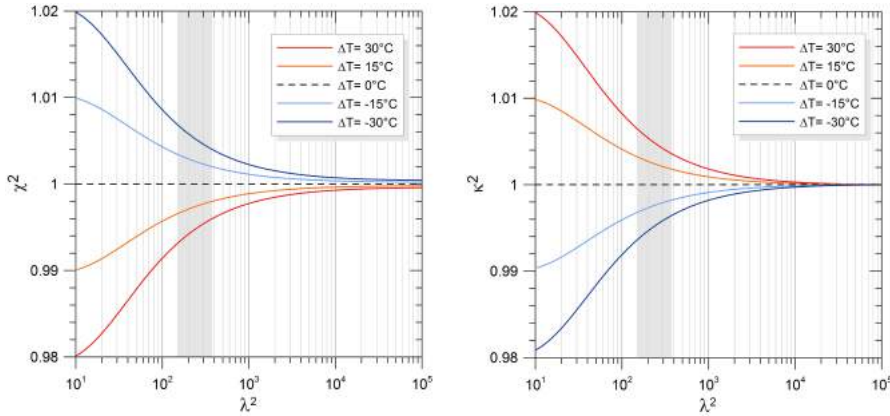

Figure 4.2: Behavior of the *tension loss* (a) and *sag augmentation* (b) $factor$ for varying the Irvine's parameter λ^2 and for different values of temperature variation ΔT.

being $y_u(x)$ the static profile of the undamaged cable. Moreover, once the Irvine parameter of the cable is defined:

$$\lambda^2 = \left(\frac{8f_u}{L}\right)^2 \frac{L}{L_{e,u}} \frac{E_c A_c}{H_u} \tag{4.5}$$

where $L_{e,u}$ represents the effective length of the undamaged cable, the dependence of the factors defined in 4.2 and 4.3 upon such parameter is quite easy to be demonstrated. This relationship allows to perform some preliminary parametric analysis enabling the evaluation of the effects of temperature and damage on the same κ^2 and χ^2. In the following Figs. 4.2 - 4.5, the obtained results are presented by specializing the just introduced model with the geometrical characteristics of the New Carquinez bridge (the adopted data are resumed later on in table 4.1). In the anlysis, the Irvine parameter is varied from 10 to 10^5, but as reported by Luco and Turmo in [90], the values representative of real bridges, highlighted with a grey stripe in the figures, range only from 148 to 376 with an average value of 220.

In Fig. 4.2 the effects of temperature variation on *tension loss* and *sag augmentation* $factor$ are evaluated at first. It can be easily observed that while ΔT spans from -30 to 30 ^{o}C, χ^2 tends to decrease whereas κ^2 increases almost linearly, which can be considered physically meaningful in most of cases. Such linear behavior is underlined in Fig. 4.3 where the relationship between the considered factors is focused in the range of λ^2 for real bridges.

Following a similar approach, analogous analysis are carried out for varying the Irvine parameter and the damage intensity factor η which is the most significant

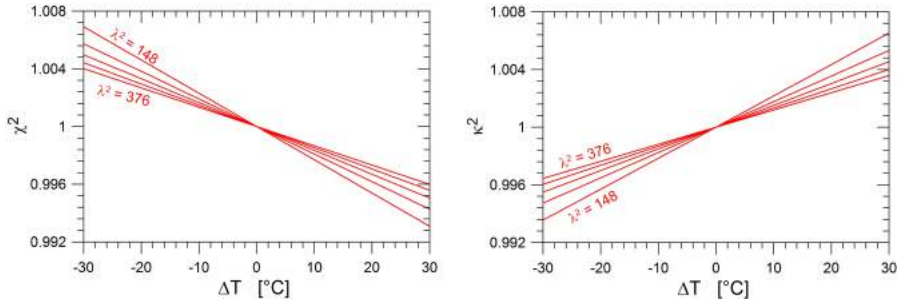

Figure 4.3: Variation of the *tension loss* (a) and *sag augmentation* (b) *factor* for varying temperature variation ΔT and different values of the Irvine's parameter in the range of values for real bridges.

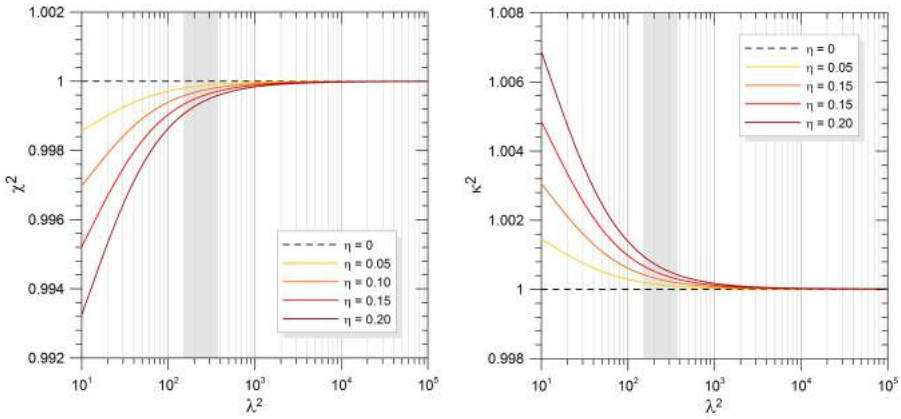

Figure 4.4: Behavior of the *tension loss* (a) and *sag augmentation* (b) *factor* for varying the Irvine's parameter λ^2 and for different values of damage intensity factor η.

damage characteristic in the adopted model as pointed out in previous studies (see for instance [81, 87]). The results, depicted in Fig.s 4.4 and 4.5, are obtained for a fixed damage extention $\delta = 0.05$ and position $\gamma = \delta/2$ (damage in the proximity to one support) and by varying η from 0 to 0.2, that means a remarkable cross section reduction of the 20% in the damaged cable. More detailed justifications concerning the chosen values of such paramenter will be given later on in Sec. 4.4 and 4.5. As expected, the effects of damage upon κ^2 and χ^2 are always smaller than those produced by changing temperature, and weakly non linear. Moreover it is worth to notice that the effect of damage occurrence tends to decrease for higher values of λ^2.

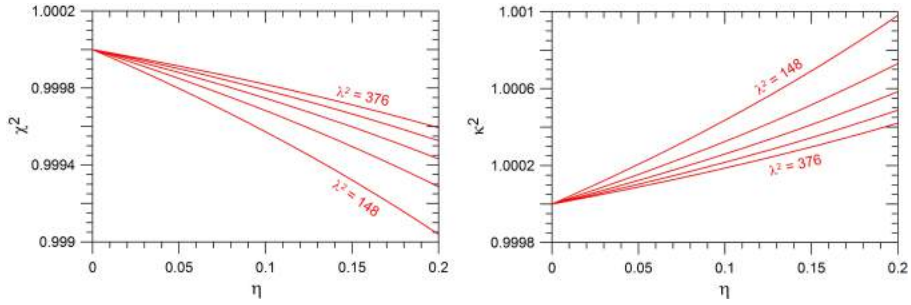

Figure 4.5: Variation of the *tension loss* (a) and *sag augmentation* (b) *factor* for varying damage intensity factor η and different values of the Irvine's parameter in the range of values for real bridges.

4.1.2 Equations of motion under wind loading

The wind blows in the horizontal cross-deck direction and the mean wind speed is denoted by U. The along-wind (horizontal) turbulence component is denoted by $u(x,t)$ while the across-wind (vertical) turbulence component is denoted by $w(x,t)$, t denoting time and x being the abscissa along the girder. Wind effects on the deck determine aerodynamic and aeroelastic loads, L_{tot} and M_{tot}, representing lift and pitching moment per unit length, Fig. 4.1. Under the classic hypothesis of validity of superposition principle, L_{tot} and M_{tot} are given by the sum of buffeting and self-excited components.

The motion of the bridge is described by means of two generalized displacement functions (Fig. 4.1 (b)): flexural vertical deflection $v(x,t)$ and twist rotation $\theta(x,t)$ about the longitudinal centerline of the deck. The following non-dimensional variables are also conveniently introduced for the problem at hand:

$$\begin{array}{llll} \overline{x} = \frac{x}{L} & \overline{v} = \frac{v}{8f_u} & \overline{t} = \frac{t}{L}\sqrt{\frac{2H_u}{m}} & \overline{u} = \frac{u}{U} \\ \overline{w} = \frac{w}{U} & \overline{U} = U\sqrt{\frac{m}{2H_u}} & \overline{B} = \frac{B}{L} & \overline{\theta} = \frac{4bH_u\theta}{mgL^2} \end{array} \tag{4.6}$$

where m is the mass per unit-length of girder and cables, B is the reference width of the deck and g denotes gravity acceleration.

The wind-excited response of the bridge is studied in the modal space, through standard variables' separation. Vertical and torsional modal amplitudes are denoted as $\zeta_i^v(\overline{t})$ and $\zeta_i^\theta(\overline{t})$ $(i = 1, 2, \ldots, \infty)$, while corresponding eigenfunctions are $\phi_i^v(\overline{x})$ and $\phi_i^\theta(\overline{x})$. The expressions of $\phi_i^v(\overline{x})$ and $\phi_i^\theta(\overline{x})$, as well as of the non-dimensional natural circular frequencies, $\overline{\omega}_i^v$, $\overline{\omega}_i^\theta$, of the damaged bridge were derived in [88] and the reader is referred to that study for the details. The

non-dimensional circular frequencies, $\overline{\omega}_i$, are defined in terms of the dimensional ones, ω_i, as $\overline{\omega}_i = \omega_i L\sqrt{m/2H_u}$.

The equations of motion of the i-th vertical and torsional modes are

$$\ddot{\zeta}_i^v(\bar{t}) + 2\overline{\xi}_i^v\overline{\omega}_i^v\dot{\zeta}_i^v(\bar{t}) + \overline{\omega}_i^{v\,2}\zeta_i^v(\bar{t}) = -\Lambda_{b,i}^v(\bar{t}) - \Lambda_{se,i}^v(\bar{t}) \tag{4.7}$$

$$\ddot{\zeta}_i^\theta(\bar{t}) + 2\overline{\xi}_i^\theta\overline{\omega}_i^\theta\dot{\zeta}_i^\theta(\bar{t}) + \overline{\omega}_i^{\theta\,2}\zeta_i^\theta(\bar{t}) = \frac{1}{\varrho_t^2}\left(\Lambda_{b,i}^\theta(\bar{t}) + \Lambda_{se,i}^\theta(\bar{t})\right) \tag{4.8}$$

where $\varrho_t^2 = I_m/(mb^2)$, I_m being the combined mass polar moment of inertia per unit length of girder and cables, $\overline{\xi}_i^v$ and $\overline{\xi}_i^\theta$ are modal damping ratios, while $\Lambda_{b,i}^v$, $\Lambda_{b,i}^\theta$, $\Lambda_{se,i}^v$ and $\Lambda_{se,i}^\theta$ are the i-th vertical and torsional modal components of buffeting and self-excited wind loads, respectively, whose expressions are reported in Appendix A.1 for the sake of brevity.

After straightforward computations, Eqs. (4.7,4.8) are grouped and rendered in first order form as follows:

$$\dot{\mathbf{x}}(\bar{t}) = \mathbf{A}(\overline{U})\mathbf{x}(\bar{t}) + \mathbf{B}\mathbf{\Lambda}(\bar{t}) \tag{4.9}$$

where $\mathbf{x}(\bar{t}) = [\mathbf{q}(\bar{t})\ \dot{\mathbf{q}}(\bar{t})\ \mathbf{z}(\bar{t})]^T$ is the state vector, $\mathbf{A}(\overline{U})$ is the aeroelastic system matrix, containing inertial, damping and stiffness terms, including aeroelastic contributions to these quantities, $\mathbf{\Lambda}(\bar{t})$ is the buffeting wind loading vector, and $\mathbf{B}$ is the collocation matrix. Vectors $\mathbf{q}(\bar{t})$, $\mathbf{z}(\bar{t})$ and $\mathbf{\Lambda}(\bar{t})$ are defined as:

$$\begin{aligned}
&\mathbf{q}(\bar{t}) = [\zeta_1^v(\bar{t})\ \zeta_2^v(\bar{t})\ \ldots\ \zeta_n^v(\bar{t})\ \zeta_1^\theta(\bar{t})\ \zeta_2^\theta(\bar{t})\ \ldots\ \zeta_n^\theta(\bar{t})]^T\\
&\mathbf{z}(\bar{t}) = [\mathbf{z}^{Lv}(\bar{t})\ \mathbf{z}^{L\theta}(\bar{t})\ \mathbf{z}^{M\theta}(\bar{t})\ \mathbf{z}^{Mv}(\bar{t})]^T\\
&\mathbf{\Lambda}(\bar{t}) = [-\Lambda_{b,1}^v(\bar{t})\ -\Lambda_{b,2}^v(\bar{t})\ \ldots\ -\Lambda_{b,n}^v(\bar{t})\ \frac{\Lambda_{b,1}^\theta(\bar{t})}{\varrho_t^2}\ \frac{\Lambda_{b,2}^\theta(\bar{t})}{\varrho_t^2}\ \ldots\ \frac{\Lambda_{b,n}^\theta(\bar{t})}{\varrho_t^2}]^T
\end{aligned} \tag{4.10}$$

where n is the number of vertical and torsional modes retained in the model and $\mathbf{z}^{Rr}(\bar{t})$ $(R = L, M,\ r = v, \theta)$ are vectors containing additional aerodynamic state variables related to self-excited loads, whose expressions are reported in A.1.

Eq. (4.9) governs the multimodal aeroelastic vibration of damaged suspension bridges under wind action. It is especially noteworthy that the aeroelastic system matrix, $\mathbf{A}(\overline{U})$, and, consequently, the modal properties of the system, depend upon both damage characteristics and wind speed.

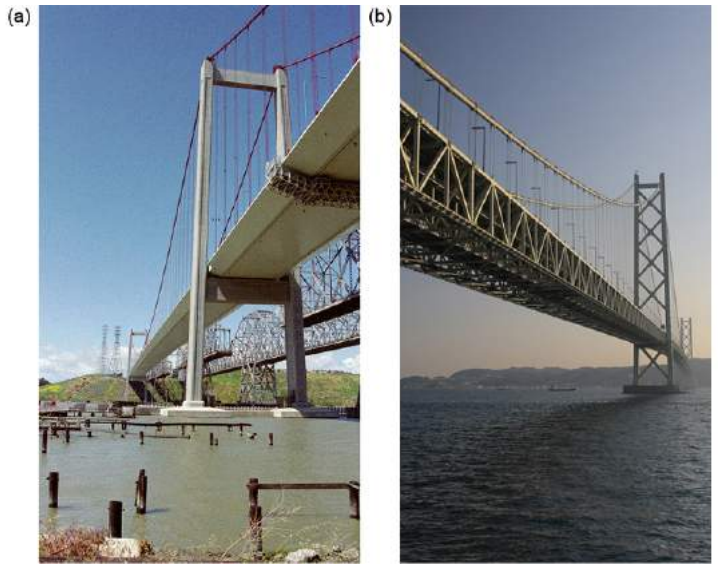

Figure 4.6: Photo of the New Carquinez Bridge (a) and of the Akashi Akaikyo Bridge (b).

4.2 Wind effects on eigenfrequencies

This section is devoted to evaluating apparent variations in modal frequencies induced by wind action. The evaluation and quantification of such effects are obtained by specializing the previously introduced continuum model of suspension bridge with the geometrical and aerodynamic characteristics of two bridges with completely different behavior under wind action: the New Carquinez Bridge (USA) and the Akashi Kaikyo Bridge (J), (Fig. 4.6).

In order to investigate apparent changes in natural frequencies due to changes in incoming wind speed, U, the eigenvalue problem of the aeroelastic system, readily obtained from Eq. (4.9), is solved for U varying from 0 to 20 m/s and the corresponding natural frequencies are extracted from the complex eigenvalues of matrix $\mathbf{A}(\overline{U})$.

The results concerning the first three symmetric and antisymmetric, vertical and torsional, modes are presented in terms of ratios between apparent natural frequencies (those obtained for $U > 0$) and structural ones (those obtained for $U = 0$).

The hereafter, the following notation will be adopted to indicate the modes:

Table 4.1: Main geometrical and aerodynamic characteristics adopted in the parametric analysis and rapresentative of the NCB.

Parameter	Value	Parameter	Value	Parameter	Value
L[m]	728	a_1^{Lv}	0.630	b_1^{Lv}	0.425
B[m]	25.6	$a_1^{L\theta}$	2.0594	$b_1^{L\theta}$	0.0796
c_L	0.12	a_1^{Mv}	2.0420	b_1^{Mv}	0.0943
c_D	0.14	$a_1^{M\theta}$	1.7863	$b_1^{M\theta}$	12.4768
c_M	0.02	c'_L	5.0	c'_M	0.9740

V stands for vertical, T for torsional, A and S stand for antysimmetric and symmetric, respectively, while the number denotes the order of the mode.

4.2.1 New Carquinez Bridge

The first considered case of study is representative of the New Carquinez Bridge (NCB), USA, in terms of geometry, mechanical properties and aerodynamic characteristics of the deck. Geometrical and mechanical details on this bridge can be found in [87, 91].

The NCB is characterized by a streamlined box type cross section and can be considered as moderately sensitive to wind action. Aerodynamic and aeroelastic parameters used for specializing the analytical model to this bridge are summarized in Table 4.1, where, as reported in A.1, c_L, c_D, c_M represent lift, drag and moment aerodynamic coefficients of the deck, c'_L and c'_M are first derivatives of c_L and c_M with respect to wind angle of attack, while a_i^{Rr} and b_i^{Rr} ($R = L, M$, $r = v, \theta$) are indicial function coefficients. The natural frequencies of the bridge obtained from the eigenproblem solution of the analytical model are summarized in Table 4.2. Modal damping ratios of 0.5% are assumed in all 12 modes retained in the analytical model.

As it can be observed from these results, relative variations in the most sensitive frequency are the order of about 0.1% under a variation of 1m/s in wind speed. Such variations are comparatively more significant in vertical modes than in torsional ones and tend to decrease in higher order modes in both cases.

Table 4.2: Values of the natural frequencies of the NCB evaluated by the analytical model of the bridge.

	Symmetric		Antisymmetric	
	vertical[Hz]	torsional[Hz]	vertical[Hz]	torsional[Hz]
1	0.198	0.538	0.134	0.698
2	0.307	1.057	0.313	1.395
3	0.436	1.746	0.566	2.093

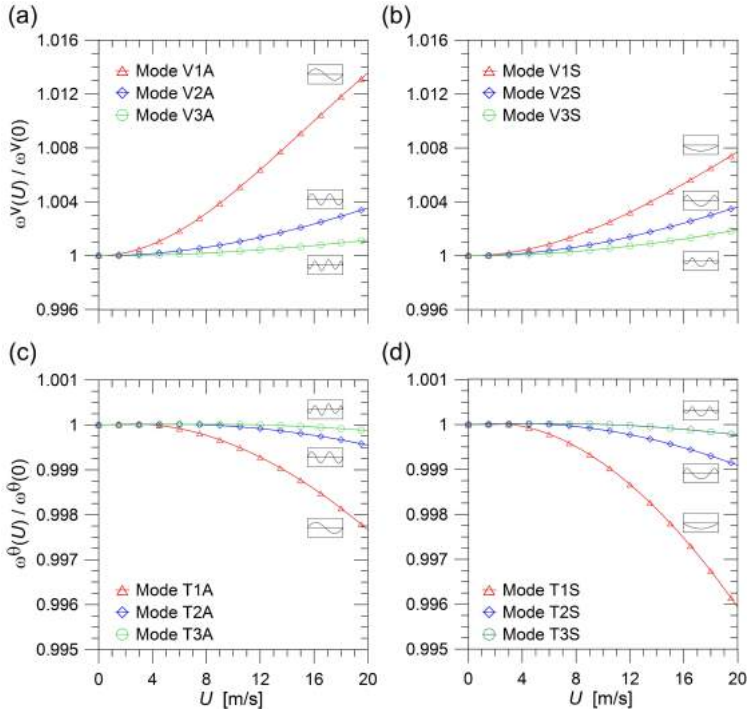

Figure 4.7: Frequency ratios of vertical and torsional modes for varying mean wind speed of the NCB: first three antisymmetric (a) and symmetric (b) vertical modes and first three antisymmetric (c) and symmetric (d) torsional modes.

Table 4.3: Main geometrical and aerodynamic characteristics adopted in the parametric analysis and rapresentative of the AKB.

Parameter	Value	Parameter	Value	Parameter	Value
L[m]	1991	a_1^{Lv}	$[-0.365\ -11.652]$	b_1^{Lv}	[0.021 7.235]
B[m]	35.5	$a_1^{L\theta}$	$[-0.392\ -3.653]$	$b_1^{L\theta}$	[0.021 1.155]
c_L	0.02465	a_1^{Mv}	0.039	b_1^{Mv}	0.000
c_D	0.42050	$a_1^{M\theta}$	[0.0730 1.758]	$b_1^{M\theta}$	[0.025 7.098]
c_M	0.01317	c'_L	1.19175	c'_M	0.30653

Table 4.4: Values of the natural frequencies of the AKB evaluated by the analytical model of the bridge.

	Symmetric		Antisymmetric	
	vertical[Hz]	torsional[Hz]	vertical[Hz]	torsional[Hz]
1	0.113	0.173	0.080	0.137
2	0.170	0.230	0.170	0.274
3	0.226	0.345	0.279	0.411

4.2.2 Akashi Kaikyo Bridge

With the purpose of facing a completely different behavior of the bridge under wind action a second case of study is considered by specializing the analitic model of the bridge with the geometry, mechanical properties and aerodynamic characteristics of the Akashi Kaikyo Bridge, (AKB).

The AKB is the longest suspension bridge in the world and links the city of Kobe to Iwaya on Awaji Island, in Japan. It is characterized by a truss type stiffned cross section and it can be considered rigid under an aerodynamical point of view. Geometrical and mechanical details on this bridge can be found in [92] while the aerodynamic and aeroelastic parameters used for specializing the analytical model to this bridge are summarized in Table 4.3 where it is worth noting that we have two coefficients a_i^{Rr} and b_i^{Rr} $(R = L, M,\ r = v, \theta)$ because the approximation of the indicial funcions is obtained in this case by adopting two exponential groups. As in the previous subsection Tab. 4.4 summarize frequencies of the first twelve modes of the AKB obtained from the eigenproblem solution of the analytical model.

The obtained results, depicted in Fig. 4.8, show as expected, a completely

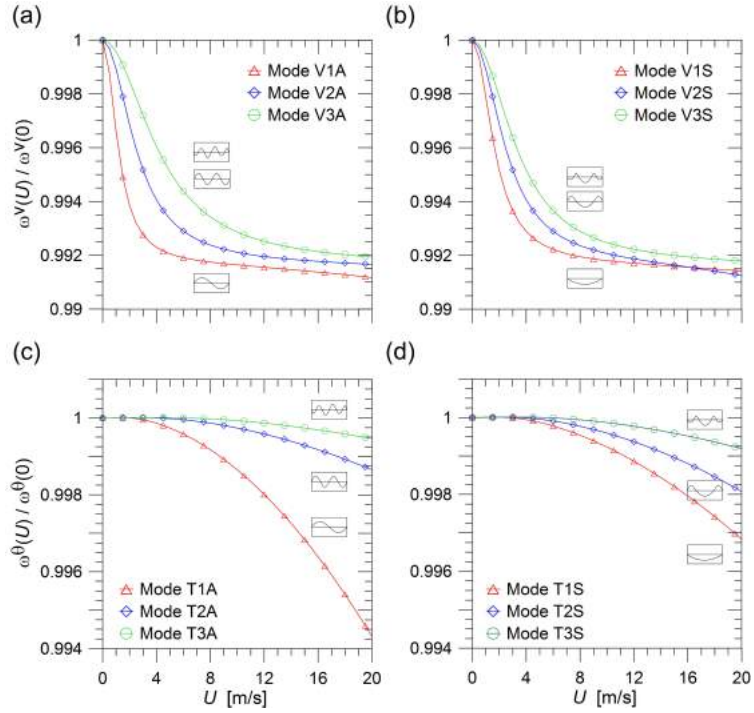

Figure 4.8: Frequency ratios of vertical and torsional modes for varying mean wind speed of the AKB: first three antisymmetric (a) and symmetric (b) vertical modes and first three antisymmetric (c) and symmetric (d) torsional modes.

different behavior compared with the NCB. First of all, despite the maximum apparent variations of the modal frequencies are more or less of the same order of those obtained in the previous case, the sensitivity to wind action of the AKB seems to be more relevant for lower values of the incoming wind speed, those from 0 to 8m/s to be more precise. In this range relative variations in the most sensitive frequency are the order of about 0.2% under a variation of 1m/s in wind speed, while for higher values such variations stabilize. Similarly to the case of the NCB, also in the AKB the vertical modes are more sensitive to wind action even if the differences with the torsional ones are less marked. However, unlike the NCB, the AKB exhibit a more marked non linear relationship among the frequencies. Fig. 4.9, for instance, elucidates this diffent behavior by plotting at each different value of $U \in [0 \div 20\text{m/s}]$, the first vertical antisymmetric frequency versus the first torsional antisymmetric one for both the NCB (Fig. 4.9(a))and AKB (Fig. 4.9(b)).

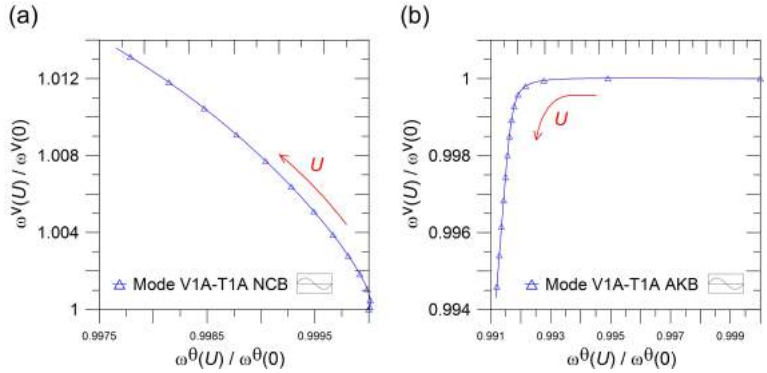

Figure 4.9: Plot of the trend between the first antinsymmetric vertical frequency ratio and the first antisymmetric torsional one for the NCB (a) and the AKB (b).

4.3 Temperature effects on eigenfrequencies

The effects induced on modal frequencies by variations of temperature are also evaluated through a deterministic analysis: the eigenvalue problem of the aeroelastic system, Eq. 4.9, is solved for increasing the value of the variation of temperature ΔT between -30 and 30 ^{o}C, as previously done for evaluating the effects on *tension loss* and *sag augmentation factors*. Throughout these two parameters, as already described in 4.1.1, the thermal effects are accounted for in the continuum model of the suspension bridge.

In order to separately evaluate the effects due to temperature variation ΔT on bridge modal frequencies, the following presented results are obtained in absence of damage and for changing ΔT only from the reference state as defined in 4.1.1. Fig.s 4.10 and 4.11 show for the NCB and AKB, respectively, the trend of the frequency ratios here defined similarly to what was previously stated in Fig. 4.2, as the ratio between apparent natural frequencies obtained for $\Delta T \neq 0$ and structural ones (those obtained for $\Delta T = 0$). First of all, it can be easily observed for both bridges a similar linear trend between frequencies and temperature variation which can be considered realistic in most cases especially given that, in the present model, only thermal effects on the main cables are accounted for, disregarding any kind of global or local effects of temperature on deck sections. This last assumption leads to changes in modal frequencies induced by temperature variation smaller than what can be generally observed in real cases (see for instance [39]). However, such simplification can be considered satisfactory and realistic in the present implementation producing variations in modal frequencies at least comparable with those induced by wind

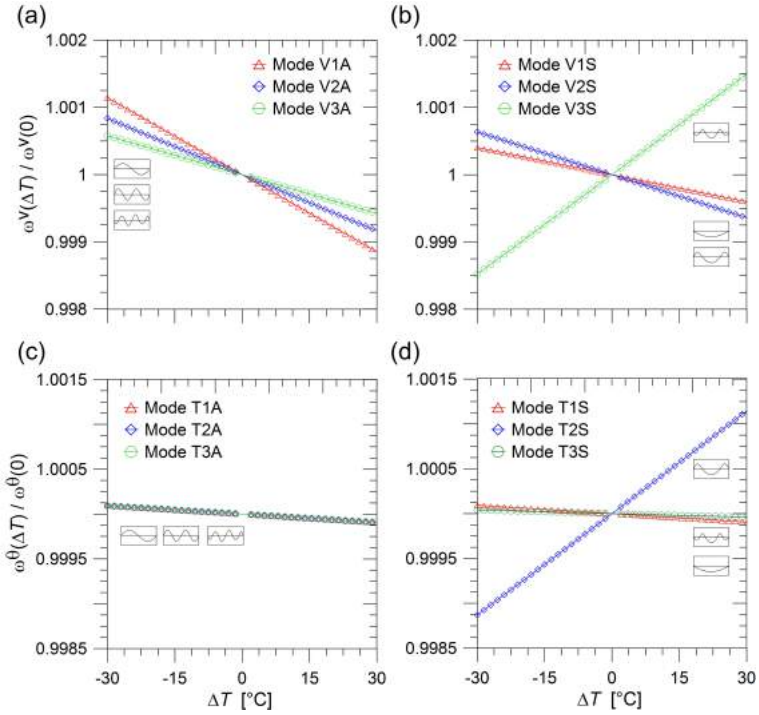

Figure 4.10: Frequency ratios of vertical and torsional modes of the NCB for increasing the temperature variation ΔT: first three antisymmetric (a) and symmetric (b) vertical modes and first three antisymmetric (c) and symmetric (d) torsional modes.

action (Fig.s 4.7 and 4.8) and always bigger than those induced by damage occurrence in the main cable (see the following Sec. 4.4). Moreover considering thermal effects on main cables of suspension bridge perfectly suits with the final aim of the present application where multivariate statistical analysis will be adopted with the purpose of identifying damage occurrence in one main cable indeed.

The trend of the frequency ratios of vertical modes for both the NCB and AKB reveals a similar behavior coherently to what has been stated in the preceding general dissertation in Sec. 4.1.1, pointing out, however, a clearly higher sensitivity of the AKB to ΔT. The variation of the most sensitive vertical modal freqency is around 0.05% under a variation of 1 ^{o}C. Similar observations can be done regarding the torsional modes which are however less sensitive to temperature variation with the exception of the modes T2S for the NCB and T1S for the AKB. Moreover, in the case of torsional modes analysis it is interesting to notice how the third torsional simmetric mode has an opposite trend for the NCB and the AKB. This is probably due to the different values

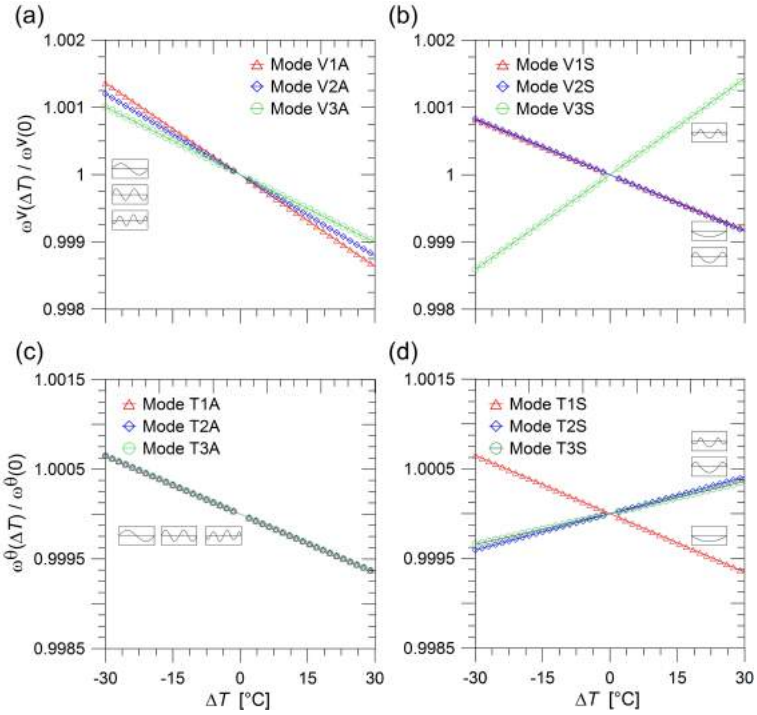

Figure 4.11: Frequency ratios of vertical and torsional modes of the AKB for increasing the temperature variation ΔT: first three antisymmetric (a) and symmetric (b) vertical modes and first three antisymmetric (c) and symmetric (d) torsional modes.

of the Irvine's parameter λ^2 for the two bridges.

4.4 Damage effects on eigenfrequencies

An analysis similar to that presented in previous Sections, is also carried out to evaluate main cable damage effects on natural frequencies. In this way, a direct comparison with wind and thermal effects is possible.

As sketched in the previous Sec. 4.1 and described more in details in [88], main cable damage in the analytical model is completely described by its intensity factor, η, its extension factor δ and its position factor, γ, Eq.s 4.1. Natural frequencies are almost not influenced by damage position [88], which practically impedes damage localization. For this reason, in the presented analysis a fixed damage position is considered corresponding to the proximity to one support

($\gamma = \delta/2$). This, in fact, is a region where local bending stresses develop and increase the risk of wire fatigue ruptures [93].

In the carried analysis, the case $\delta = 0.05$, corresponding to a damage extension equal to 5% of the total cable span, is considered, at first, and η is varied from 0 to 0.2, corresponding to a cross section reduction in one main cable ranging from 0 to a remarkable 20%. Then, the analysis is repeated for $\eta = 0.05$ and δ varying from 0 to 0.1. These two different simulations are adopted to underline as much different aspects of damage occurrence in the main cable of suspension bridge. The former is carried out to stress the potential effects induce by a local failure in which many wires break down in a limited area, due for instance by an impulsive high tensile stress in the cable. The latter is more focused on the evaluation somehow of the effects induced by the recovery length in the cable for a fixed damage severity or, under another point of view, of the effects induced by a diffused damage due for instance to a diffused corrosion process in the cable.

Figs. 4.12-4.15 show the results of the parametric analysis in terms of ratios between damaged and undamaged frequencies for varying both the *damage intensity facor* η and the *damage extention facor* δ. As it can be observed from these results, damage-induced frequency variations are comparatively more significant in symmetric modes than in antisymmetric ones both in the NCB and in the AKB even if the former reveals a slightly higher sensitivity to damage. Moreover, in confirmation of what previously stated, η seems to be the most relevant damage parameter producing the most marked effect in modal properties. The trend of frequency ratios for varying both η and δ is almost linear and, in any case, the most sensitive modes are the second symmetric vertical and the first symmetric torsional ones, exhibiting frequency variations of about 0.3% in the NCB and 0.1% in the AKB for the maximum considered damage level. Changes in frequencies of other modes, especially of the torsional antisymmetric ones, are so small that they essentially lose any practical interest.

The comparison between wind and damage effects highlights that small variations in wind speed produce apparent changes in frequencies that can likely be more significant than those produced by a small damage. Furthermore, variations of natural frequencies with wind speed are seen to be non-linear, especially in the case of the AKB, which is a challenge for removing wind effects from identified frequency data using the procedure described in Chap. 3. Analysis results also show that frequencies are affected by damage intensity and extension in quantitatively similar ways. This implies that damage quantification is not possible using frequencies as damage sensitive features, because the same frequency shifts could be caused by different damages characterized by the same value of the product $\eta\delta$.

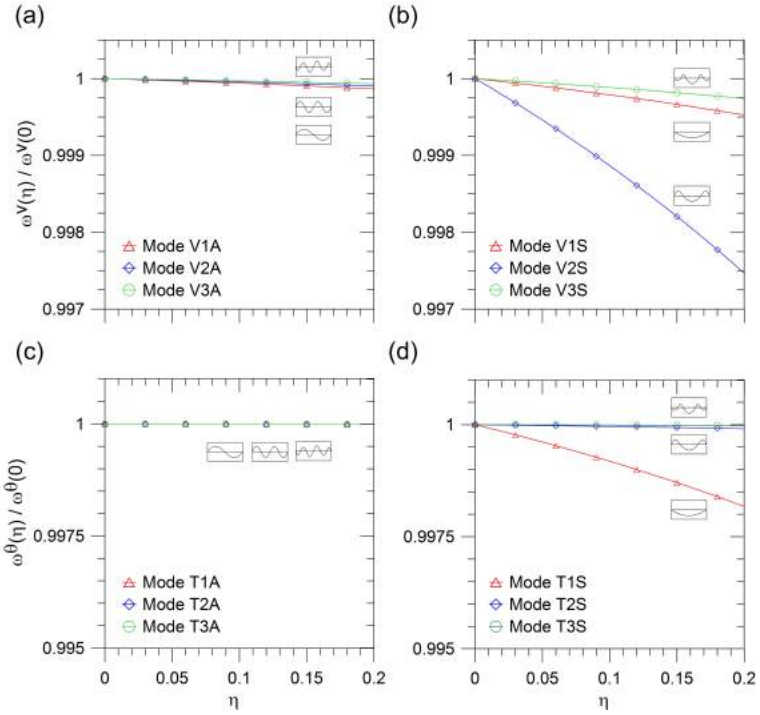

Figure 4.12: Frequency ratios of vertical and torsional modes of the NCB for varying damage intensity η ($\delta = 0.05$ and $\gamma = \delta/2$): first three antisymmetric (a) and symmetric (b) vertical modes and first three antisymmetric (c) and symmetric (d) torsional modes.

4.5 Damage detection

After the description of the analytical model and the first preliminary results concerning the evaluation of the effects induced on modal frequencies by wind temperature and damage, in the present section the multivariate statistical techniques described in the previous Chaps. 2 and 3 are finally applied to NCB and AKB continuous responses simulated under real wind and temperature time histories loading. Some details on the response simulation are produced at first, focusing the attention on the hypothesized sensors layout and on the wind and temperature data adopted for generating the bridge response. Later on, after the introduction of the artificial damage to the identified bridge frequency time histories, the capability in its detection is performed by adopting both classic regressive model and PCA-based techniques. Finally some observations on the obtained results are drawn, pointing out values and drawbacks in the

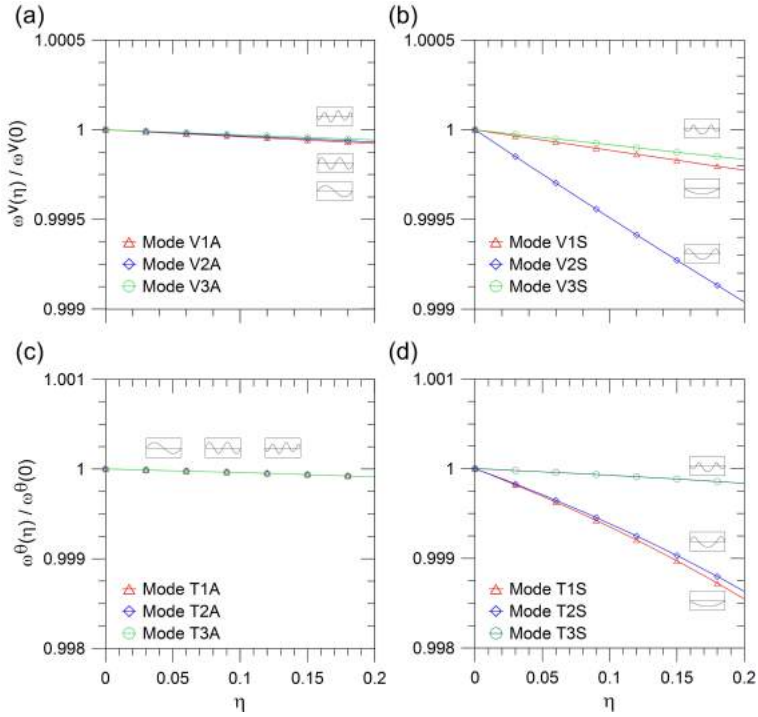

Figure 4.13: Frequency ratios of vertical and torsional modes of the AKB for varying damage intensity η ($\delta = 0.05$ and $\gamma = \delta/2$): first three antisymmetric (a) and symmetric (b) vertical modes and first three antisymmetric (c) and symmetric (d) torsional modes.

application of each technique.

4.5.1 Continuous response simulation and analysis

Aeroelastic dynamic response of the NCB and AKB under turbulent wind action, and changing temperature ΔT, is simulated for a total duration of 515 consecutive days. Modal identification is carried out by considering the vertical acceleration response of the bridge generated in 20 points along the main span. These points, whose spatial layout is shown in Figs. 4.16 and 4.17 for NCB and AKB respectively, ideally represent the locations of the sensors of a permanent monitoring system installed on the considered bridges. The sensors are located in such a way to measure vertical and torsional responses in 10 equidistant cross sections of the girder, thus permitting to identify both vertical and torsional modes.

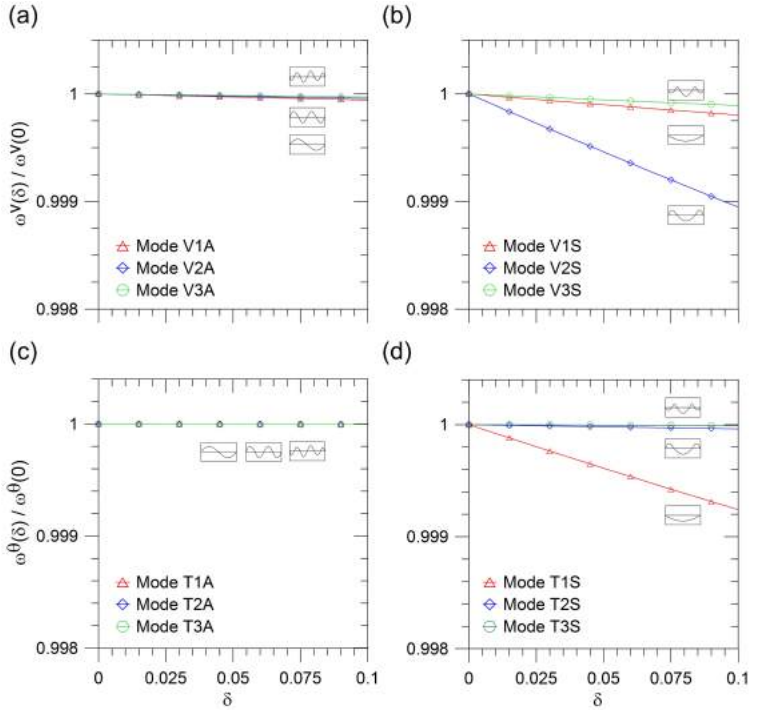

Figure 4.14: Frequency ratios of vertical and torsional modesof the NCB for varying damage extension δ ($\eta = 0.05$ and $\gamma = \delta/2$): first three antisymmetric (a) and symmetric (b) vertical modes and first three antisymmetric (c) and symmetric (d) torsional modes.

The generation of the wind-excited response of the bridges is carried out with a time step of 0.05 sec. Consecutive one-hour-long time histories of structural responses are generated by time integration of Eq. 4.9, modeling vertical and horizontal turbolent wind velocities as multivariate zero-mean Gaussian stochastic processes (Subsec. 4.1.2), with stationary characteristics within each one-hour-long time window. Generation of turbulent wind components and, particularly, of quantities defined in Eqs. A.5, A.6 in Appendix A.1, is carried out by means of the continuous representation of the wind field based on so-called *wind modes* [94], as described in [87].

One-hour mean wind speed data used in the simulation are obtained from a real wind time history downloaded from National Data Buoy Center for an open sea site at 10 m elevation. Particularly, the overall 10-minutes mean wind speed historical data collected in 2005 and 2006 for station no. 46026, LLNR 357, are selected, hourly down-sampled and converted to the site and elevation of the NCB and AKB, by using the classic logarithmic law for the wind profile, assuming a boundary layer height of 300 m. Similarly, the temperature data are

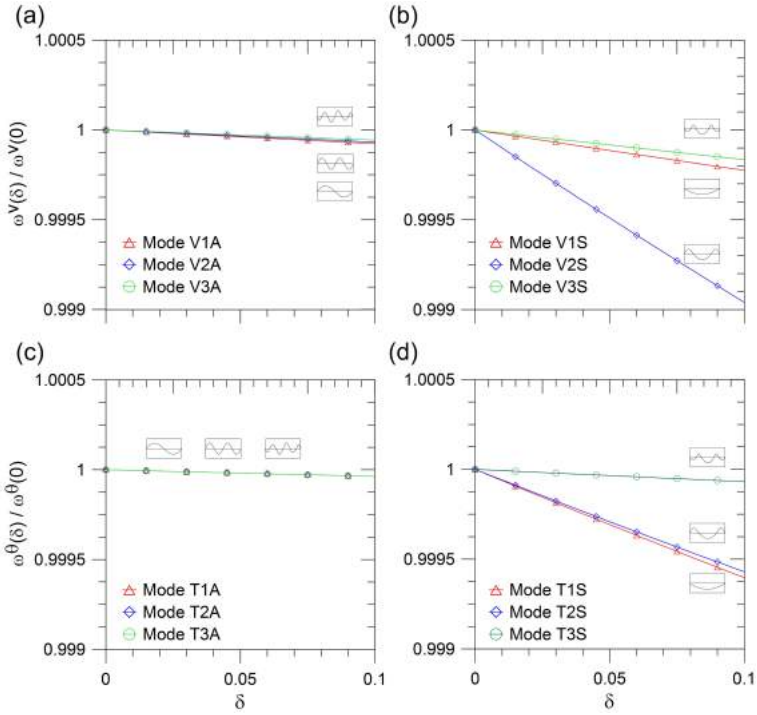

Figure 4.15: Frequency ratios of vertical and torsional modes of the AKB for varying damage extension δ ($\eta = 0.05$ and $\gamma = \delta/2$): first three antisymmetric (a) and symmetric (b) vertical modes and first three antisymmetric (c) and symmetric (d) torsional modes.

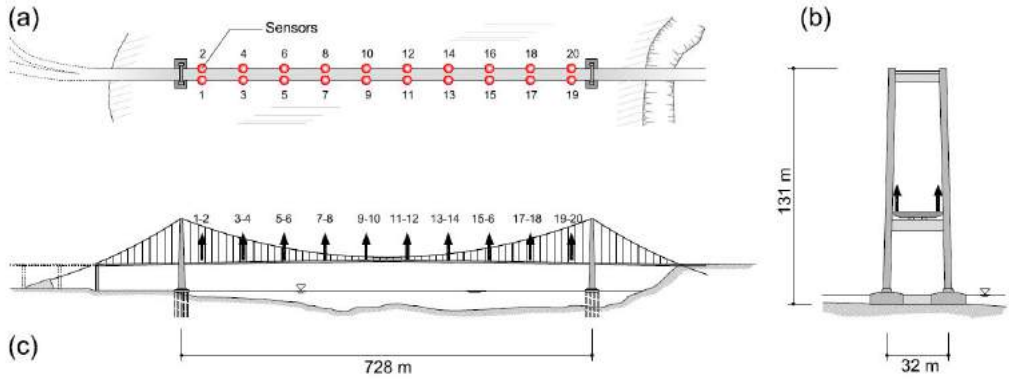

Figure 4.16: Case study bridge (NCB) with ideal sensors' layout: plan (a), cross section (b) and elevation (c).

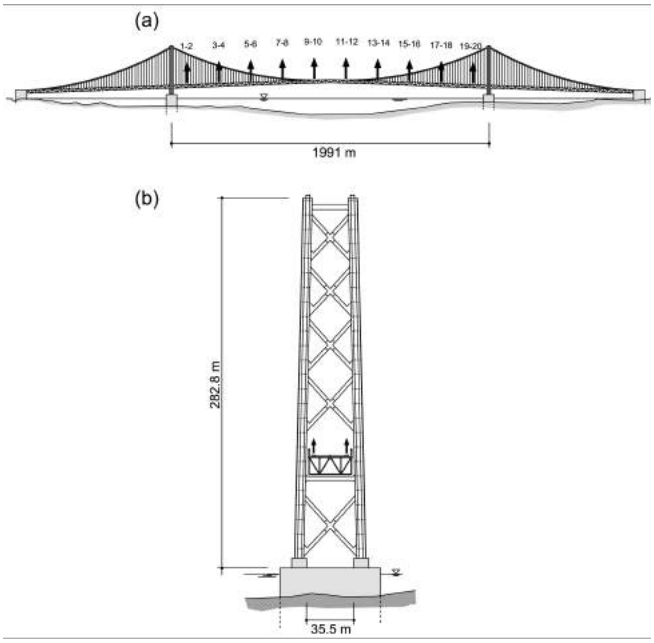

Figure 4.17: Case study bridge (AKB) with ideal sensors' layout: cross section (a) and elevation (b).

downloaded from station FTPC1-9414290, an on-shore meteorological station owned and maintained by NOAA's National Ocean Service, closer to the site of the NCB. The yearly averages of the overall hourly-sampled temperature historical data, acquired and collected in 2007 and 2008, are calculated and the variation of temperature ΔT adopted for the simulations are then estimated. For example, one year of the considered temperature and wind time histories are reported in Figs. 4.19 and 4.20 respectively, where not only the seasonal but also the daily fluctuation of such variables are clearly visible (as highlighted in the detailed view). Moreover in Fig. 4.20 (b), the histogram of mean wind speed data, computed in a period of one year to consider the seasonal periodicity of wind speed, is presented , also showing the optimally fitting Weibull probability distribution function whose characteristic parameters are $a = 7.25$ m/s (scale parameter) and $b = 1.89$ (shape parameter). It is finally necessary to state that for the purpose of generating continuous bridge acceleration time histories, the similar climatic, geographical and morphological configurations of NCB and AKB sites (see for instance Fig. 4.18), have led to reasonably adopt the same wind and temperature time histories for both bridges.

Generated turbulent wind field is based on the use of analytical spectral representation and coherence function reported in [94]. Accordingly, the autospectra, $S_{uu}(\omega)$ and $S_{ww}(\omega)$, of along-wind and across-wind turbulence components,

Figure 4.18: Geographic position of NCB and AKB.

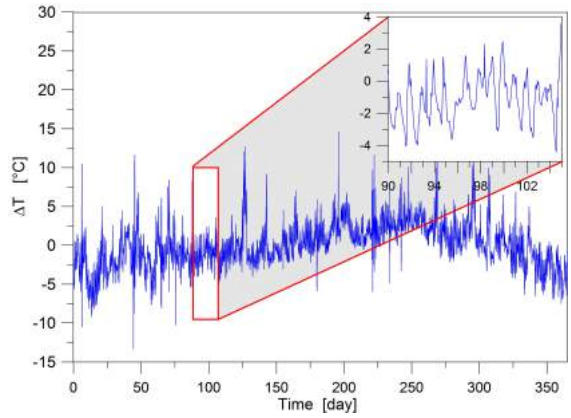

Figure 4.19: Time history of variation of temperature ΔT data adopted for the continuous response simulation of the suspension bridge model.

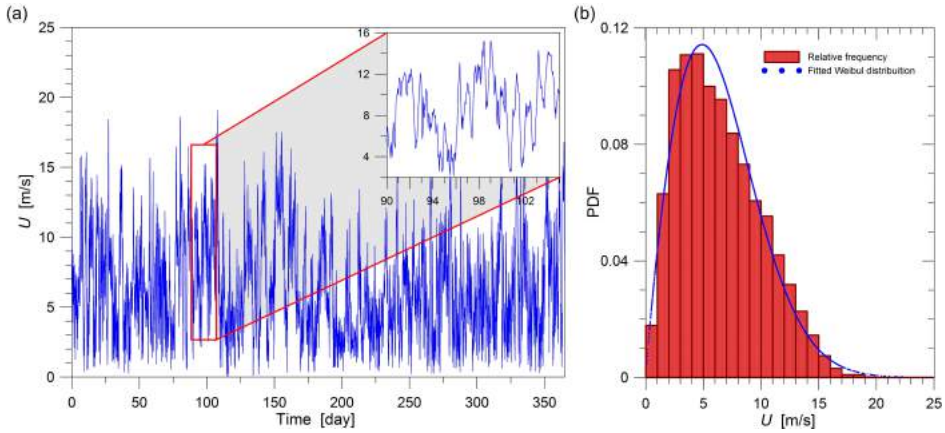

Figure 4.20: Time history of mean wind speed data used for bridge response simulation (a), histogram of the data with optimally fitting Weibull probability density function (PDF) (b).

respectively, are defined as:

$$\begin{aligned} S_{uu}(\omega) &= \frac{6.868\sigma_u^2 L_u/U}{(1+1.5\cdot 6.868\omega/(2\pi)L_u/U)^{5/3}} \\ S_{ww}(\omega) &= \frac{6.103\sigma_w^2 L_w/U}{(1+1.5\cdot 6.103\omega/(2\pi)L_w/U)^{5/3}} \end{aligned} \tag{4.11}$$

where σ_u^2 and σ_w^2 are variances of $u(x,t)$ and $w(x,t)$, respectively, while L_u and L_w are their integral length scales. These quantities are calculated according to the model presented in [95] as follows:

$$\begin{aligned} L_u &= 300\left(\frac{z}{200}\right)^{0.67+0.05\ln(z_0)} \\ L_w &= 0.1L_u \\ \sigma_u^2 &= (6-1.1\tan^{-1}(\ln(z_0)+1.75))\frac{U^2}{(2.5\ln(z/z_0))^2} \\ \sigma_w^2 &= 0.25\sigma_u^2 \end{aligned} \tag{4.12}$$

where z_0 is the roughness length (here assumed equal to 0.015 m for a coastal environment), z is the elevation of the deck (here assumed equal to 40 m) and all quantities are expressed using SI units. Coeherence function between along-wind turbulence components in two different points located at x and x' along the bridge deck is modeled through the classic exponential form

$$\mathrm{Coh}_u(x,x',\omega) = \exp\left(-\frac{|\omega|C_u|x-x'|}{2\pi U}\right) \tag{4.13}$$

where C_u is a coefficient assumed equal to 3. An analogous expression to Eq. 4.13 is adopted for the coherence of across-wind turbulence components using a coefficient $C_w = 6.5$. Along-wind and across-wind turbulence components, $u(x,t)$ and $w(x,t)$, are assumed to be statistically uncorrelated.

Once the continuous response of the two bridges has been generated the automated frequency tracking technique described in Chap. 3 is applied for the purpose of both identifying the modal properties (with particular reference to frequencies), and replacing the missing values of such quantities. In particular, the obtained time histories of identified modal frequencies highlight wind and temperature-induced fluctuations, with superimposed random errors associated with the inherent approximations in output only modal identification. As an example, the time histories of the first antisymmetric vertical modal frequency (V1A) for both the NCB and the AKB, are depicted in Figs. 4.21 (a) and 4.22 (a), showing an oscillation around their nominal values, 0.134 Hz and 0.080 Hz respectively. Moreover, a more detailed view of the dependencies of the considered frequency time histories upon environmental factors is highlighted

in Figs. 4.21 (b),(c) and 4.22 (b),(c), where the correlations of such frequencies with wind speed U and variation of temperature ΔT respectively, are clearly visible especially in the case of the NCB where there is a more regular relationship between frequencies, wind and temperature as previously clarified in the deterministic analysis (Secs. 4.2 and 4.3).

Such clear relationships are further emphasized through a correlation analysis conducted with the purpose of quantifying the dependencies not only between frequencies and environmental factors, but also among frequencies themselves: because estimated modal properties are closely correlated with wind speed and temperature variation, they are also correlated with each other indeed. This last aspect is investigated in Figs. 4.23(a) and 4.24(a), for the NCB and the AKB respectively, showing the absolute values of the obtained correlation coefficients.

The results in the case of the NCB show that the correlation between frequencies tends to decrease in the higher modes rather regularly, essentially due to a decreasing correlation with wind speed, and is less marked in the torsional ones. A similar observation can not be made in regard to the AKB, where the overlapping of more complex relationships between frequencies and environmental factors (see for instance Sec. 4.2) leads to less regular dependencies among frequencies; anyway, it can be reasonably stated that, also in this case, the correlation is generally less marked in the higher modes, especially in the torsional ones.

Obviously, correlation between frequencies and environmental factors are also investigated and the achieved outcomes are properly presented in Figs. 4.23(b)(c)and 4.24(b)(c), where the correlation coefficient between frequencies and wind speed U (b) and between frequencies and variation of temperature ΔT (c) are depicted. Correlation analysis reveals how wind effects on frequencies may potentially play a more relevant role compared with those induced by variation of temperature, being the bridge natural frequencies more significantly correlated with mean wind speed rather than with temperature. Moreover, in confirmation of what has been previously stated in the deterministic analysis of the two bridges, it is easy to observe how different is the connection among frequencies, wind and temperature for NCB and AKB: it is worth noticing, for instance, that all the modal frequencies of the AKB are anti-correlated (and slightly more markedly too) with U unlike in the case of NCB. The different relationships established among the frequencies of the two bridges are further examined in Figs. 4.25 and 4.26 where, for the NCB and the AKB respectively, different modal frequency time histories are plotted versus the first antisymmetric vertical mode one, assumed as reference. This clear difference between NCB and AKB makes both bridges as very interesting cases for the application of the damage detection techniques illustrated in Chap. 2, potentially enabling

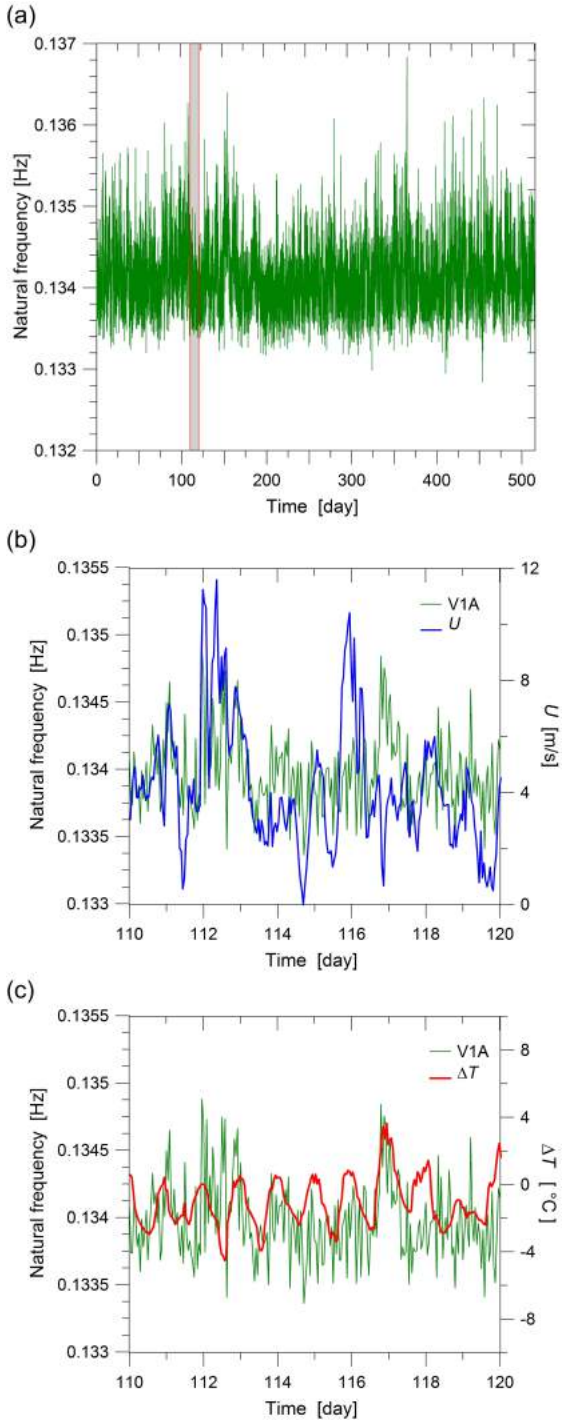

Figure 4.21: Time history of the V1A modal frequency identified from preudo-experimental bridge response data of the NCB (a) and detailed view highlighting correlation between frequency and wind speed U (b) and frequency and variation of temperature ΔT (c)

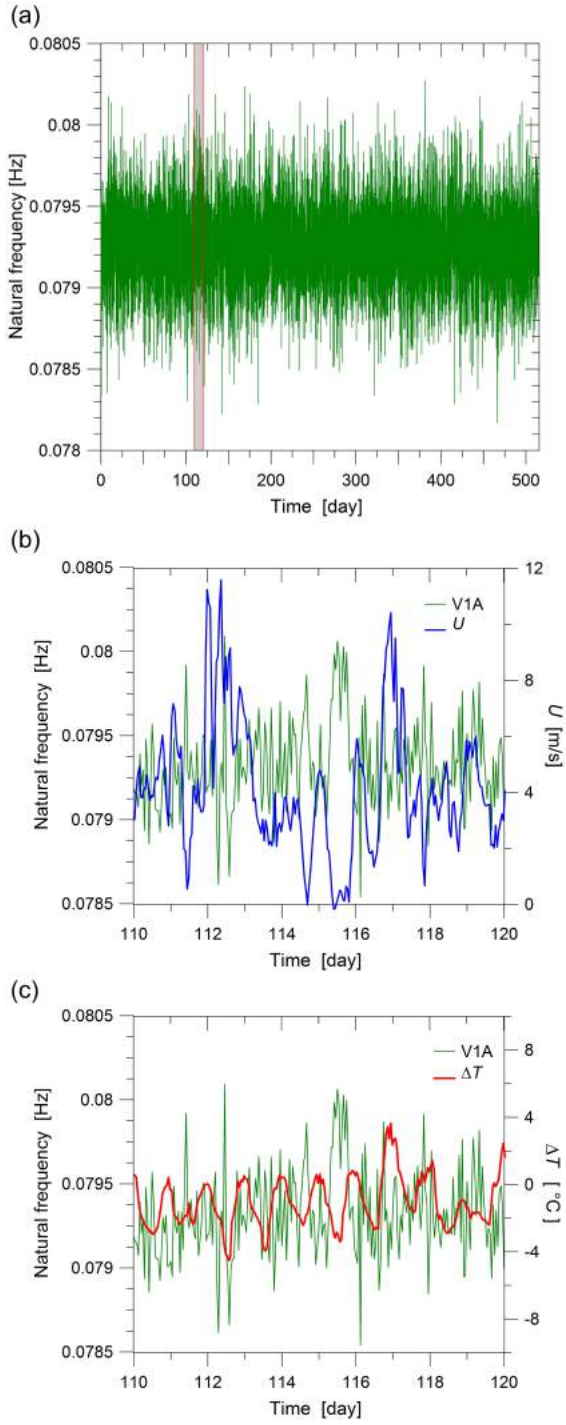

Figure 4.22: Time history of the V1A modal frequency identified from preudo-experimental bridge response data of the AKB (a) and detailed view highlighting correlation between frequency and wind speed U (b) and frequency and variation of temperature ΔT (c).

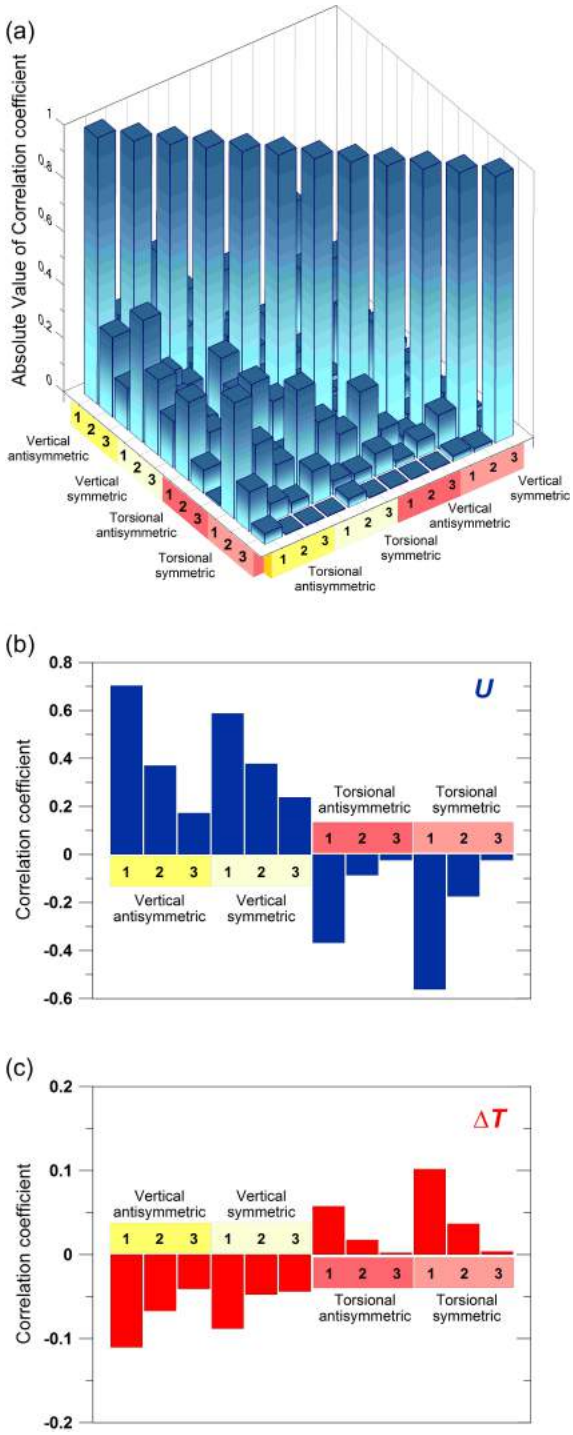

Figure 4.23: Correlation coefficients of identified frequencies between each other for the NCB(a), between frequencies and mean wind speed data U (b), and between frequencies and variation of temperature data ΔT (c).

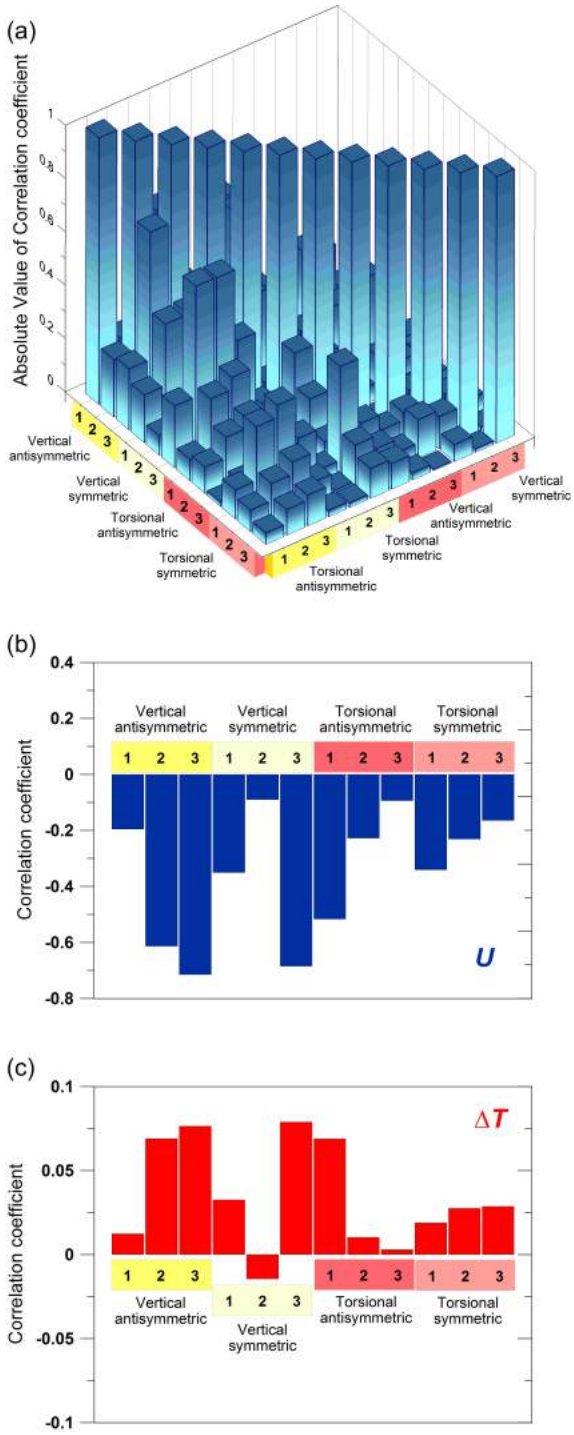

Figure 4.24: Correlation coefficients of identified frequencies between each other for the AKB (a), between frequencies and mean wind speed data U (b), and between frequencies and variation of temperature data ΔT (c).

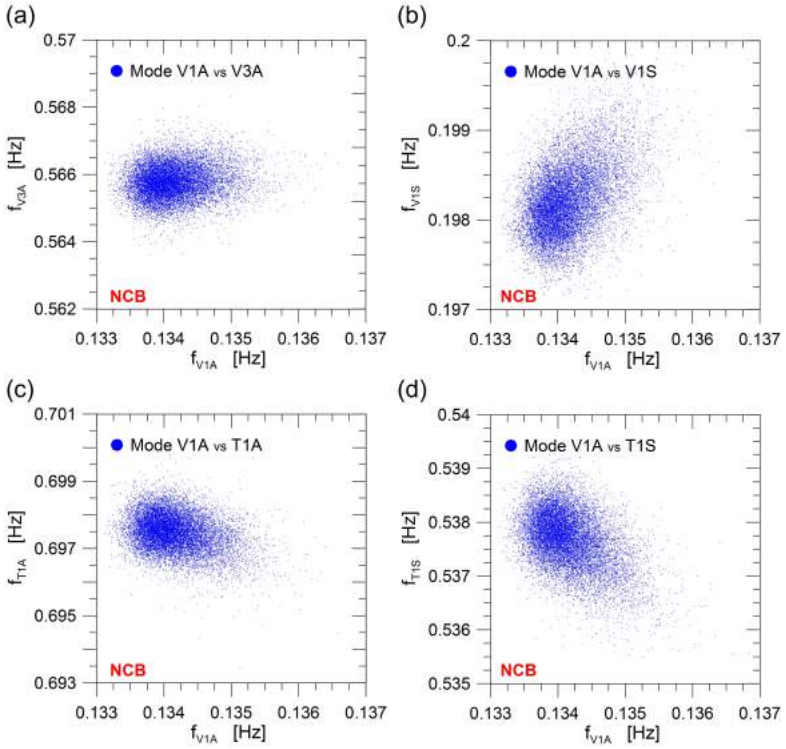

Figure 4.25: Plot of the third vertical antysimmetric (a), first vertical simmetric (b), first torsional antisymmetric (c) and first torsional simmetric (d) identified modal frequency time history of the NCB versus the first vertical antysimmetric one.

the recognition of weak points or limitation in their effectiveness.

Finally, the description of the strategy adopted for introducing artificial damage, is mandatory to be described with the purpose of later correctly reading the results of damage detection procedures. As easily deducible and explained in part in the previous Chapters of the thesis, damage occurrence in a structure is generally associated to a cross-section reduction of structural components consequence of crack formation producing a local (more rarely global), variation of the inertia properties of the structure; such variations can be generally read as changes in dynamic properties of the structure, among which modal frequencies are generally considered the most reliable to be estimated. For this reason, in the present work, these lasts are assumed as the quantities enabling damage detection and damage occurrence is simulated as an imposed frequency shift defined as in the following Eq. 4.14, applied to the identified frequency time histories:

$$\Delta f = \frac{fr_d - fr_u}{fr_u} \tag{4.14}$$

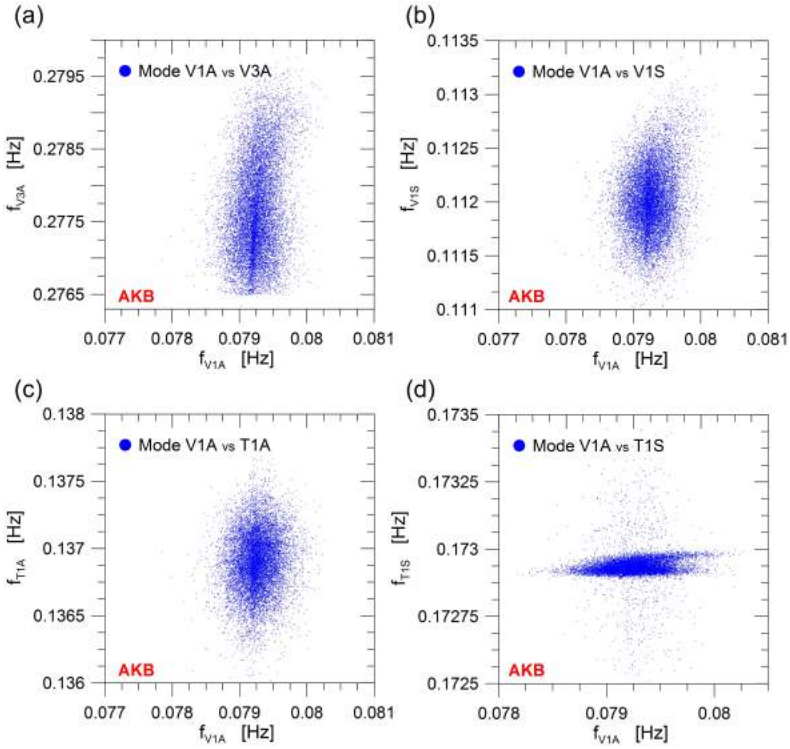

Figure 4.26: Plot of the third vertical antysimmetric (a), first vertical simmetric (b), first torsional antisymmetric (c) and first torsional simmetric (d) identified modal frequency time history of the AKB versus the first vertical antysimmetric one.

being fr_u and fr_d,the undamaged and damaged bridge frequencies estimated through the analytical model introduced in Sec.4.1. Frequency shift as just defined can be easily correlated to the frequency ratios defined earlier in the deterministic analysis for the evaluation of damage effects on structural frequencies. The application of artificial damage to identified frequency time histories produces variations which can not be detected by a simple visual inspection, making in such a way practically impossible the task of damage detection even in the case of a severe damage. For instance, in Fig.4.27 a remarkable damage characterized by $\eta = 0.10$ (extension $\delta = 0.05$ and position$\gamma = \delta/2$) is applied at day n^o 440 to the frequency time histories of both NCB and AKB: damage occurrence can not be recognized even in the detailed view of the time histories (Fig. 4.27 (c) and (d)). Unlike this approach, the application of multivariate statistical techniques can allow to clearly identify damages equal and even substantially smaller than what considered in the just presented example. For the purpose of estimating the actual effectiveness of the proposed procedure in detecting small damages the test in the following

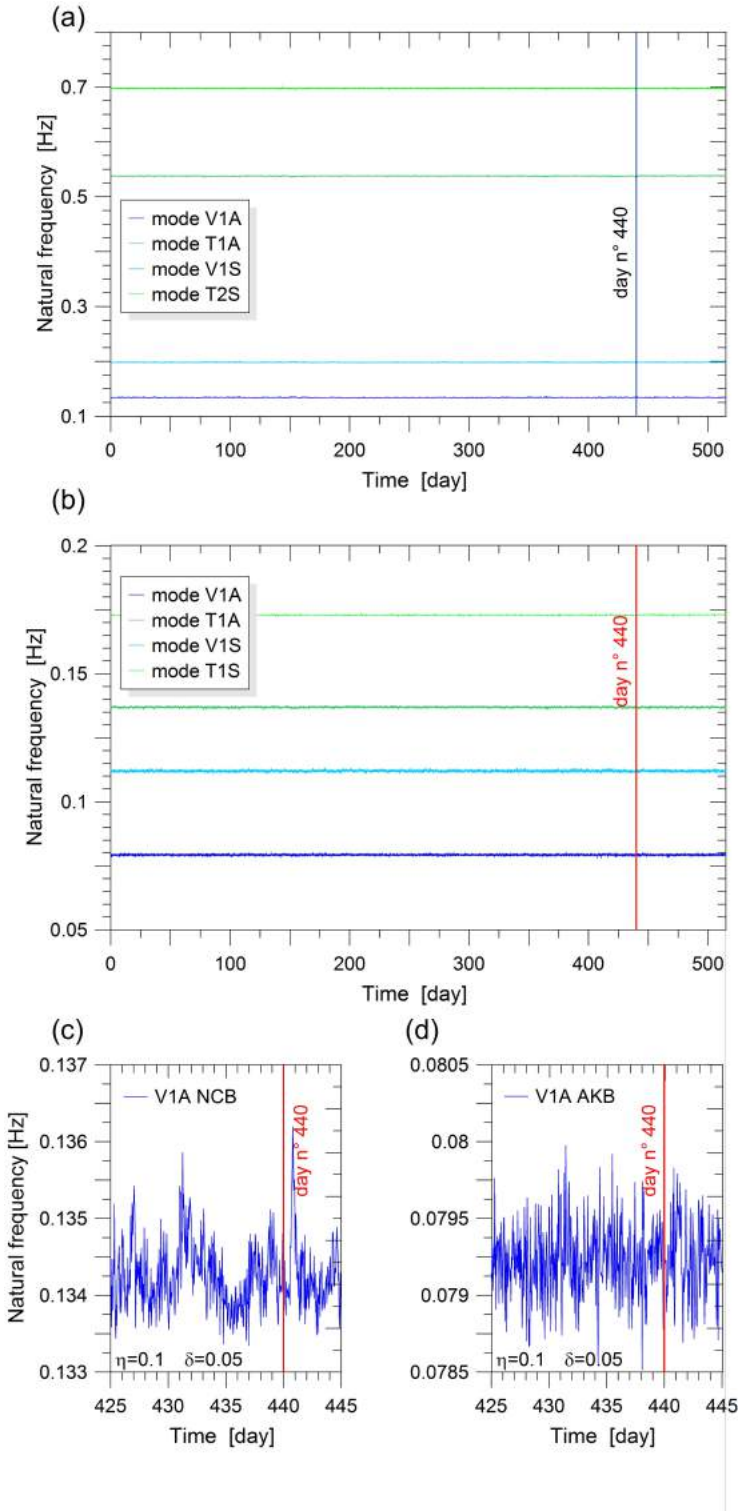

Figure 4.27: Identified frequency time histories with artificial damage addiction at day n^o 440 of the first simmetric and antisymmetric, vertical and torsional mode of the NCB (a) and AKB (b); detailed view of the first antisymmetric vertical mode of the NCB (c) and of the AKB (d) around the day of damage occurrence.

Table 4.5: Frequency ratios for AKB and NCB adopted for estimating the frequency shift in the three different damage intesity scenarios.

	New Carquinez Bridge			Akashi Kaikyo Bridge		
	DM1	DM2	DM3	DM1	DM2	DM3
mode	$\times 10^{-1}$	$\times 10^{-1}$	$\times 10^{-1}$	$\times 10^{-1}$	$\times 10^{-1}$	$\times 10^{-1}$
V1A	9.99986	9.99972	9.99939	9.99981	9.99961	9.99918
V2A	9.99999	9.99979	9.99956	9.99983	9.99966	9.99928
V3A	9.99993	9.99986	9.99969	9.99986	9.99971	9.99939
V1S	9.99951	9.99990	9.99788	9.99944	9.99886	9.99759
V2S	9.99737	9.99461	9.98866	9.99761	9.99509	9.98967
V3S	9.99973	9.99945	9.99884	9.99959	9.99916	9.99823
T1A	9.99999	9.99998	9.99995	9.99991	9.99981	9.99961
T2A	9.99999	9.99998	9.99995	9.99991	9.99981	9.99961
T3A	9.99999	9.99998	9.99995	9.99991	9.99981	9.99961
T1S	9.99810	9.99611	9.99182	9.99849	9.99692	9.99351
T2S	9.99991	9.99981	9.99959	9.99858	9.99708	9.99387
T3S	9.99998	9.99996	9.99991	9.99983	9.99965	9.99927

Sections will be conducted by considering three different damage scenarios. They are all characterized by the same damage position, close to one support ($\gamma = \delta/2$), and extension $\delta = 0.05$, while they distinguish themselves for their damage intensities: (i) $\eta = 0.025$ (small damage, DM1), (ii) $\eta = 0.05$ (moderate damage, DM2) and (iii) $\eta = 0.10$ (severe damage, DM3). Such damage scenarios produce relative changes, $\Delta f^{\max}$, of the most damage-sensitive frequencies always smaller than few per mil (at most around 2) even in the case of severe damage. In Tab. 4.5 the frequency ratios adopted for estimating the frequency shift applied to NCB and AKB frequency time histories respectively, are reported for the three different considered damage scenarios DM1, DM2 and DM3.

4.5.2 Regressive models

Classic linear multivariate regressive model is applied at first in order to succesively compare the effectiveness of its use for structural health monitoring with those of less conventional statistical tools fundamentally based on a proper application of the Principal Component Analysis. First of all it is worth specifying how for the present and the following applications to the AKB two of the identified frequency time histories, the ones of V2S and T1S modes to be more precise, must be discarded because from a proper data analysis it

has arisen that they contain a very high number of missing, and so artificially reconstructed, values. All that can be considered admissible as well as rather realistic, being usable for SHM only the steadily identified frequencies as well as the most damage sensitive ones. However, while this last condition can not be always verified apart from the cases in which a perfectly tuned FE model is available, the former one, that is the stable and reliable identification of modal frequencies during time, is the mandatory condition for applying SHM multivariate statistical techniques. Moreover even if the aforementioned frequency time histories may present a sufficiently large sample size for MLR analysis, they are not surely sufficient for a proper use with the following PCA-based techniques. For this reason, in order to have a comparison between different techniques applied in the same conditions, they are not considered in the following analysis.

The adopted model is already fully implemented in commercially available softwares. In the specific case, ready made tools of MATLAB by The MathWorks Inc., is used, providing an optimization of β coefficients (predictors) too. In Fig.4.28 the capability in estimating frequency time histories of modes V1A and T1A of both the NCB and the AKB, are presented. After that, the capability of the just built linear models in damage detection is tested. Through the cleaning procedure illustrated in Chap. 3, for a group averaging size gr equal to 24, the control charts are built corresponding to the previously described three different damage scenarios DM1, DM2 and DM3. As it can be observed while a satisfactory success rate is achieved in the case of the NCB, similar results are not carried out in that of the AKB where the more relevant non-linearities produce a clear loss of effectiveness in the procedure. Then the constructed MLR models are adopted in the same damage scenario, DM2, for varying the group averaging size gr with the purpose of evaluating the performance in early damage detection. It is clear from the results proposed in Fig. 4.30, how the variation of gr, its growth to be more precise, produce an evident improvement of the outliers percentage in the NCB while it can not be said the same for the AKB where such percentage continues to remain quite poor.

4.5.3 PCA-based techniques

In the present section the multivariate statistical PCA-based techniques for structural health assessment, introduced in 2 are tested in the same damage scenarios presented in 4.5.1 and adopted beforehand in classical linear regressive model approach (Sec. 4.5.2). At the beginning with the purpose of a proper application of the investigated techniques some analysis are carried out for

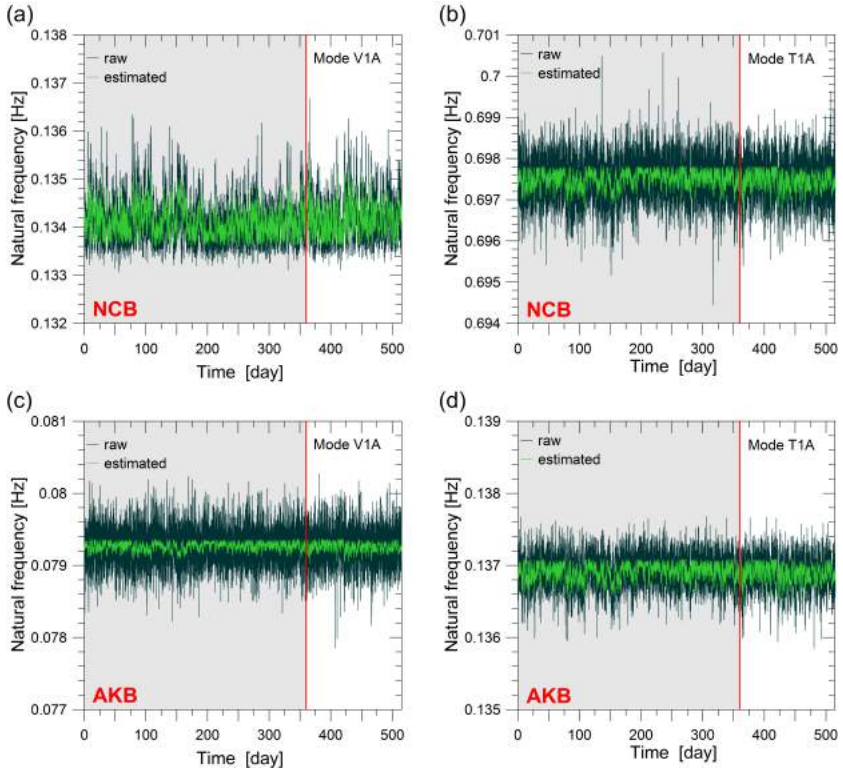

Figure 4.28: Frequency time histories of V1A and T1A modes of the NCB (a-b)and AKB (c-d), identified (dark green) through SSI procedure and then estimated (bright green) through linear regressive model.

optimizing the parameters involved in the procedures, that is, number of retained principal components l in the Linear PCA and, again, number of retained principal components l and number of clusters $q$in the case of Local PCA. After such preliminary parameters assessment, linear PCA and Local PCA are applied in the previously described damage scenarios in order to verify their capability in damage detection and finally some additional analysis are performed to get the final purpose of a strict comparison between the actual effectiveness of the two different approaches.

4.5.3.1 Linear PCA

As a first step towards an effective SHM through the application of the classical Linear PCA, some preliminary analysis are carried out in order to evaluate the importance of each PC in terms of variance of the data, so as to achieve an

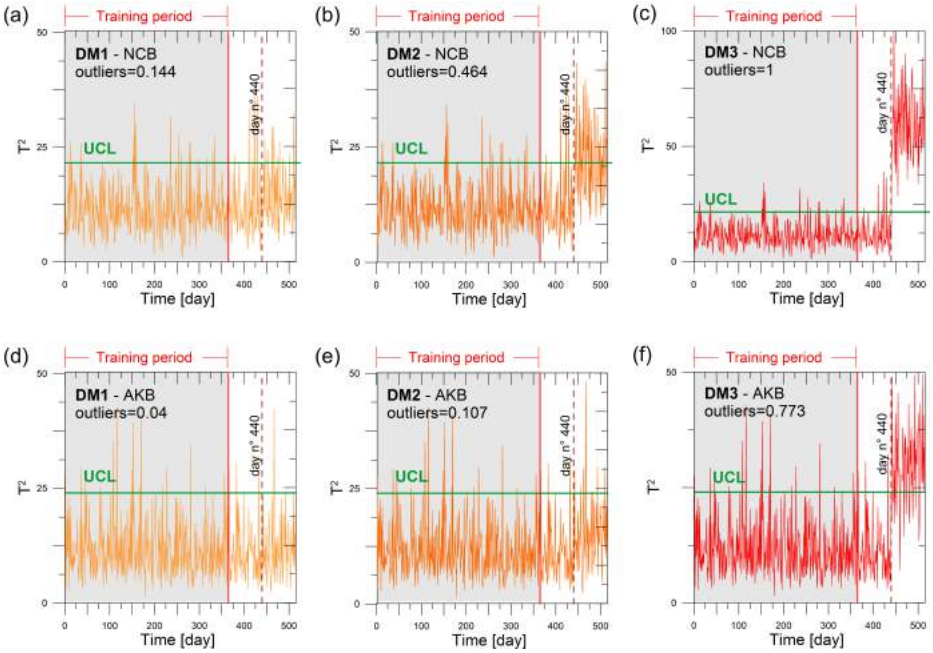

Figure 4.29: Control charts of NCB and AKB obtained for damage scenarios DM1 (a)(d), DM2 (b)(e) and DM3 (c)(f) through the application of MLR models.

effective removal of environmental effects from identified frequencies. Using the procedure described in Subsection 3.2.2, a proper choice of the number of retained PCs seems to be crucial to accurately remove wind and thermal effects from identified eigenfrequencies, by reducing the dimension of the problem without loss of effectiveness in SHM. Such a number can range from 1 to the number n of variables considered in the problem, that is the number of identified modal frequenceis of the bridge. Actually, the maximum value which can allow to obtain statistically meaningful results, corresponds to $n-1$. For this reason in the case of the NCB an overall maximum number of 11 PCs can be retained while in the case of the AKB this number reduces to 9 because of the elimination of modes V2S and T1S frequency time histories for the reasons previously advanced in SubSec. 4.5.2.

In order to have a first idea concerning the role played by the number of retained PCs (dimension, l, of the rectangular matrix $\hat{\mathbf{T}}$) in the cleaning procedure of the natural frequencies, Figs. 4.31 and 4.32 present the results obtained for different values of l in the study cases of NCB and AKB, respectively. Specifically, Fig. 4.31 (a), (b) and (f),(g) show raw and cleaned data for modes V1A and T1A when retaining 3 and 10 PCs, respectively, while, in the same figure, (c),(d),(e) and (h),(i),(l) present the corresponding histograms. A

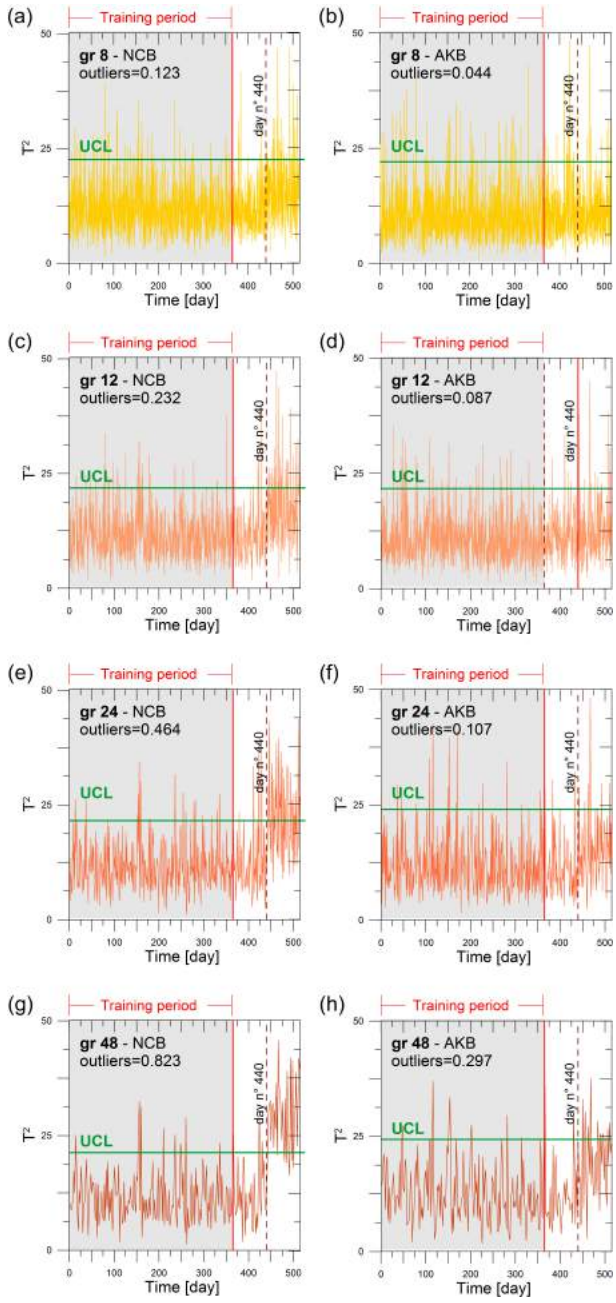

Figure 4.30: Linear PCA control charts of NCB and AKB in the case of damage scenarios DM2, obtained through MLR models and for varying the group averaging size: $gr = 12$ in (a)(b), $gr = 12$ in (c)(d), $gr = 24$ in (e)(f) and $gr = 48$ in (g)(h).

similar procedure is applied in the case of the AKB and the obtained results are presented in Fig. 4.32 for l equal to 3 and 7, respectively. The cleaned data are those contained in matrix $\mathbf{Y}^*$, Eq. (3.3), and the PC coefficients are computed considering a training period of one year. The results show that the time history of both the first antisymmetric vertical and the first antisymmetric torsional modal frequencies is cleaned by application of PCA in a very effective manner especially in the case of the AKB, where the use of a lower number of features tends to increase the weight of the firs PCs in terms of variance. Moreover it is noted that, as l is increased, the modified observation matrix, $\hat{\mathbf{Y}}$, tends to the raw observation matrix, $\mathbf{Y}$, while the residual, $\mathbf{e}$, tends to zero (see Subsection 3.2.2). For this reason, the variance of the cleaned natural frequency data, $\mathbf{Y}^*$, decreases by increasing l. This last aspect is clearly observed in the representation of raw and cleaned data through histograms: especially in the case of the AKB, (see for instance Figs. 4.32(e) and (l)) the histograms of the data cleaned by retaining the highest number of PCs are extremely narrow.

Once these preliminary tests have been carried out an unambiguous and more objective criterion is established for setting the number of PCs l one has to retain for an optimal SHM. Being 5% the percentage of permitted outliers in the training period, as imposed in the procedure for calculating the UCL in SubSec. 3.2.3, the optimal number of retained PCs is then established as the number capable of guaranteeing a similar outliers percentage in the observation period. In Fig. 4.33 the outliers percentage for varying the length of observation period is plotted for different values of the retained PCs l, estimated through one year of training period. From the obtained results, a larger number of l seems to be necessary to steadily have a number of outliers in the observation period around the imposed 5%. For any values of l the number of outliers stabilizes towards the imposed threshold for increasing the length of the training period, but it can be also stated that for a sufficiently high number of retained PCs such percentage is permanently around or even under the 5%. Therefore, in order to have confirmation of this trend, additional parametric analysis are performed by fixing observation and damaged periods, and by evaluating for different damage scenarios the so called Outliers Ratio (OR), defined as follows:

$$OR = \frac{Out_{dmg} - Out_{obs}}{Out_{trn}} \tag{4.15}$$

where $Out_{Out_{dmg}}$, $Out_{Out_{obs}}$ and Out_{trn} are the percentage of outliers in damaged, observation and training period s respectively. In Fig. 4.34 the results concerning this analysis are shown: OR is plotted versus l for five different values of η which ranges from 0 to 0.2. As it can be observed both in the case of NCB (Fig. 4.34(a)) and AKB (Fig. 4.34(b)), the choice falls again in a range of l always higher than what could be initially predictable, being only two the environmental factors influencing bridges modal properties but

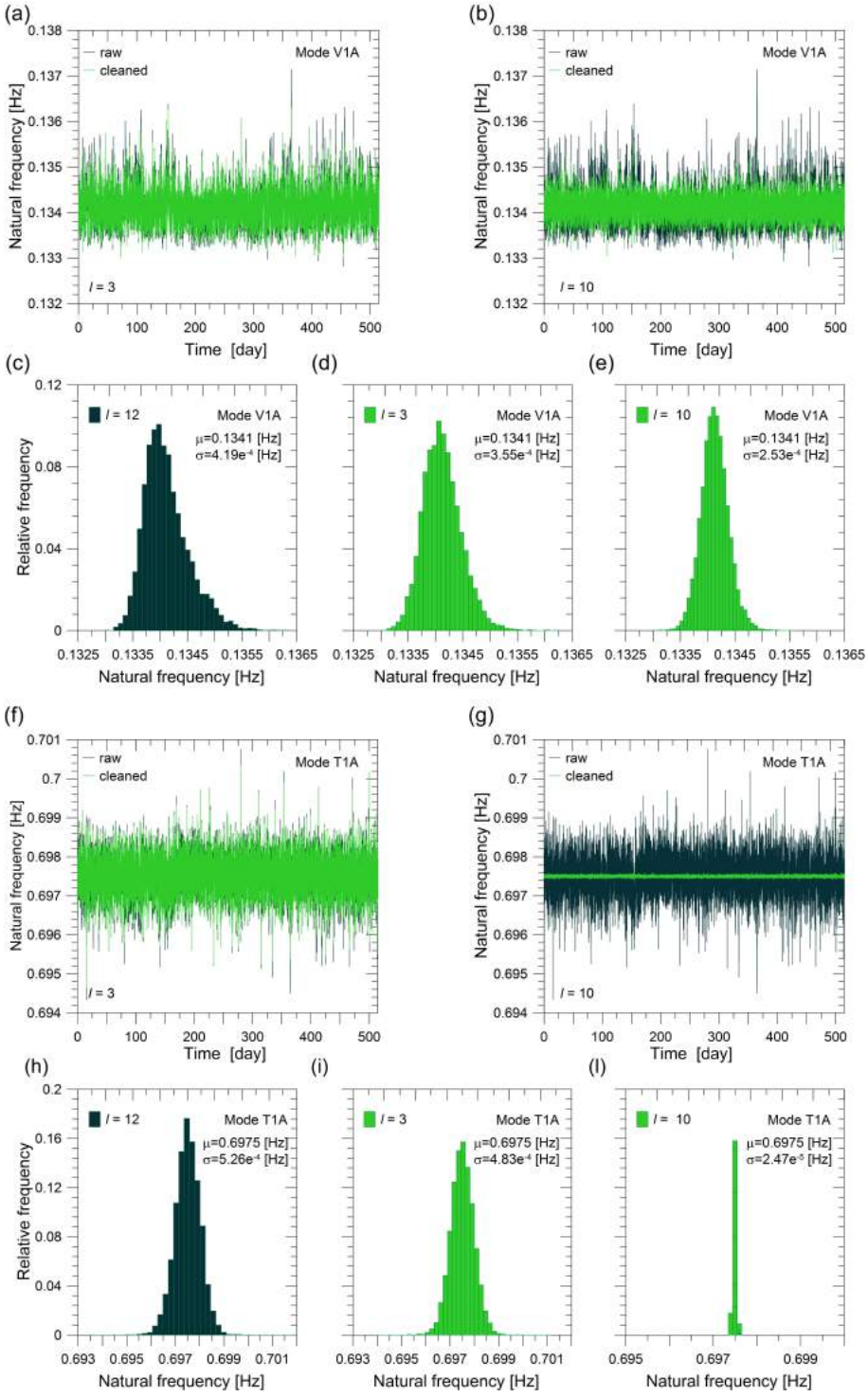

Figure 4.31: Time histories of identified frequency of V1A and T1A modes of the NCB before and after application of Linear PCA: results with 3 (a-b)and 10 (f-g) retained PCs. Histograms corresponding to raw and cleaned data for the V1A mode (c-e) and T1A mode (h-l).

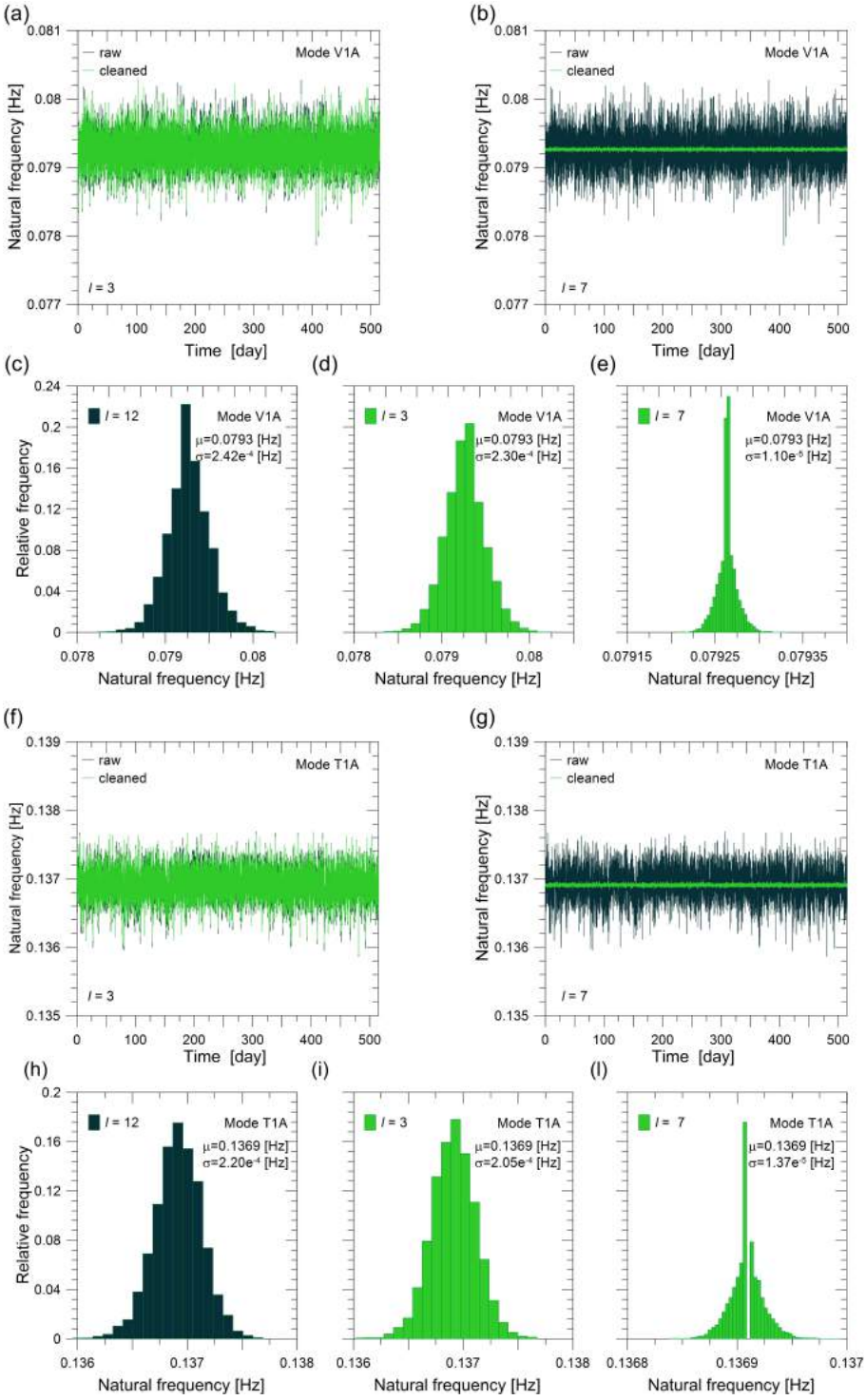

Figure 4.32: Time histories of identified frequency of V1A and T1A modes of the AKB before and after application of Linear PCA: results with 3 (a-b)and 7 (f-g) retained PCs. Histograms corresponding to raw and cleaned data for the V1A mode (c-e) and T1A mode (h-l).

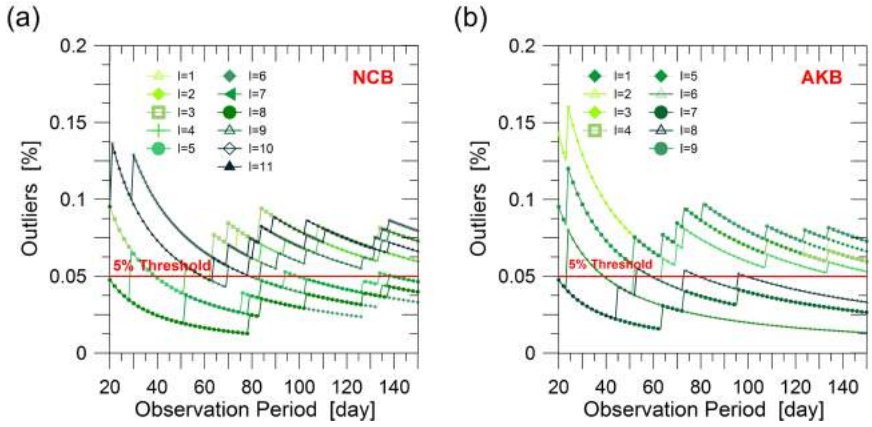

Figure 4.33: Results of the analysis for optimizing the parameters of linear PCA for NCB (a) and AKB (b): outliers percentage versus length of the observation period obtained for different values of the number l of retained PCs estimated over one year of training period.

being always higher than three the optimal number of retained PCs both in the NCB and in the AKB. All these remarks suggest the use of 7 and 8 PCs for NCB and AKB respectively, with the purpose of obtaining an effective cleaning of the frequency time histories from environmental effects. These values will be adopted in the following tests for building the control charts for damage detection purpose.

The first conducted analysis is aimed at verifying the capability of linear PCA

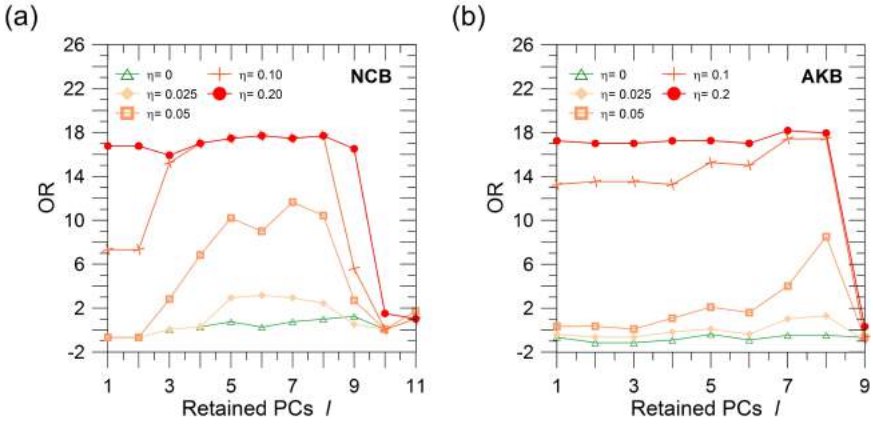

Figure 4.34: Results of the analysis for optimizing the parameters of linear PCA: OR values for varying the number of retained PCs and for different values of the damage intensity factor η in the case of NCB (a) and AKB (b).

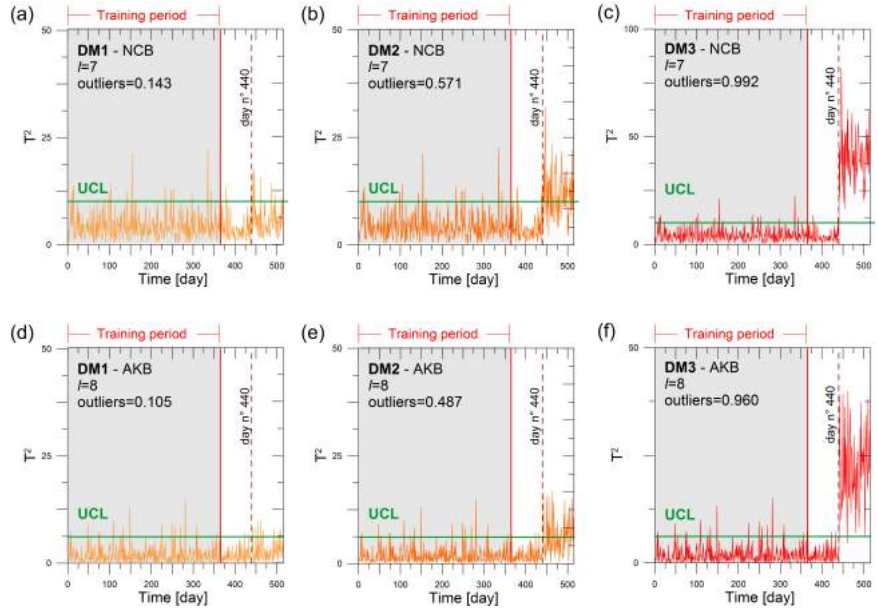

Figure 4.35: Control charts of NCB and AKB obtained for damage scenarios DM1 (a)(d), DM2 (b)(e), DM3 (c)(f), for optimally set linear PCA parameters.

in the detection of damages characterized by different severity (expressed in terms of damage intensity factor η). By adopting the same value gr of the averaging group size (see Eq. 2.20), set equal to 24 that means a value of T^2 every 24 hours, the control charts are built for the three different damage scenarios previously stated in Subsec. 4.5.1. Fig. 4.35 shows the results obtained for the NCB (a)-(c) and AKB (d)-(f). In both cases, linear PCA seems to be very effective in damage detection and it can be stated that a damage of moderate severity clearly arises from control charts producing an outliers percentage in the damaged period which is around 10 times bigger that those of the observation period. Moreover, from a discriminating observation of the control charts, it results that a small damage can not be recognized and that this technique finds a slight limitation of its effectiveness when nonlinear or weakly non linear correlations among frequencies occur: for equal parameters setting and damage intensity (DM2) the outliers percentage in the AKB is smaller than in the NCB, indeed (compare for instance Fig. 4.35(b) with Fig. 4.35(e)).

Later on, after DM2 has been assumed as a representative case study, the capability of linear PCA in early damage detection is tested by varying the group averaging size gr. The adoption of a reduced value of gr allows to enlarge the bulk of T^2 and in such a way to potentially detect in advance damage occurrence by reducing the time interval between a value of T^2 and the

following one. However this approach contrarily leads to a lower sensitivity in the calculation of the statistical distance adopted as damage sensitive feature, being the group averaging size decisive in its damage detection capability. The obtained results, depicted in Fig. 4.36, show for both the study cases how sensitive is the adopted statistical distance, T^2, to the size of gr: for the same damage intensity the outliers percentage increases 5 and 7 times for NCB and AKB respectively when gr passes from 8 to 48. Moreover the observation of the built control charts confirms the lower effectiveness of the procedure for the removal of the environmental effects in the case of the AKB where the correlation among frequencies is non linear.

4.5.3.2 Local-PCA

Similarly to the case of damage detection through the application of Linear PCA, also in the case of Local PCA some preliminary parametric analysis are carried out in order to obtain an effective SHM and to successively guarantee a proper comparison in terms of damage detection capability between the two different techniques. As previously stated, two are the main parameters which have to be set in Local PCA: the number of clusters q and the number of retained PCs l for the application of Linear PCA in each cluster.

Again, the criterion chosen for the optimal choice of the aforementioned parameters is to adopt a number of cluster and PCs capable to produce a percentage of outliers in the observation period steadily under or as close as possible to the fixed threshold of the 5% adopted as admissible limit in the training period. To this aim, in both the study cases, the number of outliers is estimated for varying the number of clusters from 2 to 8 and l from 1 to 11 and 9 for NCB and AKB respectively. The analysis are repeated for observation periods of different length, from a minimum meaningful value of 40 days to a maximum of 120. For the sake of synthesis all the results of such parametric analysis are not reported here but only some significant outcomes are summarized in the following Tab.4.6 where the outliers percentages in different training periods are reported for different combinations of the Local PCA parameters, considering an overall training period of one year for the PCs.

In the light of the results of the conducted parametric analysis the following control charts for damage detection purpose are built considering a number of clusters equal to 4 and 6 and setting the number of retained PCs to 6 and 8 for NCB and AKB, respectively. The following Figs. 4.37 and 4.38 represent the effectiveness of the procedure based on the use of Local PCA with optimally set parameters, in cleaning the environmental effects from the identified frequency

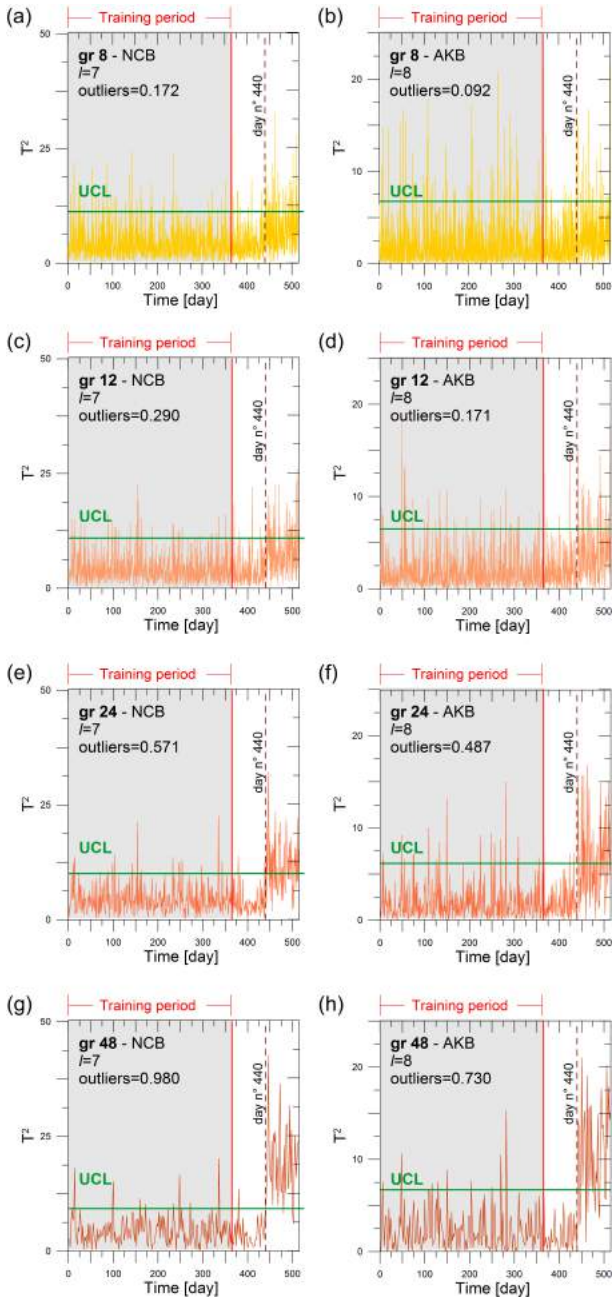

Figure 4.36: Linear PCA control charts of NCB and AKB in the case of damage scenarios DM2, obtained for optimally set Linear PCA parameters and varying the group averaging size: $gr = 12$ in (a)(b), $gr = 12$ in (c)(d), $gr = 24$ in (e)(f) and $gr = 48$ in (g)(h).

Table 4.6: Outliers percentage in the observation period for different values of the parameters of the Local PCA.

	New Carquinez Bridge				Akashi Kaikyo Bridge			
Obs. period	$q = 2$		$q = 4$		$q = 2$		$q = 6$	
[days]	$l = 2$	$l = 6$	$l = 2$	$l = 6$	$l = 2$	$l = 6$	$l = 2$	$l = 8$
40	0.025	0.050	0.025	0.050	0.025	0.075	0.050	0.100
60	0.033	0.050	0.033	0.050	0.033	0.050	0.050	0.067
80	0.088	0.038	0.05	0.075	0.088	0.013	0.100	0.075
100	0.080	0.060	0.060	0.060	0.08	0.020	0.090	0.040
120	0.075	0.050	0.058	0.05	0.075	0.042	0.058	0.067

time histories of modes V1A and T1A of both AKB and NCB. In the same figures the histograms representing the distribution of such data are reported before and after the application of the cleaning procedure. By observing data elaboration, Local PCA seems to be more effective in the case of AKB rather than in the case of the NCB. The more complex relationship among frequencies in the former bridge perfectly fits with the use of Local PCA which, on the contrary, seems to be apparently less helpful in the latter case where the weak nonlinearities would not require the use of too much complex techniques for the removal of the environmental effects. However, as immediately shown below, it will be clear how the adoption of such multivariate statistical technique allows to obtain better results in any case.

One more time, the first step consists in the evaluation of damage detection capability in the case of damages characterized by different severity. For both bridges, considering a group averaging size gr equal to 24 and Local PCA optimal parameters, the control charts are built for the three different damage scenarios DM1, DM2, DM3 previously defined. The results, shown in Fig. 4.39, demonstrate how, on equal terms, this last technique allows to obtain remarkable outliers percentages in the damaged period and that the success rate is in any case a little higher than in the case of application of linear PCA and remarkably higher than MLR models.

4.5.4 Application with measurements noise

The present dissertation is completed by the application of the investigated techniques in the case of measurements noise. Before approaching to damage detection results, brief notes concerning the response simulation in presence

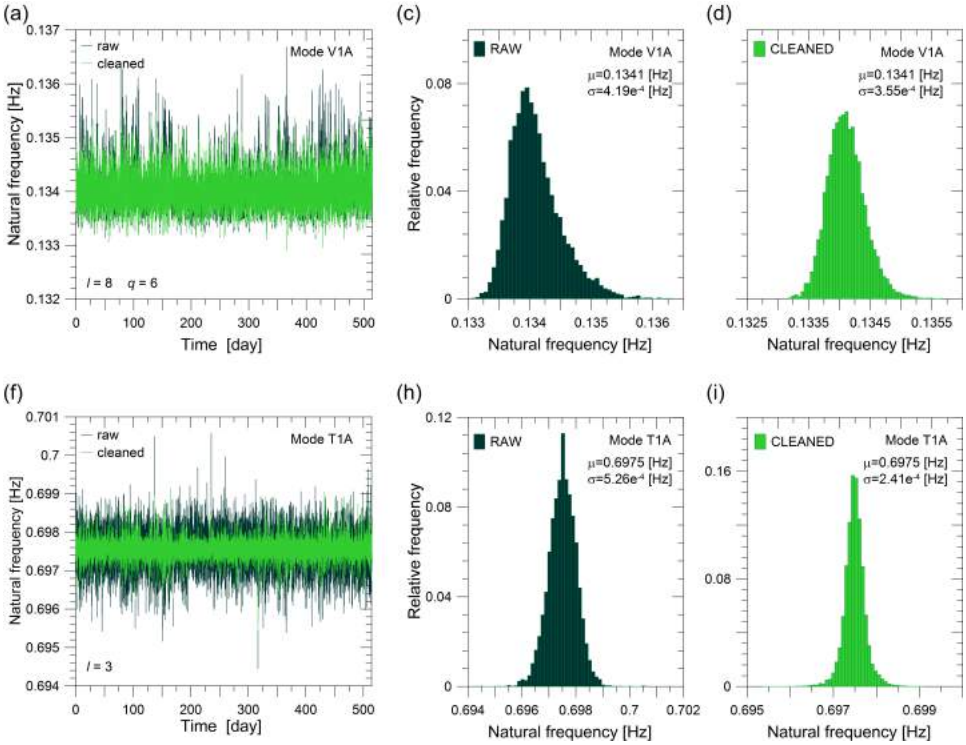

Figure 4.37: Control charts of NCB and AKB obtained for damage scenarios DM1 (a)(d), DM2 (b)(e), DM3 (c)(f), for optimally set local PCA parameters.

of noise seem to be necessary. Open field and real data measurements are always necessarily subject to disturbance sources which produce noise in the acquired data. The produced noise level varies depending on many factors, among which environmental conditions, kind of devices adopted for monitoring, type of digital/analogical converter, system of communication of the acquired data (long wiring, wireless devices, etc.) and so on. Limiting noise level on measurements is always crucial, especially in presence of low structural excitation sources, as may happen in OMA.

For this reason, in order to make more realistic and complete the following SHM techniques tests, the generated bridges response data are corrupted by noise addiction. Gaussian white noise signals are superimposed to generated responses of both NCB and AKB, and the fully automated SSI procedure is again applied for the extraction of modal properties. The standard deviation of the applied noise compared to the standard deviation of the acceleration signals, for a wind speed of 3.6 m/s corresponding to the standard deviation of U, ranges from 3.75% for the weakest acceleration signal (close to the support) to 2.6% for the strongest one (at mid-span). This noise level is similar to what

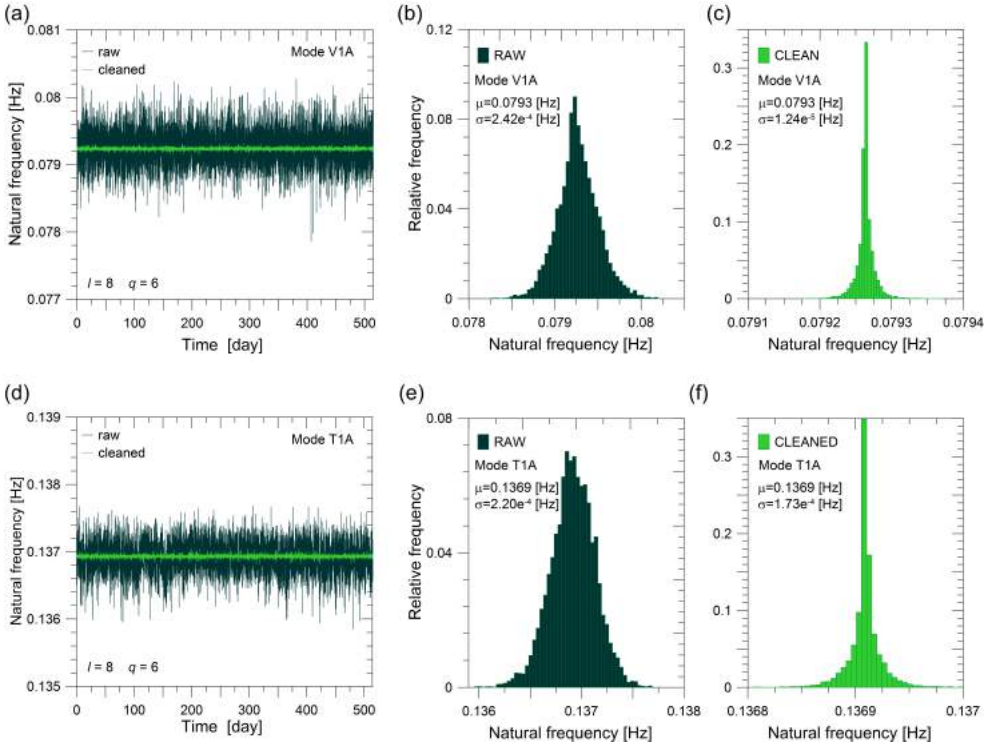

Figure 4.38: Control charts of NCB and AKB obtained for damage scenarios DM1 (a)(d), DM2 (b)(e), DM3 (c)(f), for optimally set local PCA parameters.

considered as realistic in other literature works (see for instance [66]). Noise addiction to response data has led necessarily to a higher number of missing values in the identified frequency time histories; however the percentage of such values still remain satisfactory, passing from 1.6% without noise to 2% in presence of noise and allowing in any case an effective replacement through the application of the *Expectation Maximization Algorithm* as explained in Chap. 3.

To the purpose of avoiding an useless repetition of similar analysis already performed in the previous sections, the performance evaluation of the investigated techniques in the case of measurements noise is carried out through a parametric analysis oriented to the evaluation of the outliers percentage in the damaged period for varying the damage intensity factor. Moreover, such conducted analysis permits a direct comparison with the case without noise. In Figs. 4.41 and 4.42 the obtained results are depicted for both NCB and AKB, in the case of linear PCA and local PCA application, respectively. Damage occurs at day n^0 440 with different severity that is for varying the intensity factor η which ranges from 0 to a maximum value of 0.1. The out-

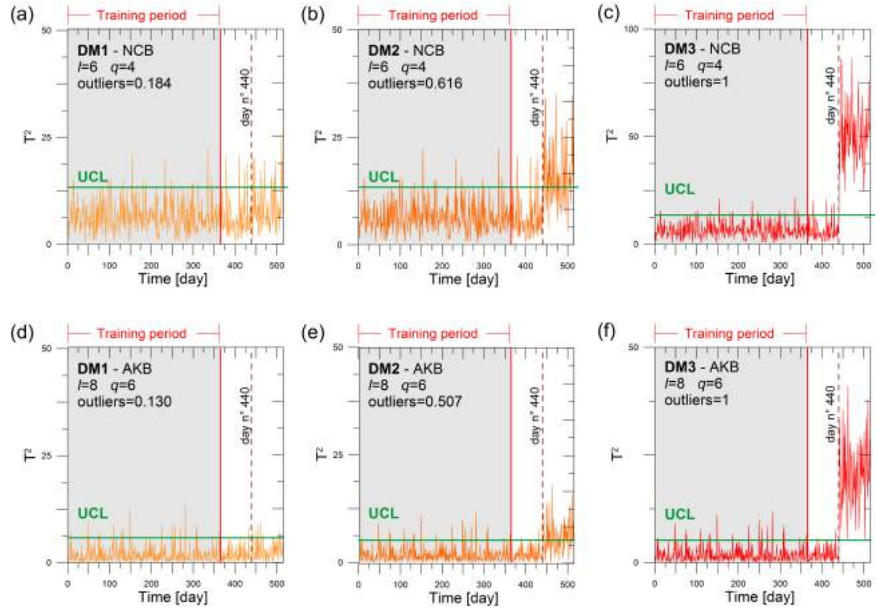

Figure 4.39: Control charts of NCB and AKB obtained for damage scenarios DM1 (a)(d), DM2 (b)(e) and DM3 (c)(f), for optimally set local PCA parameters.

liers percentage in damaged period is calculated in both cases without and with noise measurements addiction, represented in the figures by red and blue bars respectively. The results show a slightly smaller percentage of outliers in presence of noise under a moderate damage and a slightly larger presence of outliers in absence of damage. Outliers tend to stabilize for larger damage. The former aspect slightly increases the minimum level of detectable damage, while the latter determines a slightly larger number of false alarms. Assuming for instance that 40% of outliers represents a clear indication of the presence of a damage, the minimum level of detectable damage tends to increase with measurement noise. Some interesting results about it are summarized in the following Tab. 4.7 where the minimum detectable damage for the NCB and the AKB are reported with and without noise addiction for both the case of linear PCA and local PCA. It is concluded, therefore, that the procedure is robust in revealing the existence of a damage despite the presence of measurement noise.

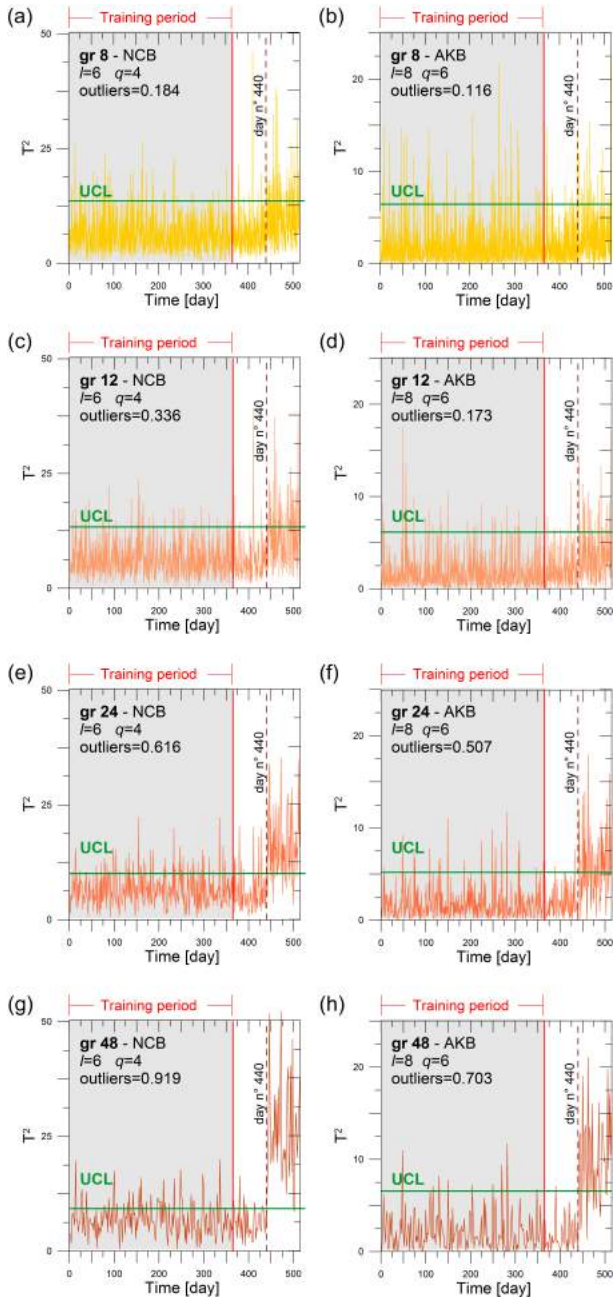

Figure 4.40: Control charts of NCB and AKB in the case of damage scenarios DM2, obtained for optimally set Local PCA parameters and varying the group averaging size: $gr = 12$ in (a)(b), $gr = 12$ in (c)(d), $gr = 24$ in (e)(f) and $gr = 48$ in (g)(h).

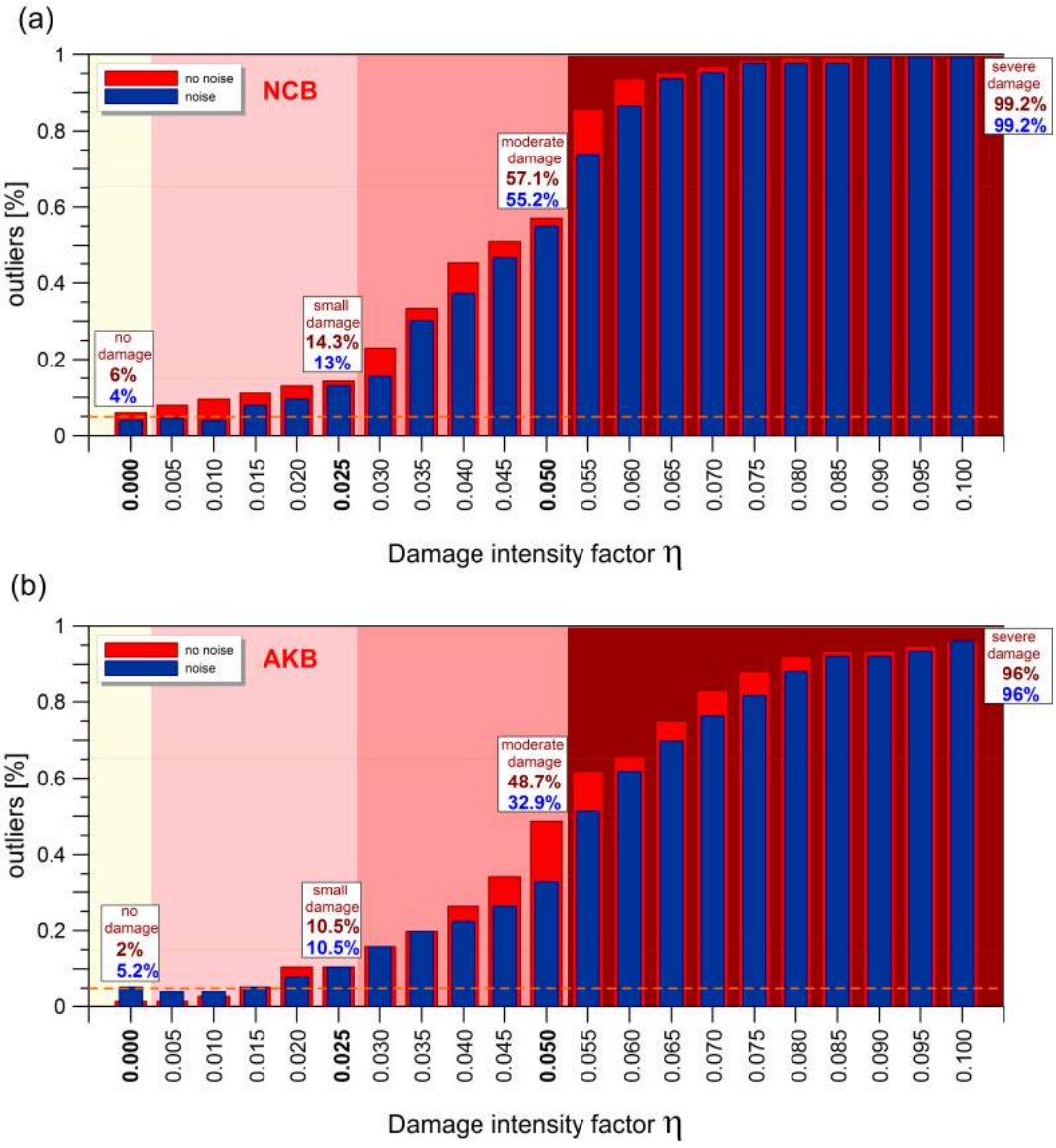

Figure 4.41: Outliers percentage in the damaged period estimated through the application of linear PCA with optimized parameters and for varying damage intensity factor η. Results obtained for the NCB (a) and AKB (b) with (blue bars) or without (red bars) noise measurements.

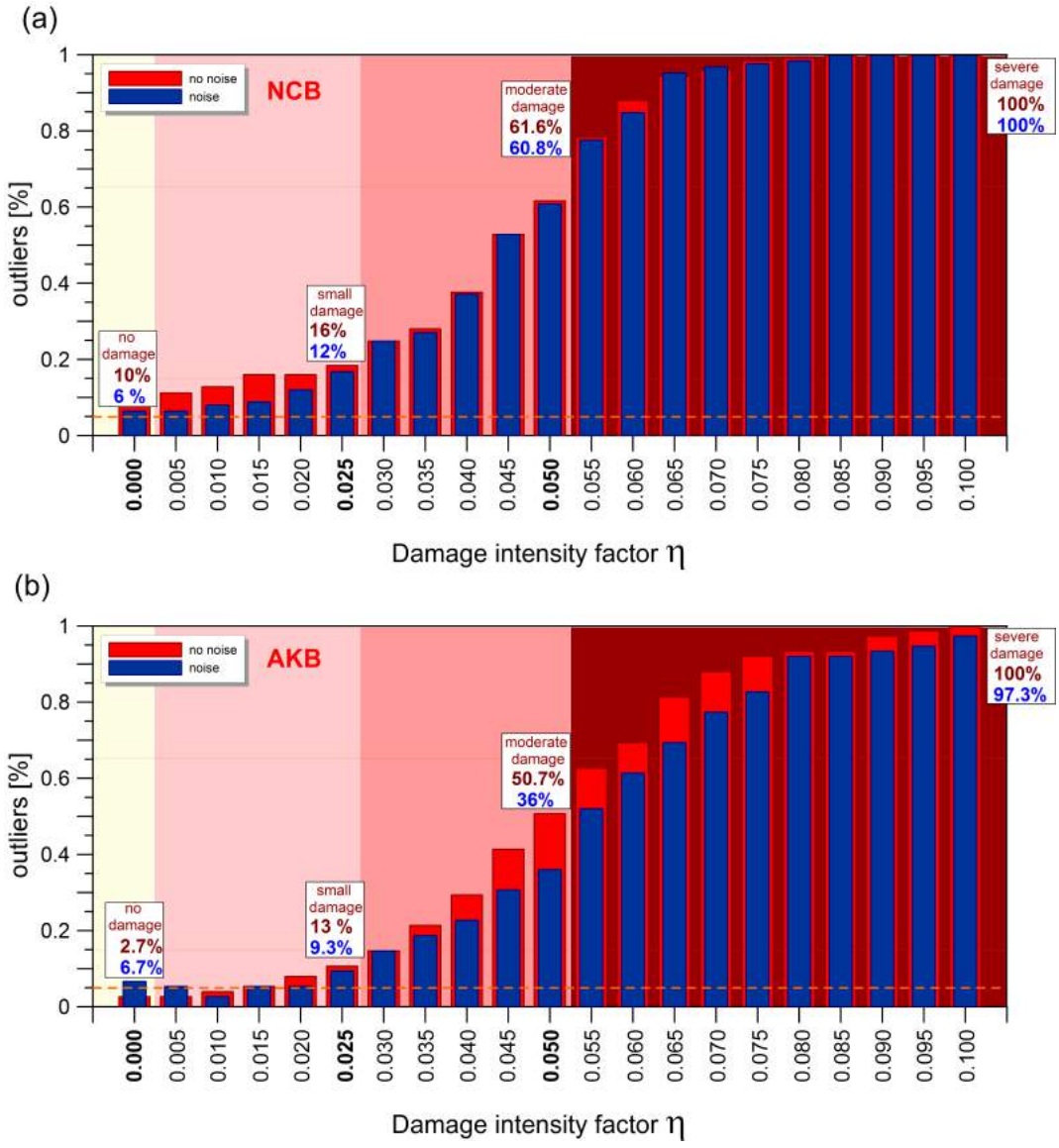

Figure 4.42: Outliers percentage in the damaged period estimated through the application of local PCA with optimized parameters and for varying damage intensity factor η. Results obtained for the NCB (a) and AKB (b) with (blue bars) or without (red bars) noise measurements.

Table 4.7: Minimum detectable damage corresponding to the 40% of outliers in the training period.

	New Carquinez Bridge		Akashi Kaikyo Bridge	
	no noise	noise	no noise	noise
linear PCA	0.0375	0.041	0.0475	0.0525
local PCA	0.042	0.042	0.044	0.051

4.6 Discussion of results

In this chapter the capability of the multivariate statistical techniques illustrated in Chap. 2 and implemented in the proposed closed loop method described in Chap. 3 are applied for assessing the health condition of a suspension bridge with main cable damage an subjected to changing environment, namely wind and temperature. In this context, novelty detection have been applied for the first time to reveal the presence of damage in structures characterized by significant variations of natural frequencies with changing wind speed.

An elastodynamic parametric bridge model with damage in one main cable and subjected to turbulent wind loading has been formulated as an extension of previous studies, accounting for aeroelastic effects through indicial functions. The model has been employed for comparing damage-induced variations of natural frequencies with those induced by temperature variation and those produced by aeroelastic effects associated with changes in incoming wind speed. This analysis, carried out by considering two sample suspension bridges with different cross sections and consequently aerodynamic behavior, demonstrated that a small changes in the incoming wind speed and variation of temperature produce apparent frequency variations that can likely be more significant than those produced by a small damage.

The analytic model has been also used for generating long-term bridge response data under turbulent wind loading and changing temperature. Natural frequency estimates have been extracted from such pseudo-experimental data and have been used for revealing the presence of a damage through MLR models and PCA-based techniques. The results demonstrated that such mutivariate statistical analysis procedures are able to remove environmental effects from frequency estimates and, with a proper tuning of some salient parameters, reveals the presence of small damages consisting of little reductions of the cross section of one main cable that produce relative variations of the most

damage-sensitive frequency smaller than 0.1%. Owing to the robustness of the adopted output-only modal identification procedure, the possibility of revealing a relatively small structural damage was confirmed also in the case of data corrupted by noise. The aforementioned analysis has been carried out considering a damage located in the region, close to one support, where wires of suspension bridges typically break as a consequence of fretting fatigue triggered by parasitic bending stresses. However, considering that natural frequencies of suspension bridges are essentially not influenced by damage position along one maincable, as it was shown in previous work, the presented results can be extended to any other possible damage location.

Results presented in this chapter show that multivariate statistical analysis tools, are globally effective for SHM also in the case of dynamic properties being significantly and non-linearly affected by changes in environmental conditions, in particular wind. Although not permitting a full damage identification, that is, damage quantification and localization (see Subsec. 2.1.1), but only disclosure of the existence of damage, such techniques seem therefore to be readily implementable in full-scale monitoring systems for long-span bridges and to provide useful information for condition-based maintenance of such structures.

Moreover the adoption of different techniques for the extraction of damage sensitive features, has allowed to strictly compare their effectiveness in the removal of the considered environmental conditions effects and, consequently, to properly detect damage occurrence. More specifically, the application of techniques based on the hypothesis of linear correlation among structural dynamic features (MLR and Linear PCA), has revealed, when on the contrary non-linear correlations are present, some limitations if compared with more sophisticated techniques (Local PCA), which can allow somehow to account for such non-linearities.

The presented results have been entirely based on simulated data considering aeroelastic and thermal effects and measurement noise. Further work will be necessary to extend the presented results to also consider other external factors, especially concerning the operational conditions such as traffic load, as well as to consider aspects of the structural behavior that were not included in the simulation, such as non-linearities and lateral movement of the deck.

5

APPLICATION TO SHM OF A REAL LONG-SPAN ARCH BRIDGE

Proving the actual effectiveness of SHM techniques necessarily passes for their application not only on artificially generated data but above all on data obtained from real field measurements possibly of full scale structures. For this reason, this chapter is devoted to the application of the procedure for damage identification proposed in Chap. 3, to real bridge monitoring data. The real measurements data are obtained from the permanent monitoring system installed on the Infante Dom Enrique bridge over Douro river in Porto (PT) and are a courtesy of ViBest (Laboratory of Vibration and Structural Monitoring). The outstanding arch structure of the bridge is briefly described at first, giving some details on the construction stages and on the permanent monitoring system with which the bridge has been equipped since 2007. The available data, consisting in temperature measurements and in frequency time histories identified from bridge acceleration acquisitions, are then analyzed and after artificial damage introduction, the capability in damage detection of the adopted SHM techniques is verified for different damage scenarios. The case of an artificially imposed enhanced non-linear correlation between identified natural frequencies is also considered in the analysis in order to gain generality and to better highlight advantages and limitations of the investigated techniques.

Contents

5.1 Introduction 115
5.2 Infante Dom Enrique arch bridge 116
5.2.1 Description of the structure 116
5.2.2 Monitoring system 120
5.3 Damage detection 122
5.3.1 Permanent monitoring data analysis 122
5.3.2 Regressive model 131
5.3.3 PCA-based techniques 134
5.4 Discussion of results 144

5.1 Introduction

The application of the multivariate statistical techniques described in Chap. 2 and implemented in one single automated tool (Chap. 3), has revealed a great potentiality in damage detection as clearly emerged from the results presented in the previous Chap. 4. Many works have recently confirmed this by applying different methods, all mainly based on statistical approaches, and testing them basically on data generated through the use of proper analytical models or sometimes on data obtained from mock-up models of simplified structures such as concrete beams, steel plates and so on.

For this reason, the main constraining condition influencing the absolute positive judgment on the actual use of such techniques for damage detection purpose, lies in the inability to fully reproduce both with analytical models and with proper laboratory tests, the operational conditions in which a real structure operates. That is why application to real field measurements possibly of full scale structures, seems to be at the moment the only considerable further step capable of validating the use of SHM tecniques. Unfortunately achieving such kind of data is not trivial, especially in the field of bridge monitoring both because bridges equipped with permanent monitoring system are not so common and because companies which oversee SHM systems tend to be careful in supplying these data. However,thanks to a collaboration born with the Laboratory of Vibrations and Structural Monitoring, ViBest, of the Facultade de Engenharia Universitade do Porto (FEUP), two years of monitoring data of the Infante Bridge over the Douro River in Porto, are made available and the test of the proposed procedure made possible also on real bridge measurements.

The data consist in temperature measurements and in bridge modal frequency time histories identified through different techniques both in time and frequency domain. In the following Sections, such data are described more in detail and, based on previous works conducted at ViBest, they are used for testing the investigated SHM techniques. In this way, a strict comparison between classical regressive models and PCA-based techniques will be carried out. In addiction, the case of an artificially imposed enhanced non-linear correlation between identified natural frequencies is also considered in the analysis in order to gain generality and to better highlight advantages and limitations in the use of the aforementioned techniques.

5.2 Infante Dom Enrique arch bridge

The navigable Douro river offers to people who up it, the chance of passing underneath an incredible series of world-renowned bridges linking the cities of Porto, on the north side, and of Gaia on the south one, (see Fig. 5.1). In the last two centuries the landscape of such thousand-year old history land has been deeply marked and adorned by the construction of bridges that, in many cases, constituted authentic miracles for bridge engineering of the times. Between them it is necessary to remember the Luiz I Bridge (Fig. 5.1(f)), designed by Théophile Seyring, opened in 1886 setting a *world record*; the beautiful Arrabida Bridge (Fig. 5.1(g)), an arch bridge which spans an overall length of 272 m, opened in June 1963 setting for a while a *world record* for reinforced concrete bridges; finally the São João Bridge, a railway bridge opened to traffic in June 1991, which was until 2006 the *world record* in portal prestressed concrete railway bridges with a central span 250 m long. The last to be built among these outstanding bridges is the Dom Infante Enrique Bridge (Fig. 5.1(e)), opened in 2002, which consists of a shallow and extremely thin arch. Spanning a remarkable distance of 280 m it is the second largest arch bridge in Europe surpassed only by the Krk Bridge, in Croatia, with a span of 390 m.

5.2.1 Description of the structure

At the end of 20^{th} century, the public call for tenders for the design and built of the Infante Dom Henrique Bridge, over the river Douro, located halfway between the 19^{th} century Luiz I and Maria Pia Bridges, demanded for a solution that should match the technical and aesthetic qualities of those two bridges, which are both considered great works of engineering [96, 97]. The same name chosen for the bridge enlarged further the responsibility, being Infante Dom Henrique not only one of the most eminent personality of the city of Oporto and Portugal but also a considerable figure for Europe which had been led by him on the adventure to meet other civilizations. For all these reasons the new bridge had to abide by the following fundamental conceptual characteristics:

- high respect for the river underneath and to the magnificent historic bridges in Porto not competing with them but trying, on the other hand, to come up with new solution elegant and careful in the form but innovative in the technical solution;

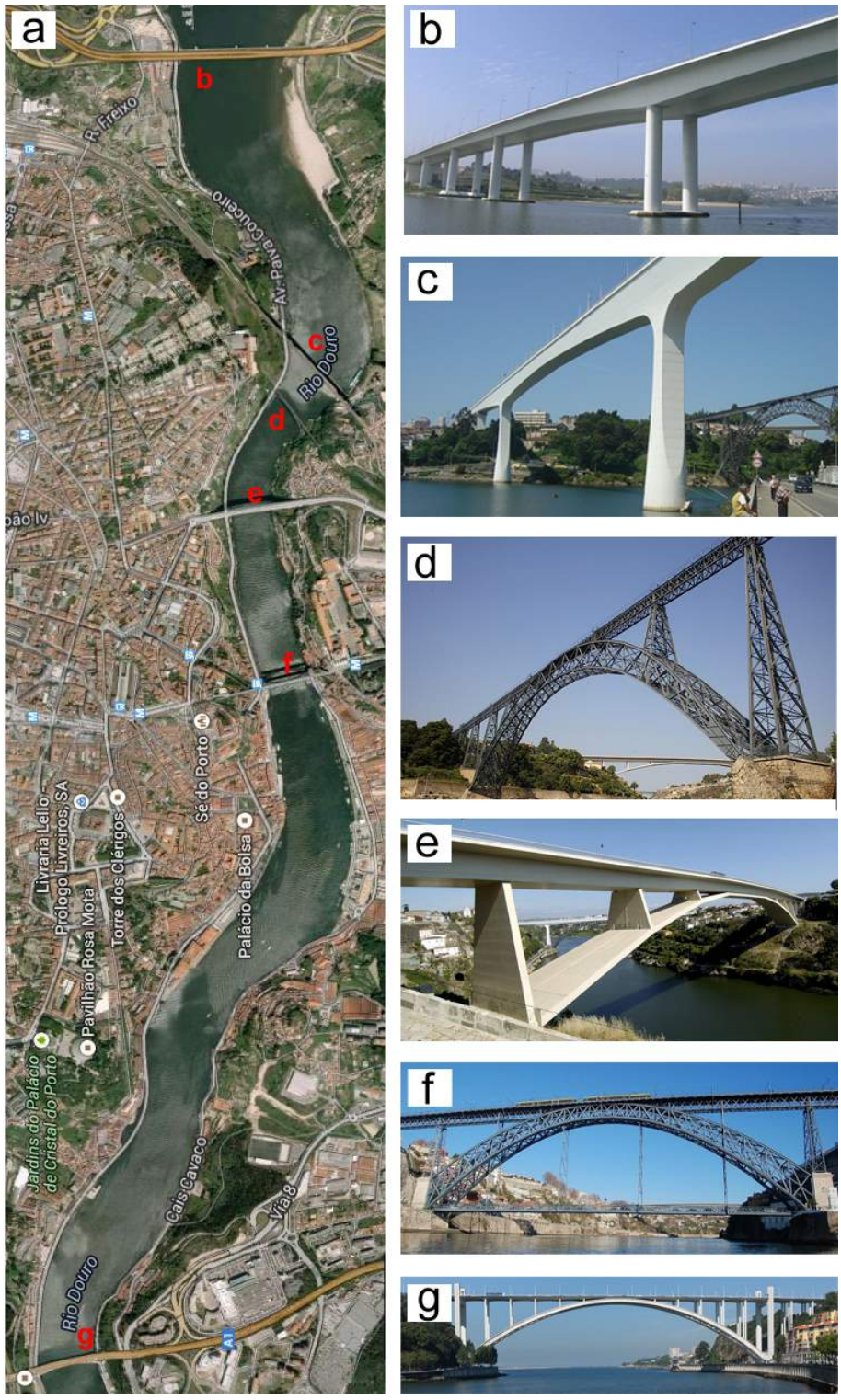

Figure 5.1: Aerial view of the bridges across Douro River in Porto (a), Freixo bridge (b), São João Bridge (c), Maria Pia Bridge (d), Infante Bridge (e), Luìs I Bridge (f), Arràbida Bridge (g).

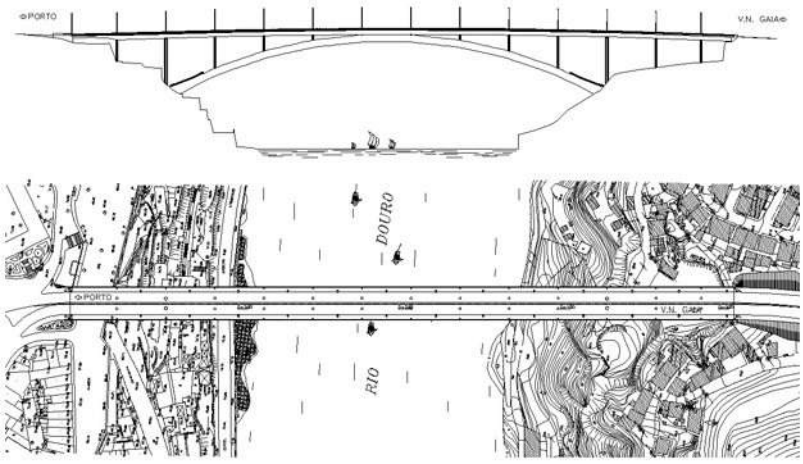

Figure 5.2: Draft of the conceptual design of the Infante Dom Enrique Bridge.

- high respect towards the city of Porto and to its particular profile with no elements above the deck of the bridge.

The designers of the bridge received these recommendations and the results is a very slender arch bridge which appears in a discrete manner and does not contain any decoration, nothing that does not comply with the functional requirements. Everything in the bridge has a purpose that is both structural and functional. For this reason it has virtue of simplicity, structural purity and geometric regularity(Fig. 5.2).

The Infante Dom Enrique Bridge is a "Maillart" type of arch bridge, built by creating rigid triangular structural systems requiring temporary struts and diagonals to complement those bars provided by the arch and the deck. The equilibrium of the two half-bridges cantilevering over the river at a height of more than 70 meters was achieved by cable anchorages into the granite slopes, together with concrete-ground struts forming rigid triangular structural systems with the deck and temporary diagonals [98]. Its structure is composed of two mutually interacting fundamental elements: a very rigid prestressed reinforced concrete box beam, 4.50 m in height, supported on a very flexible reinforced concrete arch, 1.50 m thick, as shown in the elevation and cross-sections in Fig. 5.3. In the 70 m central stretch of the bridge, the arch combines with the deck to form a box section that is 6 m in height. The lateral faces of this section bear an indentation that gives the impression of continuity to the masses corresponding to the deck and the arch. The span between abutments

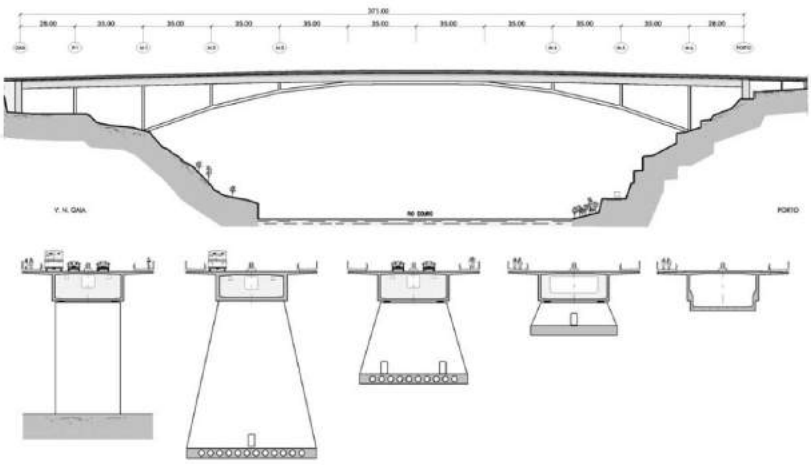

Figure 5.3: Elevation and cross-sections of the Infante Dom Enrique Bridge.

of the arch is 280 m and the rise till the crown of the arch is 25 m, thus with a shallowness ratio greater than 11/1([97]). However the excellent aesthetic attribute of the bridge involved great problems in its construction, difficulties overcome only through the use of remarkable technological advances necessary both for the great dimension of the bridge and because of the following relevant features:

- as previously mentioned the Infante Dom Enrique Bridge is the second longest arch bridge in Europe;
- it holds the world record for straight segmental arches; its constant thicknesses of 1.5 m (around $L/187$) conveys and extreme slenderness, more marked than what the usual one adopted in common rigid arch where the length-to-thickness ratio usually span between $L/40$ and $L/187$;
- the rise of $f = 25$ m means a shallowness for the arch of $L/f = 11.2$ (see Fig. 5.4) that has no parallel in the field of large span arch bridge
- Its "static coefficient" ($L^2/f > 3000$), proportional to the axial force at the crow of the arch, as reported in Eq. , is the largest of any concrete arch bridge built to this date.

$$H = \frac{p}{8} \cdot \left(\frac{L^2}{f} \right) \tag{5.1}$$

where p is the uniform dead load.

The construction method was to progress by cantilevering the deck and the arch from each side of the river. This process has been possible thanks the

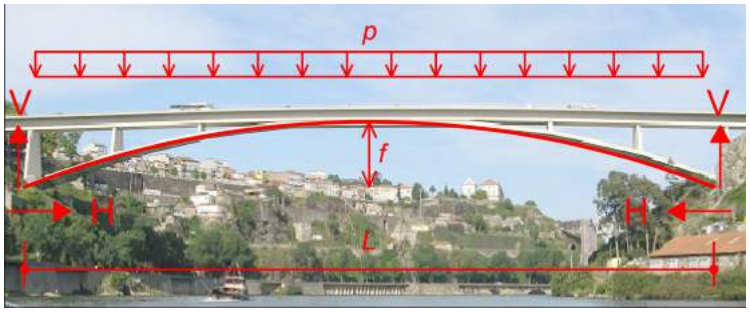

Figure 5.4: Maillart arch scheme applied to the Infante Dom Enrique Bridge.

construction of two temporary pillars which allow to reduce the span from 280 m to 210 m, during construction. The 70 m central span was built by typical cast-in-place segmental box-beam construction methods. Moreover a complex system of temporary tensile diagonal bars and vertical compression bars are installed ensuring that the two bridge cantilever were tied back to the deck abutments until the deck and arch met at the centre of the bridge.

During the construction of the bridge several highly innovative techniques and procedures are introduced, addressing a geometrical precision criteria never demanded before. First of all, the positioning of the support platform for the arch formwork was adjusted to the millimeter by using two automatic and computerized hydraulic system. A centralized computer system allowed to monitor the behavior of the the bridge during all its construction phases. The same construction, internal tension control and removal of the temporary structures necessary for bridge erection have been carried out with the use of high technology solution and innovative procedures.

.

5.2.2 Monitoring system

Since 2007 the Infante Dom Enrique Bridge has been equipped with a permanent monitoring system which is in continuous operation since the month of September of the same year. The installed system, whose scheme is synthetically represented in Fig. 5.5, is a so called *decentralized system* that is a system where more than one acquisition system is adopted: in particular, in the considered study case, two GPS-synchronized local digitizers are placed

The description of the structure and many of the presented figure are explicitly based on [96, 97, 98, 99]

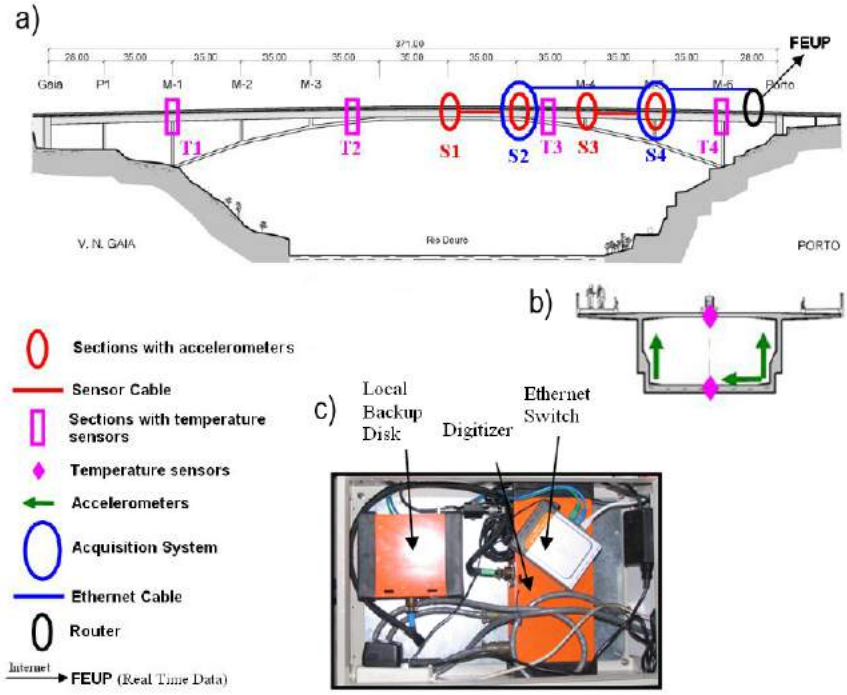

Figure 5.5: Scheme of the monitoring system installed on the Infante Dom Enrique Bridge: sensors layout (a), tipical instrumented cross-section (b), acquisition system block (c). Figure from [100].

in sections S4 and S2 in order to minimize the electrical interferences due to long wiring. Field measurements obtained with this system configuration have revealed to be already more than satisfactory; for this reason, being the distance between the two digitizers short enough, the problem of noise limitation is no further optimized though the adoption of fiber optical cables, for instance, which is generally suggested for distances between devices longer than 90 m or in any case, when the configuration of the structure makes the same structure vulnerable to lightning (typically in vertical slender structures).

Above the two digitizers, the monitoring system is composed by an overall number of 12 accelerometers, 8 temperature sensors (marked in Fig. 5.5) embedded in the concrete structure of the bridge, local backup disks and an ultra low-power field processor that allows the conversion in text files of the data acquired by the sensors and their transfer by a local network to Vibest at FEUP. All the equipment is located inside the deck box girder, being therefore well protected from the environmental threats. The accelerometers, (model FBA ES-U2 produced by Kinemetrics Inc.), are force balance accelerometers with high sensitivity, capable to guarantee a good dynamic characterization

of the structure also at low frequency levels. Since the structure revealed from previously performed Ambient Vibration Tests (AVT) an high level of symmetry of its mode shapes, the sensors are installed in four different sections in half bridge only. Each section is equipped with three accelerometers disposed as underlined in 5.5(b) in order to properly deduce the torsional movement of the bridge.

The permanent dynamic monitoring system is complemented by a static monitoring system installed on the bridge during its erection in order to control the construction phases (as previously mentioned). Moreover during the first six months of monitoring activity, the system has been also integrated by a local meteorological station with the purpose of an evaluation in situ of environmental condition such as wind speed humidity and temperature. More details concerning the technical characteristic of each devices are provided in the following references [100] and [101].

5.3 Damage detection

In the present section a brief general overview on the data acquired by the continuous monitoring of the Infante Dom Enrique bridge is given. Some considerations on the data are drawn with particular reference to the correlations that the identified frequency time histories exhibit with each other and with environmental factors (temperature in the specific case). Synthetic details are also given concerning the Finite Element modeling of the bridge developed by the same research group at FEUP during the dynamical investigation. The same FEM has been adopted to evaluate the variation in terms of frequencies produced by different hypothetical damage scenarios. Finally, following what previously done in Chap. 4, the investigated multivariate statistical techniques are applied for the purpose of evaluating their capability in damage detection in the case of real bridge monitoring data.

5.3.1 Permanent monitoring data analysis

Acceleration signals of 30 minutes are acquired with a sampling frequency of 50 Hz. Even if this choice could reduce the capability of the following procedures in a rapid detection of anomalies in which the structure may occur, the adoption of longer acceleration time histories surely leads to improve the accuracy of

modal parameters estimation and consequently to potentially detect smaller variation produced by damage.

After their acquisition, accelerations are properly post-processed: a low-pass filtering is applied at first allowing offsets elimination and then a data re-sampling to 12.5 Hz is performed. The treated data have been analyzed in depth by the members of research group at FEUP working on the project on the monitoring of the Infante Bridge. The results carried out are extensively described in many literature works (see for instance [100, 101, 102]) and especially in the PhD Thesis of Filipe Manuel Rodrigues Leite Magalhães [103](member of the research group of the Infante and current Assistant Professor at FEUP). Such analysis essentially focused on the statistical characterization of the acceleration measurements and, through the RMS of such signals, pointed out many interesting remarks among which that the lateral acceleration in average is roughly equal to one half of the vertical one and the relationship existing between the same RMS and traffic loading especially during the rush hours.

Once these preliminary calculations are carried out, some automated modal identification techniques both in frequency and time domain (Chap. 3), are applied to the treated data in order to extract the modal properties of the bridge for each collected setup. More specifically, an automated FDD for the frequency domain and both SSI-COV and PolyMAX techniques in the time domain are applied to this purpose. Such techniques, properly set by the researchers of ViBest, have allowed to steadily identify twelve modal frequencies, whose time histories over two year of continuous monitoring are plotted in Fig. 5.6. In the following applications for damage detection purpose only the results extracted through PolyMAX method are adopted being the success rate in the identification as high as in the case of the other methods but being the standard deviation in frequencies estimates rather smaller. The results of PolyMAX identification, as presented in [103], are summarized in Tab. 5.1 where the following notation for the modes is adopted: the number indicates the order of the mode, L stands for *lateral* mode, V for *vertical bending*, T for *torsional* while VA represents a vertical bending mode of the arch with residual components at the deck (see [103]).

It is worth observing from data in Tab. 5.1 how the adoption of 30 minutes acceleration time histories allows to gain a remarkable success rate, always higher than 99%, and how the standard deviation in frequencies estimates is considerably smaller than that obtained in the case of modal damping or MAC. These remarks further support what has been previously stated in Chap. 2, namely that, despite the excellent potential properties of other dynamic characteristics in damage detection, modal frequencies still remain the most reliable tool to this purpose.

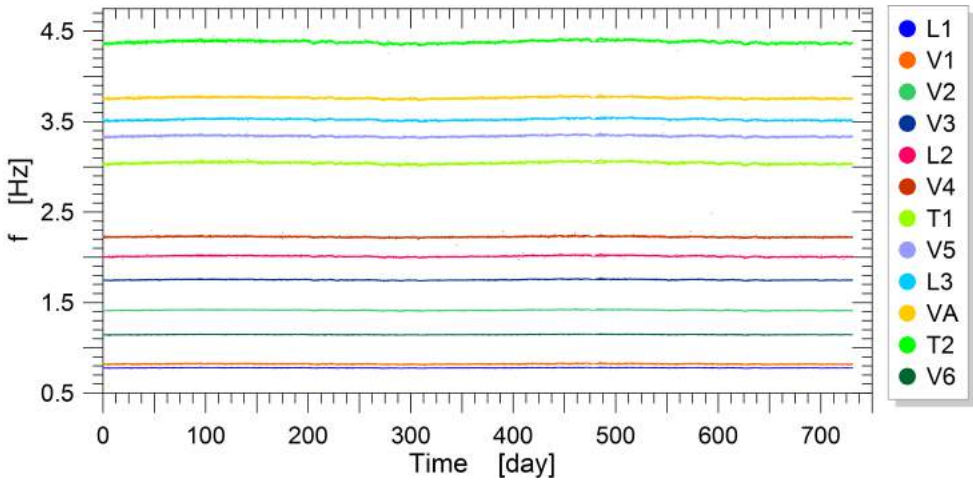

Figure 5.6: Frequency time histories of the Infante Bridge monitoring system obtained through the automated PoliMAX identification technique.

.

Table 5.1: Modal parameters of the Infante Dom Enrique Bridge identified through PolyMAX modal identification technique.

n^o mode	type	f_{mean} [Hz]	f_{std} [Hz]	ξ_{mean} [%]	ξ_{std} [%]	MAC_{mean}	MAC_{min}	Success rate [%]
1	L1	0, 7777	0.0019	0.4379	0.0933	0.9962	0.8257	99.994
2	V1	0, 8208	0.0041	1.1841	03741	0.9981	0.9537	99.988
3	V2	1, 1459	0.0025	0.4404	0.0846	0.9998	0.9946	100
4	V3	1, 4154	0.0042	0.4482	0.0912	0.9992	0.9774	100
5	L2	1, 7509	0.0049	0.4411	0.0809	0.9915	0.8109	99.937
6	V4	2, 0113	0.0073	0.4751	0.0979	0.9986	0.8096	99.325
7	T1	2, 2248	0.0061	0.4424	0.1089	0.9990	0.8028	99.873
8	V5	3, 0408	0.0111	0.4344	0.0987	0.9993	0.9033	100
9	L3	3, 3371	0.0086	0.4820	0.0904	0.9945	0.8210	99.896
10	VA	3, 5214	0.0094	0.3553	0.0733	0.9908	0.8018	99.042
11	T2	3, 7603	0.0097	0.4419	0.0833	0.9925	0.8058	99.671
12	V6	4, 3785	0.0149	0.5352	0.1108	0.9989	0.9082q	100

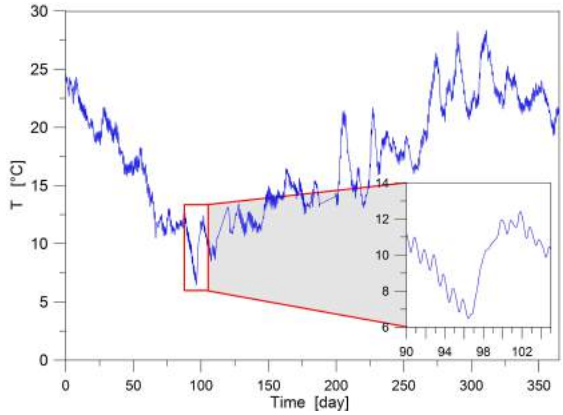

Figure 5.7: One year mean temperature T time history acquired by the temperature sensors of the Infante Bridge monitoring system.

Despite deepened analysis of the data are already carried out at FEUP and shown in many papers, a preliminary fact-finding work is mandatory for becoming familiar with the frequency time histories of the Infante bridge made available. For this reason, following what previously done in Chap. 4, the first step consists in the analysis aimed at the evaluation of the correlation existing between frequencies and frequencies and between frequencies and temperature whose time history has been also made available. First of all only one temperature time history characterizing the bridge site is extracted from the eight available ones: four bridge sections are equipped with two temperature sensors (in the top and bottom flange respectively) indeed. This target is met by simply averaging the data acquired by the eight sensors; the obtained results are depicted in Fig. 5.7.

Secondly, the correlation analysis is carried out. Figs. 5.8 and 5.9 summarize the obtained results. In the former figure, modes L1 (a), V1 (c) and T1 (e) time histories over two years of continuous monitoring are depicted underlying their seasonal and daily fluctuations. In addiction to this, in the detailed view (Fig. 5.8 (b), (d) and (f)), ten days of variation of the same frequencies are superimposed to the corresponding temperature time history: at a first glance it is immediately deducible that frequency and temperature are closely related to each other and that an increasing in temperature reasonably produce a decrease in modal frequencies and vice versa. Moreover, due to the relationship between modal parameters and environmental factors (temperature in the specific case), a close correlation among frequencies is foreseeable. Such dependences are numerically determined through the calculation of the correlation coefficients whose trend is graphically represented in Fig. 5.9. As expected frequencies are remarkably correlated to each other (Fig. 5.9 (a)) even if modes V1 and T1

reveal a slightly weak dependence, being also less correlated with temperature variation. In fact, looking at Fig. 5.9 (b), beside the confirmed marked anti-correlation between frequencies and temperature (the absolute values of correlation coefficients are always bigger than 0.6), it appears quite clearly what has been just stated concerning modes V1 an T1.

With a view to applying the identified frequency time histories for damage detection purpose it could be also interesting to have a general idea about the kind of relationship existing between them. Differently to what previously done in Chap. 4, a numerical model which also allows to account for environmental factors is not available in this case. for this reason the only way to gain such kind of evaluation is to plot frequency time histories against each other in order to visually grasp the potential existence of linear or non-linear correlations among them. Despite this method is the fastest one, and a very direct way to extract this information in a qualitative way, it is necessary to remember that quantification and evaluation of relationship in the hyperplane constituted by the twelve modal frequencies are not trivial problems to be addressed and furthermore they are merely not in the aim of the present dissertation even if potentially relevant for a correct reading of the following results. In Fig.5.10 the synthetic results of a more deepened analysis are shown. The choice of the plotted frequencies is non random but reflects well definite observation on the data, especially in the light of the following considerations:

- V1 and L1 modes are the less sensitive to temperature and damage effects (see the following Sec. 5.3.1.1) respectively;
- V2 and V3 modes are the lowest ones after V1 and represent important cases to be investigated essentially for two reasons: the former consists in the fact that lower modes are generally the most reliably identified (confirmed by the success rate of 100%, see Tab. 5.1) and the latter is that vertical modes are in most cases vary damage sensitive;
- VA mode is the most damage sensitive to damage scenario DM4 (Sec. 5.3.1.1), the most severe one among those that have been considered, and will be exploited for this reason for the comparison between Linear and Local PCA (see Subsec. 5.3.3.3) in presence of artificially introduced non -linear correlations.

Fig. 5.10 mainly reveals a prevalent linear behavior which is coherent with the characteristics of the structure that, despite its very slender structural scheme, is made of concrete revealing for this reason a remarkable sensitivity essentially to changing temperature. However, some weak non linearities can be read in Fig. 5.10(c) and (d) and affect the mutual behavior between other modes not reported here for sake of synthesis. Again it is appropriate remarking that the estimation of relationships among frequencies, here presented only in a

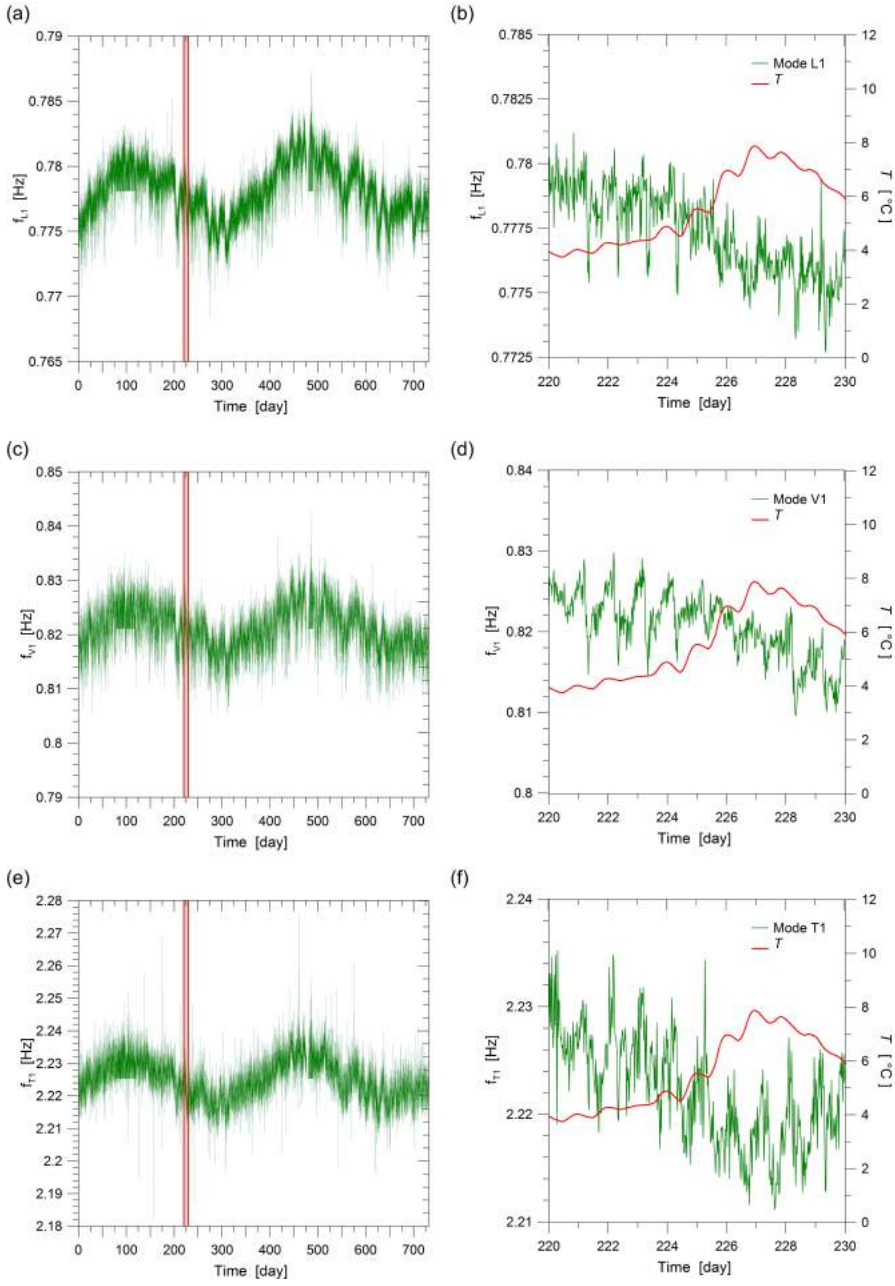

Figure 5.8: Identified frequency time histories of modes L1 (a), V1 (c), T1 (e). Detailed view of the daily fluctuations for the same modes, (b) (d) and (f) respectively, overlapped with the corresponding variation of temperature.

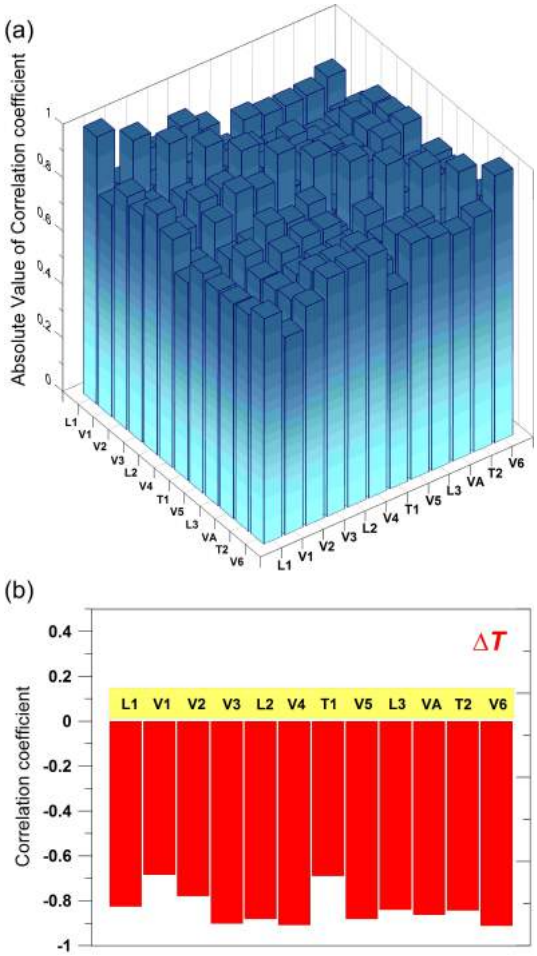

Figure 5.9: Correlation coefficients of identified frequencies between each other for the Infante Dom Enrique bridge (a) and between frequencies and variation of temperature data ΔT (b).

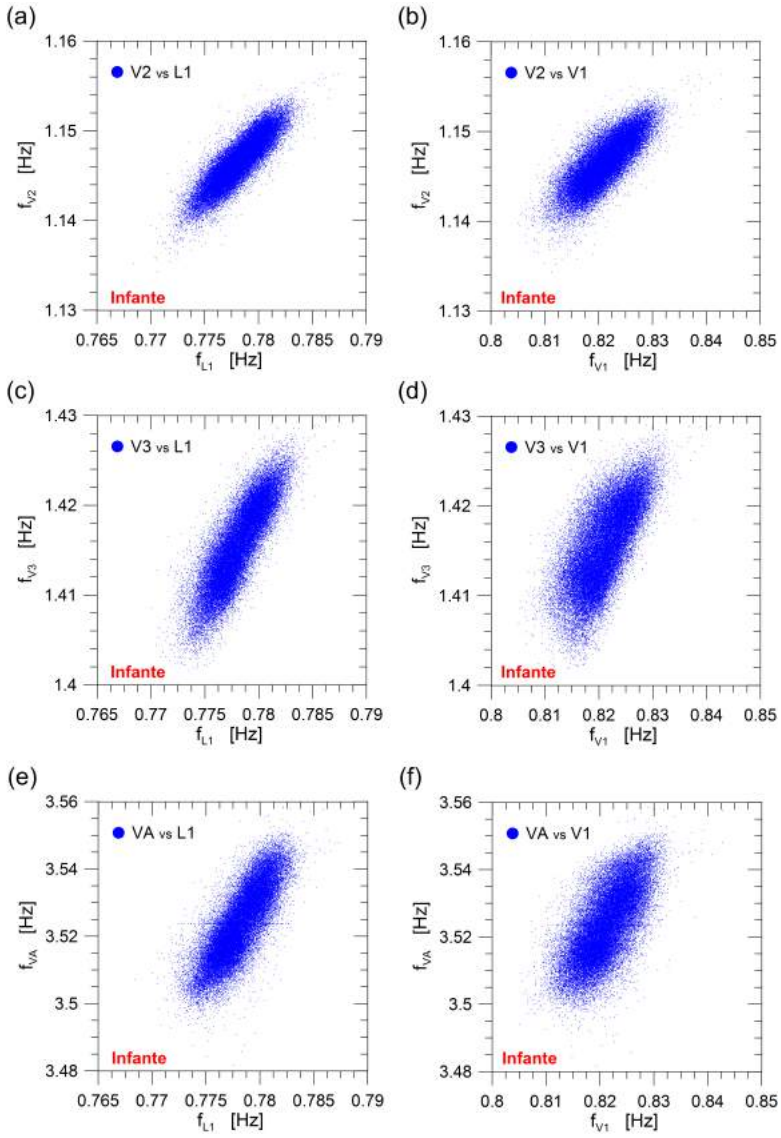

Figure 5.10: Plot of the identified frequency time histories of modes V2, V3 and VA versus the ones of mode L1 (a),(c),(e) and V1 (b),(d),(f), respectively.

qualitative manner, is not a trivial problem and generally out of the aim of the thesis.

5.3.1.1 Numerical modeling

In order to go on towards the application of damage detection techniques, a short consideration should be devoted on the numerical modeling developed at FEUP for a correct interpretation of the dynamic behavior arisen from AVT of the Infante bridge, and successively for evaluating damage effects on modal parameters. The bridge is modeled with the ANSYS software using 3D bar finite elements characterized by cross section properties (area, moments of inertia, torsion moment of inertia and shear deflection constants) consistent with the geometry of the deck, arch and columns. The same materials constituting FE model elements behave in the same way of real materials being their properties equal to those provided by in situ tests performed during bridge construction. To be more precise, an elasticity modulus of 37 GPa is adopted for deck and arch concrete and an elasticity modulus of 34 GPa (value defined by EC2 (CEN 2004) for a C35745 concrete) is considered for the columns.

Most of the problems met during the modeling of the Infante bridge consisted in the evaluation of the behavior of the connection between deck and substructure (arch and column) because, in the real bridge, for low levels of excitation (that is the common condition), friction forces produced in the connection can prevent rotation and displacement giving back, in this way, the modeling of their behavior very difficult. For this reason four different models of the bridge have been developed with the final result of the so called "$Model$ 4" (see [103]) where MAC is bigger than 0.95 for all the twelve considered modes while errors in modal frequencies estimates are always smaller than 5%.

Once the model has been developed and optimally tuned, with the purpose of evaluating damage effects on modal properties four different damage scenarios are considered plausible in the bridge and simulated, as commonly done in literature, in a simplified manner through a reduction of the inertia in limited segments of selected components of the bridge. In the specific case all damages whose position and extension are represented in Fig. 5.11 have been simulated by a reduction in the vertical bending inertia of 10% over the lengths of $8.75m$, $10.0m$, $3.0m$ and $5.0m$ for DM1, DM2, DM3 and DM4 respectively .

The assumed configuration for the hypothesized fault conditions can be considered as representative of quite small damages that do not compromise in any case the safety of the bridge and can be deem, on the other hand, as the consequences of the beginning of a deterioration process or as the result of

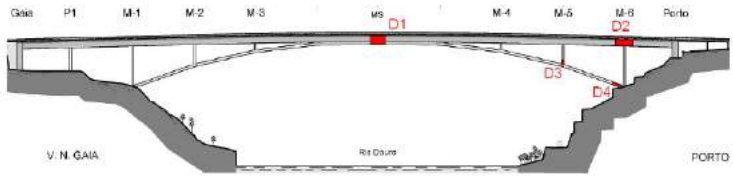

Figure 5.11: Lateral view of the Infante Dom Enrique bridge with the highlighted position of the four hypothesized damage scenarios.

Table 5.2: Characteristics of the 12 steadily identified modes of the Infante Dom Enrique Bridge and frequency shift corresponding to the four different damage scenarios hypothesized for the bridge.

Frequencies			Damage scenario frequency shift			
$n^o mode$	*type*	*value* [Hz]	$DM1$	$DM2$	$DM3$	$DM4$
1	L1	$0,7777$	0	0	0	0
2	V1	$0,8208$	0	-0.19	-0.108	-0.059
3	V2	$1,1459$	-0.112	-0.025	-0.007	-0.014
4	V3	$1,4154$	-0.126	-0.16	-0.133	-0.072
5	L2	$1,7509$	0	0	0	0
6	V4	$2,0113$	-0.001	-0.141	-0.028	-0.1
7	T1	$2,2248$	0.038	0	0	0
8	V5	$3,0408$	-0.137	-0.079	-0.045	-0.248
9	L3	$3,3371$	0.009	0	0	0
10	VA	$3,5214$	$-0,001$	$-0,011$	$-0,251$	$-0,323$
11	T2	$3,7603$	0	0.001	0	0
12	V6	$4,3785$	-0.001	-0.006	-0.001	-0.022

some extreme action. In Tab. 5.2 the relative variations of the considered modal frequencies Δf (Eq.4.14) for each damage scenario are reported. It can be observed that vertical bending modes are the most sensitive to damage occurrence, coherently to what previously observed in Chap. 4 even if for a different structural bridge scheme. Moreover, it is worth underlining how variation induced in modal frequencies are very small (of few per mil) also in this case.

5.3.2 Regressive model

Following the same approach adopted for the continuum model of suspension bridge in the previous chapter, a classic linear multivariate regressive model is

applied at first in order to later compare the effectiveness of its use for structural health monitoring in the case of real bridge data with those of PCA-based techniques. First of all, it is worth specifying that, despite from FE model analysis two modes (the first two lateral ones, L1 and L2 to be more precise) have revealed insensitivity to damage occurrence, the regressive model and the following applications will be carried out considering all the identified frequency time histories, including those of the just mentioned lateral modes. The reason of this choice lies in the fact that without knowing *a priori* the sensitivity or insensitivity to damage of modes, the only reasonable condition for discarding a mode in the application to SHM by multivariate statistical techniques, is the unreliability in its identification, and it is not the case of modes L1 and L2 which are characterized, on the contrary, by a success rate close to the 100% (see Tab. 5.1).

As already specified in Sec. 4.5.2 the considered MLR model is fully implemented in MATLAB, including the procedure for β coefficients optimization. For the sake of synthesis, the results concerning damage detection are immediately presented. In Fig. 5.12 the control charts are built for the four different considered damage scenarios by setting the group averaging size gr equal to 24, considering one year of training period for the model and by artificially adding damage as a frequency shift at day n^o 545.

As it can be observed, the success rate in damage detection is very high in all the four different scenarios. This achievement can be attributed to two distinct concurrent reasons. First of all, in confirmation to what stated in Subsec. 5.3.1 and clearly observable in Fig. 5.10, the prevalent linear correlation among features makes very effective the application of the multivariate linear regressive model. Secondly, the acquisition every half an hour, instead of hourly data as in the numerical application, offers a bigger statistical sample size (two times bigger than the suspension bridge study case) which allows a better estimation of the parameters of the regressive model. In the control charts a new coefficient is introduced, namely OR_{dmg}. It is defined as the ratio between the outliers percentage in damaged period and in observation period, that is:

$$OR_{dmg} = \frac{Out_{dmg}}{Out_{obs}} \tag{5.2}$$

Effectively its adoption would be necessary only in the following PCA-based techniques applications but to be coherent in the presentation of the results such coefficient is introduced and calculated also in SHM by regressive model. OR_{dmg} coefficient represents a very simple and rapid way to evaluate how much bigger the percentage of outliers in the damaged period is expected to be in comparison with that in the observation period. After this first application the capability in early damage detection is tested for damage scenarios DM3

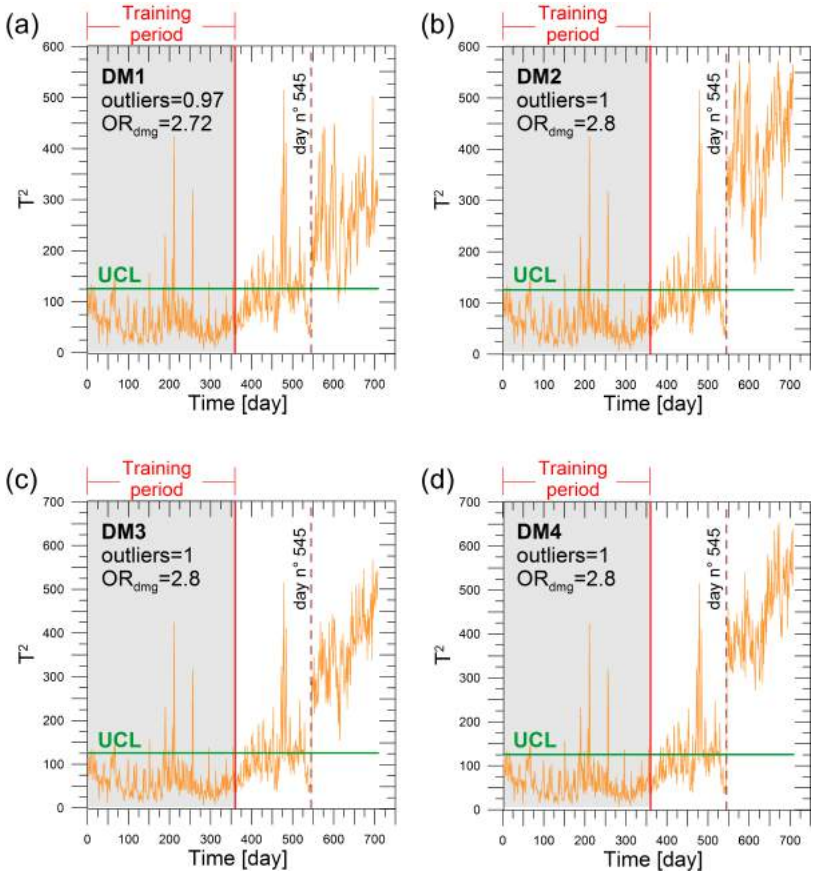

Figure 5.12: Control charts obtained with regressive models for the four different damage scenarios hypothesized for the Infante Dom Enrique bridge.

and DM4 which can be considered the most severe ones in terms of induced variation of resonant frequencies. The analysis are repeated for varying gr from 8 to 48 and the corresponding control charts are depicted in Fig. 5.13. What can be observed essentially is that for increasing the group averaging size, while a slight increment of the outliers percentage occurs, the OR_{dmg} considerably decreases being such coefficient for gr equal to 8 almost 3 times bigger than in the case for gr equal to 48, for both the considered damage scenarios.

5.3.3 PCA-based techniques

In the present section the multivariate statistical PCA-based techniques for structural health assessment (Chap. 2) are tested in the case of real bridge data for the different damage scenarios previously introduced and described in Subsec. 5.3.1.1. Unlike in the previous case of multivariate regressive model application, where parameter optimization is already implemented in the adopted routines, in the case of PCA-based techniques a choice of criteria enabling the optimal setting of the involved parameters must be properly established being exceedingly crucial to gain a good performance in damage detection. The parameters involved in the procedures, similarly to what previously stated in Chap. 4, are the number of retained principal components l in the Linear PCA and, again, number of retained principal components l and number of clusters q in the case of Local PCA. After parameter optimization and the application of Linear and Local PCA to the four considered damage scenarios, a strict comparison among these two last techniques is carried out in order to verify their capability in small damage detection and their effectiveness in the case of data with remarkable artificially added non-linear correlation among frequencies.

5.3.3.1 Linear PCA

Again, the first step towards an effective SHM through the application of the classical Linear PCA, consists in a preliminary evaluation of the weight of the retained PCs in the procedure adopted for the removal of the environmental effects on frequencies aimed at addressing an optimal damage detection. Being equal to 12 the overall number n of steadily identified modal frequencies, and so of the features which can be applied in the statistical process control, the number of retained PCs can potentially range from 1 to $n-1$, that is 11. Differently from the numerical case considered in Chap. 4, nothing is known

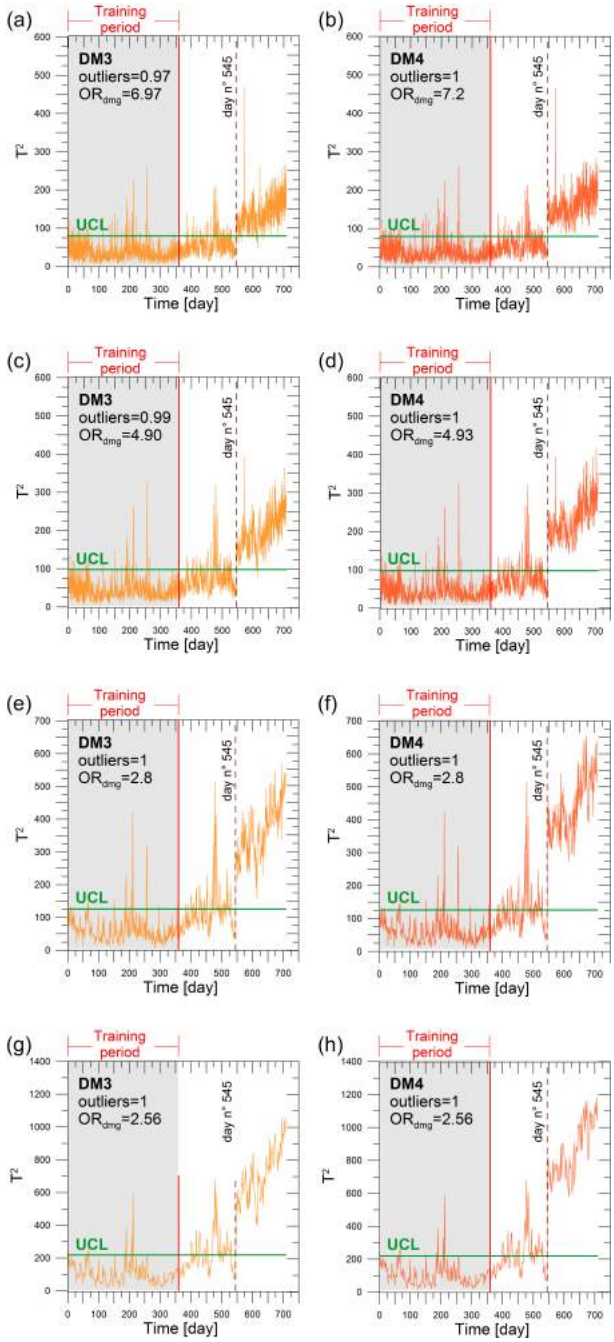

Figure 5.13: Control charts for damage scenarios DM3 and DM4 of the Infante Dom Enrique bridge obtained with regressive models for varying the group averaging size *gr* from 8 to 48..

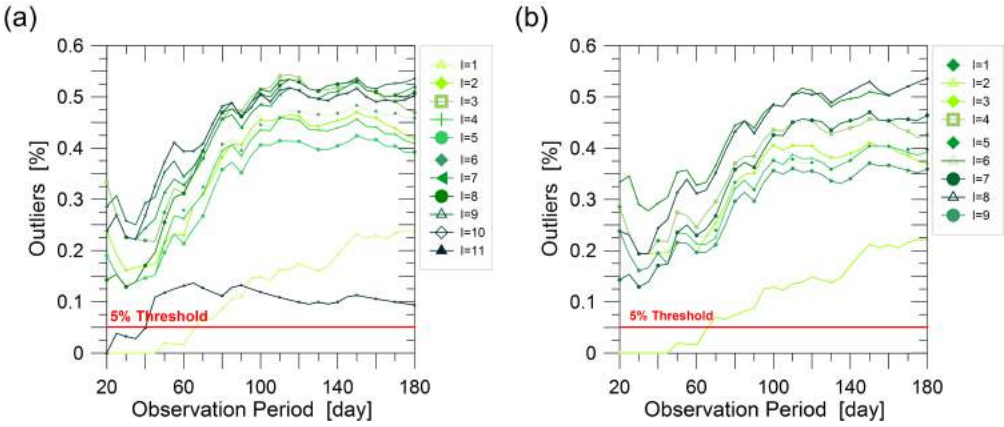

Figure 5.14: Outliers percentage in the observation period for varying the length of the same observation period from 20 to 180 and the number l of the retained PCs. Results obtained considering all the available frequency time histories (a) and, to the contrary, discarding those damage insensitive (b).

about the external environmental and operational agent that mainly influence variations in resonant frequencies, even if the wide literature in the field suggests that in the case of concrete medium-span bridges humidity, temperature and traffic generally fulfill a leading role.

One more time, the objective criterion established for setting the number of PCs l one has to retain for an optimal SHM is to choose a number capable to guarantee in the observation period a number of outliers as close as possible to the imposed 5% of outliers in the training period. In Fig. 5.14 (a) the preliminary results are presented, and more specifically, the outliers percentage for varying the length of observation period is plotted for different values l of the retained PCs, estimated through one year of training period and considering all the twelve available features and a group averaging size gr equal to 24. What can be observed at first glance is that, in the case of real bridge data, the application of Linear PCA seems to loose effectiveness in cleaning the environmental effects, being the outliers percentage in the observation period always strongly higher than the desired 5%. Secondly, it appears quite clear how, on the contrary, an extreme choice of retained PCs (only 1 and 11) allows to considerably reduce this gap.

With the purpose of better understanding the reason of this result and if could be related to the presence of a copious number of features, some of which potentially weakly affected by environmental factors, the analysis are repeated accounting for only 10 features and discarding the resonant frequencies insensitive to damage that is those of $L1$ and $L2$ modes. This choice makes sense also in light of the experience reported in many literature works that lateral

Table 5.3: Outliers ratio, OR, obtained adopting 12 and 10 frequency time histories and for varying the number l of retained principal components.

freq	retained PCs l										
tot	1	2	3	4	5	6	7	8	9	10	11
12	4.67	7.82	8.74	7.62	7.31	8.63	9.85	9.65	10.26	9.65	1.83
10	4.37	6.91	7.92	7.31	6.70	7.41	10.16	8.84	10.16	/	/

modes generally reveal low sensitivity both to damage and to environmental facts. As a matter of fact this additional investigation shows a slightly better behavior as reported in Fig. 5.14 (b), but above all reveals that the optimal results obtained in Fig. 5.14 (a) for extreme values of l substantially disappear. The calculation in both the different situations of the OR as defined in Eq. 4.15 confirms what graphically observed (see Tab. 5.3).

To further investigate if this aspect could enable or not damage detection capability and to consequently adopt the most proper number l, the OR_{dmg} coefficient (Eq. 5.2) is introduced with the purpose of establishing if, despite the high outliers rate in the observation period, damage still remains detectable or not. In both cases, with 12 and 10, OR_{dmg} is calculated in the four different damage scenarios for varying l from 1 to the maximum admitted value. The results presented in Fig. 5.15 show that damage detection is still possible, being OR_{dmg} always bigger than 1.5, and that the results gained for extreme values of l are not reliable. Moreover a natural remark arising from this preliminary analysis is that, in the case of real bridge data, one year of training period could not be sufficient to set the PCs in the best possible manner. Few additional considerations on this last aspect are carried out in Appendix A.4. In conclusion, for the following applications l is set to 5 being the intermediate number of retained PCs that supply the best results both in terms of OR and OR_{dmg}. Furthermore, all the 12 available features are considered being formally more correct in the most generic case where a modal frequency is steadily identified but no available FE model can certainly inform about the sensitivity or not to damage.

Then the control charts built by considering Linear PCA in the cleaning procedure are represented in Fig. 5.16. The procedure seems to be very effective even if weakly worse in comparison to those obtained through regressive model in terms both of outliers percentage and in OR_{dmg}. Finally the early damage detection capability is evaluated, always in damage scenarios DM3 and DM4, by imposing gr equal to 8, 12, 24 and 48 respectively. Even in this case the results, shown in Fig. 5.17 reveal higher potentialities in the adoption of regressive models rather than with Linear PCA.

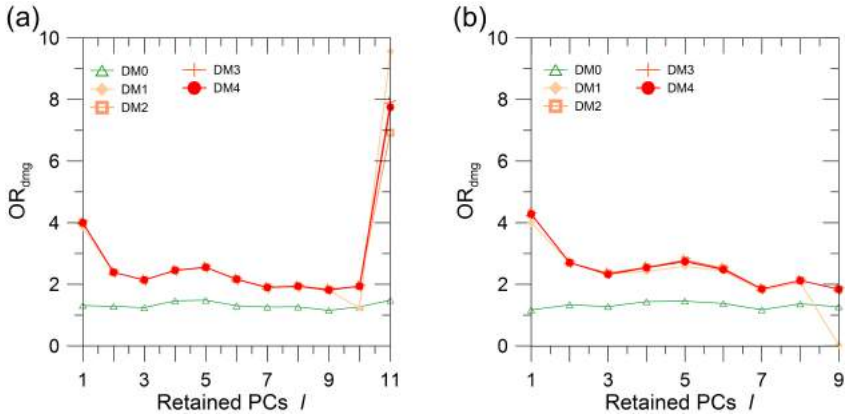

Figure 5.15: OR_{dmg} obtained through the use of Linear PCA for the four different damage scenarios hypothesized for the Infante Dom Enrique bridge and carried out considering all the available frequency time histories (a) and, to the contrary, discarding those damage insensitive (b).

5.3.3.2 Local PCA

Also in the case of Local PCA some preliminary parametric analysis are carried out in order to obtain an effective SHM and to successively guarantee a proper comparison in terms of damage detection capability between the two different techniques. The two main parameters of Local PCA, that is the number of clusters q and the number of retained PCs l for the application of Linear PCA in each cluster, are established, again, through the criterion of imposing the 5% of outliers in the observation period. Contrarily to what happened in the previous application of the linear methods (regressive models and Liner PCA), in the case of Local PCA OR seems to be steadily closer to the imposed threshold even if always higher.

In addiction to that, another empirical criterion is adopted to the purpose of having confirmation on the optimal choice of q and l. Being available different damage scenarios, they are previously tested with a parametric analysis where the outliers percentages in the damaged period are calculated for varying both q (from 2 to 10) and l (from 1 to 11). The general results of these mandatory preliminary investigations are not reported here for sake of synthesis and because not trivial to be summarized. Anyway for the following application q and l are set equal to 4 and 8 respectively.

The first application is always the test of Local PCA in the four damage scenarios with a group averaging size gr equal to 24. Both graphically and numerically (through OR_{dmg} coefficient values), it clearly appears that the

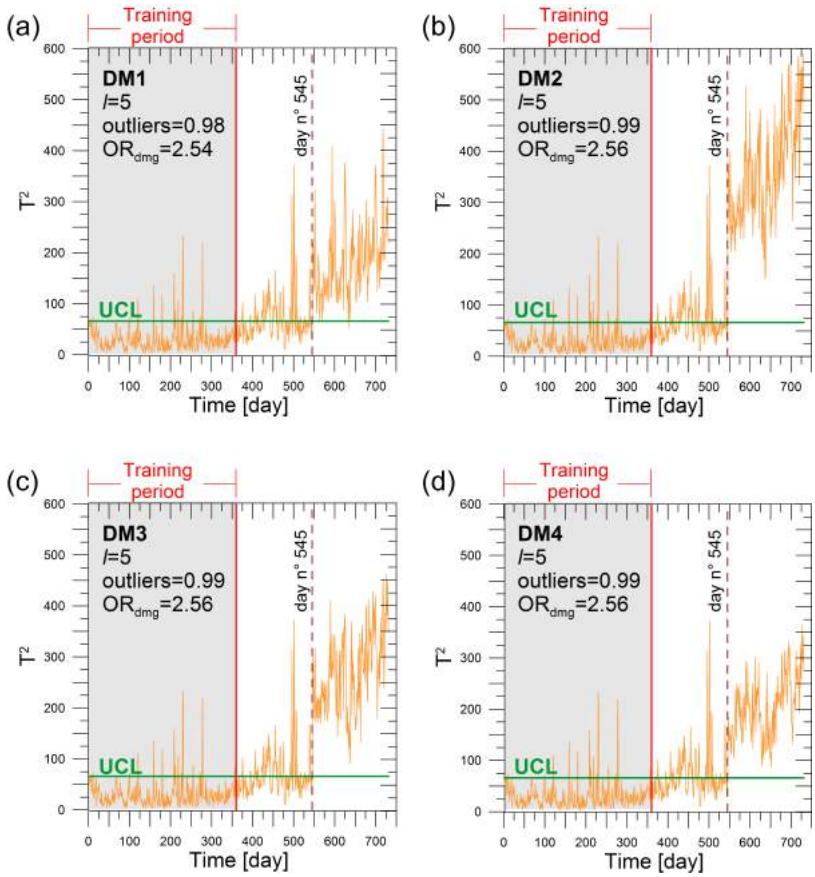

Figure 5.16: Control charts obtained for the four different damage scenarios hypothesized for the Infante Dom Enrique bridge with optimally set parameters of the linear PCA.

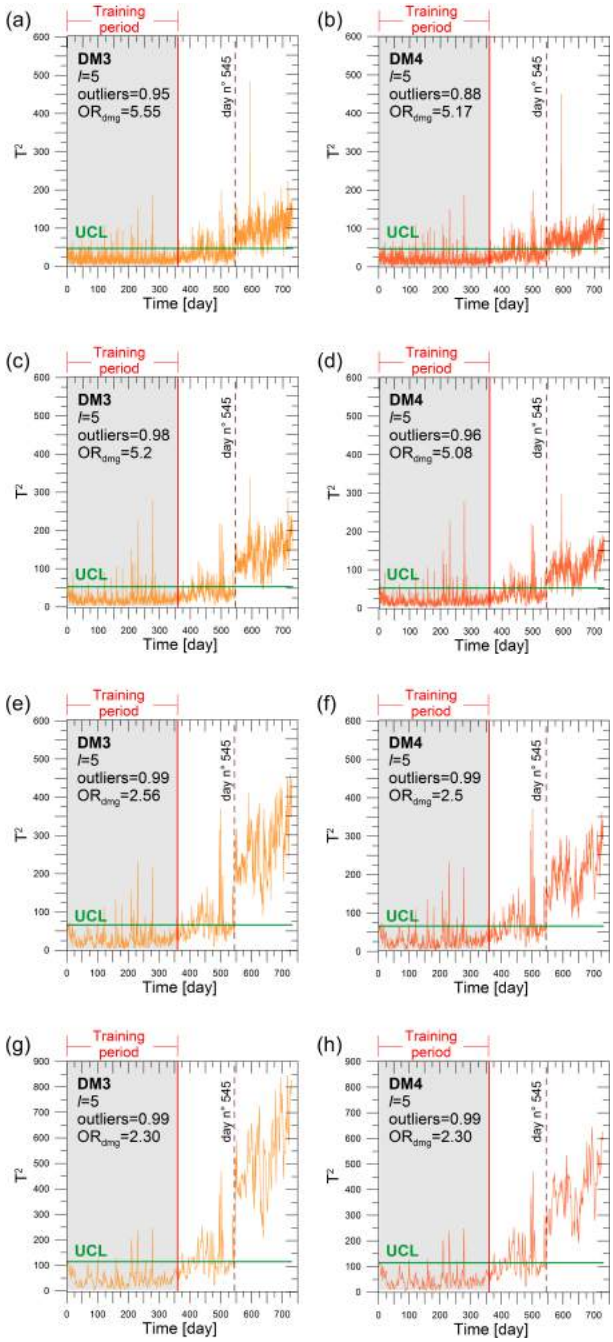

Figure 5.17: Control charts for damage scenarios DM3 and DM4 of the Infante Dom Enrique bridge obtained with optimally set parameters of the Linear PCA for varying the group averaging size gr from 8 to 48.

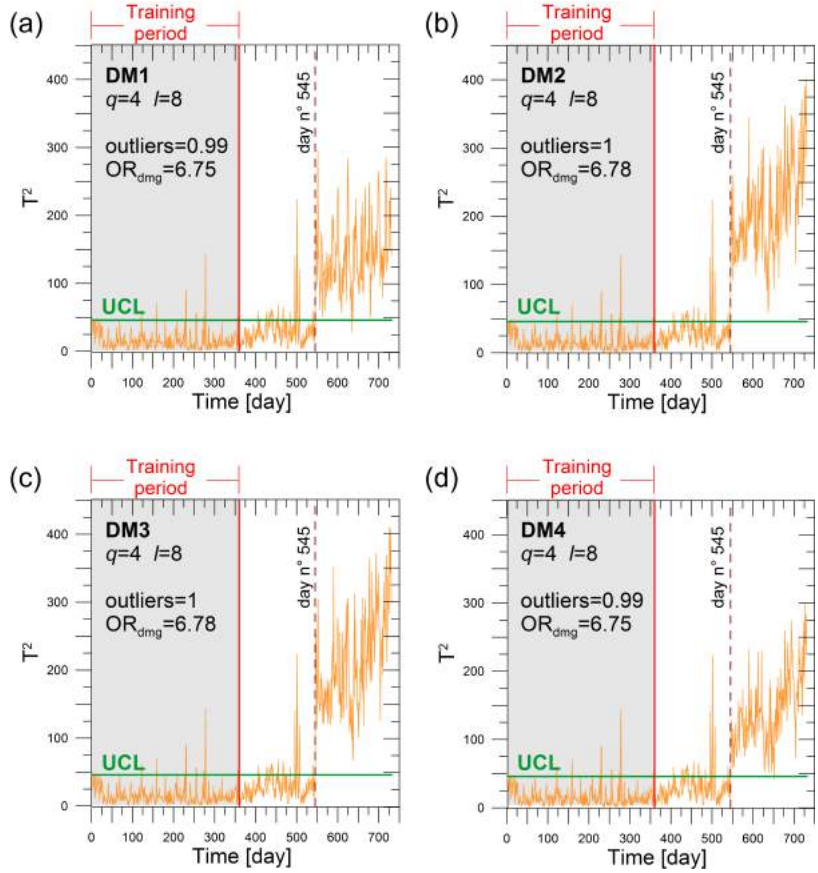

Figure 5.18: Control charts obtained for the four different damage scenarios hypothesized for the Infante Dom Enrique bridge with optimally set parameters of the Local PCA.

gained results, depicted in Fig. 5.18, express a deeply different, in particular better, situation in comparison with MLR models and Linear PCA applications. Actually, despite no significant variations of the outliers percentage in the damaged period occur, already optimized in the previous applications, OR_{dmg} coefficient notably increases being more than two times higher than by using the other methods.

Also in the application for early damage detection the situation seems to be more promising by applying the local PCA method (see Fig. 5.19). Even if the differences in regard to the other methods tends to be less marked for decreasing gr, for almost equal percentages of outliers in the damaged period, Local PCA enhances in any case the OR_{dmg} coefficients which means, from another point of view, that the percentage of outliers in the observation period

is always more restrained, limiting in fact, the number of false positive detection during the common use of the structure.

5.3.3.3 Comparison between Linear and Local PCA

Being the performances of multivariate regressive model and Linear PCA comparable, and being, on the other hand, the application of PCA-based techniques in the main aim of the present thesis work, a more comprehensive comparison between Linear and Local PCA is necessary. For these reasons additional analyses are carried out with two main purposes:

- the determination of the minimum detectable damage;
- the check of the capability of both techniques in identify damage occurrence in presence of remarkable non linear correlation among selected features.

To address the first target, damage scenario DM4 is considered because, being comparable the effects on frequencies with DM3, the considered methods have revealed to be slightly less effective in its detection. So in the theoretical hypothesis that a linearly increasing damage severity produces a linear increment of induced frequency shifts, outliers percentage in damaged period and OR_{dmg} coefficients are calculated with Linear and Local PCA method for increasing the severity of DM4 from 0 to 1. In Fig. 5.20 the results are presented for gr equal to 8 and 24. Looking at the obtained curves, if a value of OR_{dmg} coefficient equal to 3 is assumed as representative of damage occurrence, it appears clear how in the case of early damage detection, that is for gr set to 8, the damage detected by Local PCA is more or less the one half of that detectable by Linear PCA.

Finally to further emphasize the capability of local PCA in explaining the non linear correlation among frequencies even in the cases in which such non linearities could not be read easily, as in the Infante Bridge, the correlations among the original identified frequency time histories are properly corrupted. Considering as benchmark always damage scenario DM4, by fixing as reference the frequency of mode L2, referred as f_{l2}, frequency time history of mode VA,the most sensitive to the considered damage configuration, is corrupted by adding a non linear trend (quadratic to be more precise). The corruption of only one frequency time history automatically implies the modification of its correlation with all the remaining considered features. In Fig. 5.21 (a) and (b) the data before and after corruption respectively are shown and in Fig. 5.21 (c) and (d) the corresponding histograms are presented. Finally the control

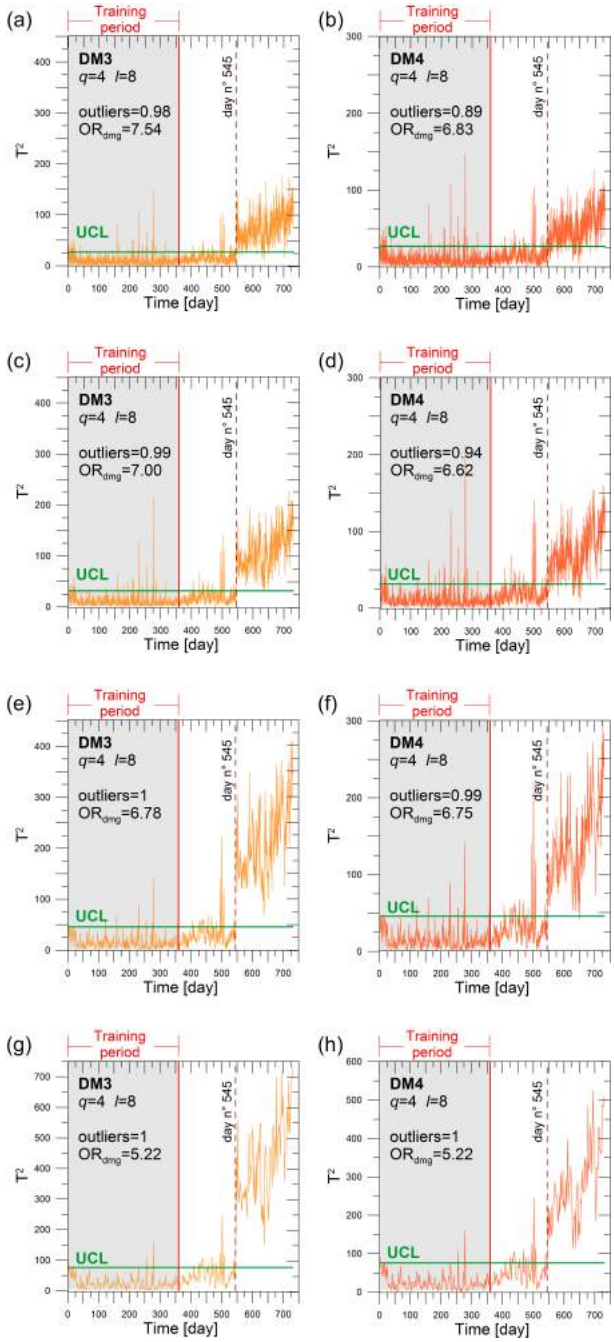

Figure 5.19: Control charts for damage scenarios DM3 and DM4 of the Infante Dom Enrique bridge obtained with optimally set parameters of the Local PCA for varying the group averaging size *gr* from 8 to 48.

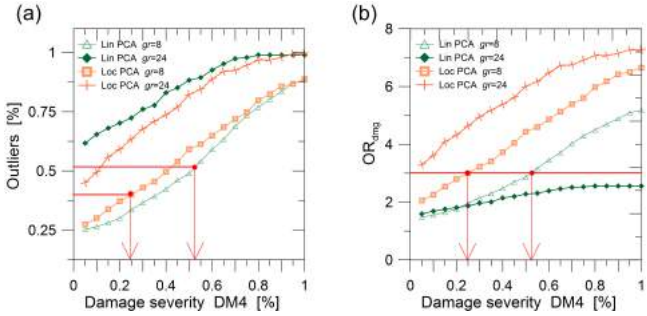

Figure 5.20: Outliers percentage in damaged period (a) and OR_{dmg} coefficients (b) for linearly increasing the severity of damage scenario DM4 obtained by applying Linear and Local PCA with gr equal to 8 and 24.

charts in the case of early damage detection (gr= 8), are built by using Linear Fig. 5.21 (d) and Local Fig. 5.21 (e) PCA underlining how in the latter case there is no substantial loss of effectiveness.

5.4 Discussion of results

In this chapter the multivariate statistical techniques described in Chap. 2 and implemented in the proposed closed loop procedure for SHM of bridges (Chap. 3), are applied to the frequency time histories data identified from the real response measurements of the Dom Infante Enrique Bridge, over Douro river in Porto (PT).

After a brief description of the structure, the frequency data together with temperature measurements, kindly made available by the ViBest of the FEUP, have been analyzed at first, underlining the correlation existing between frequencies and frequencies and between frequencies and temperature. Different potential damage scenarios are then hypothesized and the relative variations on the modal frequencies estimated. These variations, artificially applied to the frequency time histories, are adopted with the purpose of verifying the effectiveness of different damage techniques.

Both MLR and PCA-based techniques have revealed a pretty good effectiveness in damage detection. Despite no remarkable non-linear correlation among frequencies have arisen, in the case of real bridge data the techniques based on the hypothesis of linear correlation, namely MLR and Linear PCA, have shown a limited capability in the removal of the environmental effects, entailing in such a way an extremely more larger number of false positive detections in the

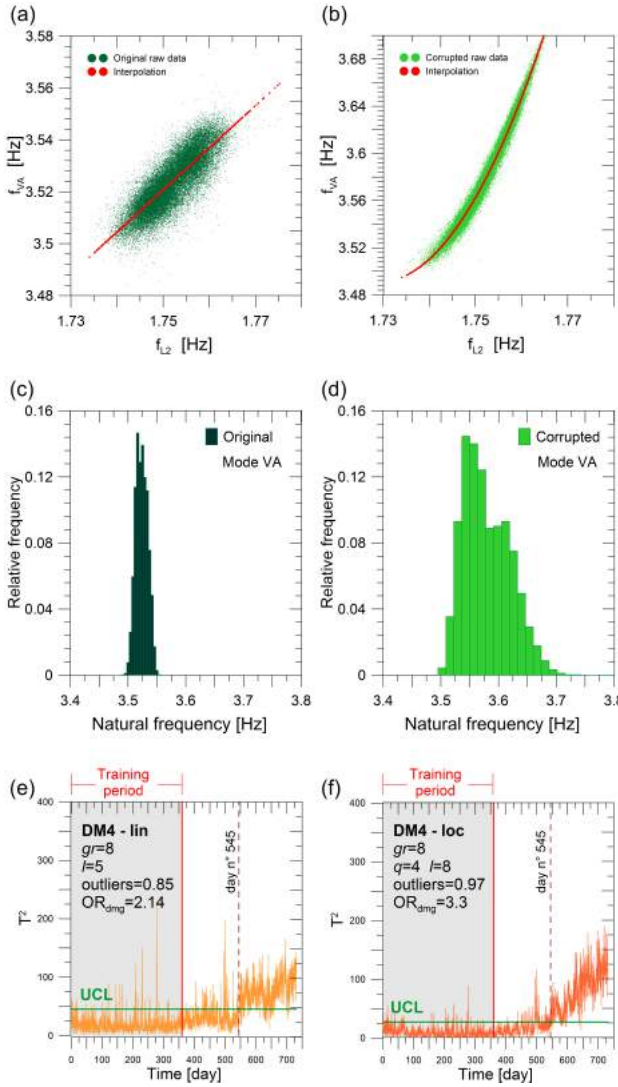

Figure 5.21: Control charts for damage scenarios DM3 and DM4 of the Infante Dom Enrique bridge obtained with optimally set parameters of the linear PCA for varying the group aeragong size *gr* from 8 to 48.

observation period, when no damage occur. This fact has suggested that for the application of such techniques training period longer than one year could be appropriate.

On the contrary, Local PCA has revealed an high reliability: not only it is comparatively effective in damage detection with the other techniques, but it also guarantees a satisfactory percentage of outliers in the observation period.

6

CONCLUSION AND RECOMMENDATION

In this concluding chapter the outcomes of the research are synthetically resumed and some future developments and improvements are traced

Contents

The present work of thesis inserts itself in the field of Structural Health Monitoring of infrastructures, with particular reference to long span bridges. Despite the adulthood reached by this practice under many points of view, there is, still now, a lack of knowledge on the actual effectiveness of the most of the developed techniques in damage detection in the case of real bridge data.

Trying to partially bridge this gap, in the present work of thesis a closed loop procedure, which goes from modal properties identification to the extraction of damage sensitive features, is presented at first. Such procedure is composed by well established tools which are however properly combined together and implemented in an automated fashion. The first chapters of the manuscript are so devoted to introduce the theoretical background especially for what concern the statistical techniques enabling damage detection.

Then the proposed methodology is fully applied to the case of a numerical suspension bridge with main cable damage. After the preliminary discussion on the evaluation of wind, temperature and damage effects on the modal frequencies of the suspension bridge, the procedure for cleaning the environmental effects from structural modal parameters is applied to one and half year of frequency time histories identified from artificially generated response of the bridge under changing temperature and wind loading. In particular the effectiveness of different implemented techniques is tested, namely MLR, Linear PCA and Local PCA.

After the introduction of an artificial damage to the frequency time histories, the control charts are built in order to check the capability in damage detection. Despite all the mentioned techniques have revealed to be very good tools, LocaL PCA has demonstrated an higher reliability especially when marked non-linear correlation among frequencies, due to wind effects, are present (as for instance in the considered case of the Akashi Kaikyo Bridge).

Then in order to clarify the real capability of the adopted techniques in cleaning environmental and operational effects and in damage detection, their application is considered to the frequency time histories identified from the real response measurements of the Dom Infante Enrique Bridge, over Douro river in Porto (PT). Accounting for a larger variety of external factors effects, such as wind temperature as well as humidity and traffic, the real bridge data represent the actual test bed for the implemented techniques.

Again damage is artificially added to the data and the damage detection procedure is applied. Despite clearly non-linear correlations among frequencies are not visible, MLR and Linear PCA evidently give worse results, not revealing loss in damage detection, but, on the contrary, showing a loss of effectiveness in the removal of environmental effects. This fact could be maybe mitigate by using training period longer than one year to set the parameters of MLR

an Linear PCA. Conversely, Local PCA preserves a very good effectiveness in both senses, and reveals to be an optimal tool for the assessment of civil infrastructures.

The obtained results confirmed that the use of statistical method is a very promising tool for the condition assessment of bridges, and that the continuous monitoring is the future of SHM, even if many more steps forward should be made especially aimed at reducing the economical impact of the monitoring system installation. The presented techniques represent a step towards this direction essentially because their application entails a very limited number of sensors. However a bigger effort should be still supported for verifying the effectiveness of such technique on the most wide range of case possible.

Finally it is worth mentioning that the absolutely generality of the adopted techniques may open the door toward their application not only to bridges but also to any type of civil structure, as for example to historical buildings and wind turbines.

ACNOWLEDGEMENTS

It is a pleasure for me to express my gratitude to the many people who have helped me or have been an important part of my life in the last three and a half years. However, I have to express special thanks:

- to my tutors Professors A.L. Materazzi and F. Ubertini from the italian side, and Professors K. Thiele and U. Peil from the german one, for providing all the necessary resources for the development of my work, for encouraging me and for sharing their experience and knowledge;

- to Professors Filipe Magalhães, and Álavaro Cunha for receiving me at their group during three month, for their hospitality and for the generous contribution to my research;

- to H2CU (Honors Center of Italian Universities) for the financial support.

RINGRAZIAMENTI

- ringrazio gli amici Chiara, Marco, Francesco M., Gabriele, Giulia, Paolo, Francesco C., Celeste, Eleonora per essere presenti nonostante la vita, soprattutto lavorativa spesso ci tenga lontani;

- ringrazio tutti colleghi di lavoro con cui ho avuto l'onore di collaborare e che hanno consentito attraverso la loro esperienza la mia crescita personale accademica e umana;

- ringrazio in particolare Antonella, Filippo e Nicola, grandi colleghi e veri amici: mi avete sempre saputo guidare, sostenere e consigliare nelle mie scelte al lavoro e fuori.

- ringrazio Tommaso ed Alessandro colleghi di dottorato, grandi compagni di avventura e amici unici;

- ringrazio la mia compagna e futura moglie, Laura, che in questi tre anni insieme ha saputo darmi la cosa più bella ed importante, una famiglia crescendo, maturando e imparando giorno dopo giorno, con me, cosa significa essere genitore. Grazie per non avermi fatto mai mancare il sostegno anche quando ero lontano e soprattutto nei momenti più difficili che ho dovuto affrontare;

- ringrazio mia figlia, Ginevra: lei più di chiunque altro è stato il motore e la ragione che ha dato senso alle tante fatiche e ai tanti sforzi sostenuti. Lei mi ha dato la forza nei lunghi periodi lontano da casa e lei, tutte le sere tornando a casa, ha cancellato ogni traccia degli affanni giornalieri con un suo sorriso. A lei che anche ha reso meravigliosamente più complesso questo mio percorso, vorrei dire che quello che ho imparato è che sono veramente poche le cose che hanno un valore nella vita e che non richiedano impegno e sacrificio per poter essere ottenute;
- ringrazio i miei genitori: vorrei che un giorno anche mia figlia provasse per me lo stesso profondo senso di gratitudine e amore che io provo per voi ... allora anche io sarei per lei il miglior genitore del mondo.
- ringrazio infine i miei nonni: la vostra assenza fisica non cambia nulla essendo con me in ogni istante della mia vita, presente e futura.

Verba volant, scripta manent

Gabriele Comanducci

Perugia, Italia, May 2015

Bibliography

[1] Holford K. M. Acoustic emission in structural health monitoring. *Key Engineering Materials*, 413:15–28, 2009.

[2] Rytter A. *Vibrational based inspection of civil engineering structures*. PhD thesis, Aalborg University, 1993.

[3] Inaudi D. Cost-benefits analysis in shm projects. In *5th international conference on structural health monitoring of intelligent infrastructure (SHMII-5)*, pages 1–9, 2011.

[4] Doebling S.W., Farrar C. R., and Prime M. B. A summary review of vibration-based damage identification methods. *Identification Methods," The Shock and Vibration Digest*, 30:91–105, 1998.

[5] Santos J. P., Crémona C., Orcesi A.D., and Silveira P. Multivariate statistical analysis for early damage detection. *Eng Struct*, 56(0):273 – 285, 2013.

[6] Chang F.-K. Structural health monitoring: current status and perspectives. In *Proc. of the International Workshop on Structural Health Monitoring (Stanford,CA, USA, Sept. 18-20, 1997)*. CRC Press, 1998.

[7] Hunt D.L., Weiss S. P., West W. M., Dunlap T. A., and Freesmeyer S. Development and implementation of a shuttle modal inspection system. In *Proc. 8th International Modal Analysis Conference (Kissimmee, FL, USA, Jan. 29-Feb. 1, 1990)* , volume 2, pages 919–925. Society for Experimental Mechanics.

[8] Wauer J. On the dynamics of cracked rotors: a literature survey. *Applied Mechanics Reviews*, 43(1):13–17, 1990.

[9] Deraemaeker A. and Worden K. *New trends in vibration based structural health monitoring*, volume 520. Springer Science & Business Media, 2012.

[10] Sinou J.-J. A review of damage detection and health monitoring of mechanical systems from changes in the measurement of linear and non-linear vibrations. *Mechanical Vibrations: Measurement, Effects and Control*, pages 643–702, 2009.

[11] Sabnavis G., Kirk R. G., Kasarda M., and Quinn D. Cracked shaft detection and diagnostics: a literature review. *Shock and Vibration Digest*, 36(4):287, 2004.

[12] Ewins D.J. *Modal testing: theory, practice and application (mechanical engineering research studies: engineering dynamics series)*. Wiley, 2003.

[13] West W. M. Illustration of the use of modal assurance criterion to detect structural changes in an orbiter test specimen. In *Proc. of the Air Force Conference on Aircraft Structural Integrity (Sacramento,CA, USA, December., 1986)*, volume 1, pages 1–6, 1986.

[14] Lieven N. and Ewins D. Spatial correlation of mode shapes: The coordinate modal assurance criterion (comac)". In *Proc. of the 6th International Modal Analysis Conference (Kissimmee, Florida, USA,1988)*, volume 1, pages 690–695, 1988.

[15] Rahai A., Bakhtiari-Nejad F., and Esfandiari A. Damage assessment of structure using incomplete measured mode shapes. *Srtruct. Control HLTH*, 14(5):808–829, 2007.

[16] Adams R.D., Cawley P., Pye C.J., and Stone B.J. A vibration technique for non-destructively assessing the integrity of structures. *J. of Mech. Eng. Sc.*, 20(2):93–100, 1978.

[17] Dilena M. and Morassi A. Identification of crack location in vibrating beams from changes in node positions. *J. Sound Vibr.*, 255(5):915–930, 2002.

[18] Maeck J. and De Roeck G. Damage assessment using vibration analysis on the z24-bridge. *Mech. Syst. Signal Pr.*, 17(1):133–142, 2003.

[19] Leonard F., Lanteigne J., Lalonde S., and Turcotte Y. Free-vibration behaviour of a cracked cantilever beam and crack detection. *Mech. Syst. Signal Pr.*, 15(3):529–548, 2001.

[20] Kyriazoglou C., Le Page B.H., and Guild F.J. Vibration damping for crack detection in composite laminates. *Composites Part A: Applied Science and Manufacturing*, 35(7):945–953, 2004.

[21] Modena C., Sonda D., and Zonta D. Damage localization in reinforced concrete structures by using damping measurements. *Key Eng Mat*, 167:132–141, 1999.

[22] Pandey A.K. and Biswas M. Damage detection in structures using changes in flexibility. *J. Sound Vibr.*, 169(1):3–17, 1994.

[23] Topole K. G. Damage evaluation via flexibility formulation. In *Smart Systems for Bridges, Structures, and Highways, Proc of SPIE*, volume 3, pages 145–154. International Society for Optics and Photonics, 1997.

[24] Jaishi B. and Ren W.-X. Damage detection by finite element model updating using modal flexibility residual. *J. Sound Vibr.*, 290(1):369–387, 2006.

[25] Bernal D. and Gunes B. Flexibility based approach for damage characterization: benchmark application. *J. Eng. Mech. - ASCE*, 130(1):61–70, 2004.

[26] Farrar C. R., Baker W.E., Bell T.M., Cone K.M., Darling T.W., Duffey T.A., Eklund A., and Migliori A. Dynamic characterization and damage detection in the i-40 bridge over the rio grande. In *Los Alamos National Laboratory repoprt LA-12767-MS*, 1994.

[27] Salawu O. S. Detection of structural damage through changes in frequency: a review. *Eng. Struct.*, 19(9):718–723, 1997.

[28] Lifshitz J. M. and Rotem A. Determination of reinforcement unbonding of composites by a vibration technique. *J Compos Mater*, 3(3):412–423, 1969.

[29] Hearn G. and Testa R. B. Modal analysis for damage detection in structures. *Journal of Strucl Eng - ASCE*, 117(10):3042–3063, 1991.

[30] Sinou J.J. Numerical investigations of a robust identification of crack location and size in beams using only changes in ratio pulsations of the cracked beams. *Struct. Eng. Mech.*, 25(6):691–716, 2007.

[31] International Society for Optics and Photonics. *Damage detection and localization using natural frequency changes*, volume 1, 1992.

[32] Messina A., Williams E.J., and Contursi T. Structural damage detection by a sensitivity and statistical-based method. *J. Sound Vibr.*, 216(5):791–808, 1998.

[33] Koh B.H. and Dyke S.J. Structural health monitoring for flexible bridge structures using correlation and sensitivity of modal data. *Computers & structures*, 85(3):117–130, 2007.

[34] Mohan V., Parivallal S., Kesavan K., Arunsundaram B., Ahmed A.K. F., and Ravisankar K. Studies on damage detection using frequency change correlation approach for health assessment. *Procedia Engineering*, 86:503–510, 2014.

[35] Deraemaeker A., Reynders E., De Roeck G., and Kullaa J. Vibration-based structural health monitoring using output-only measurements under changing environment. *Mech. Syst. Signal Pr.*, 22(1):34 – 56, 2008.

[36] Surace C. and Worden K. Novelty detection in a changing environment: A negative selection approach. *Mech. Syst. Signal Pr.*, 24(4):1114 – 1128, 2010.

[37] Cross E.J., Manson G., Worden K., and Pierce S.G. Features for damage detection with insensitivity to environmental and operational variations. *Phil. Trans. R. Soc. As.*, 2012.

[38] Moser P. and Moaveni B. Environmental effects on the identified natural frequencies of the dowling hall footbridge. *Mech. Syst. Signal Pr.*, 25(7):2336–2357, 2011.

[39] Xu Y.L., Chen B., Ng C.L., Wong K.Y., and Chan W.Y. Monitoring temperature effect on a long suspension bridge. *Structural Control and Health Monitoring*, 17(6):632–653, 2010.

[40] Peeters B. and De Roeck G. One-year monitoring of the z 24-bridge: environmental effects versus damage events. *Earthquake Eng. Struct.*, 30(2):149–171, 2001.

[41] Peeters B., Maeck J., and De Roeck G. Vibration-based damage detection in civil engineering: excitation sources and temperature effects. *Smart Mater. Struct.*, 10(3):518, 2001.

[42] Li H., Li S., Ou J., and Li H. Modal identification of bridges under varying environmental conditions: temperature and wind effects. *Structural Control and Health Monitoring*, 17(5):495–512, 2010.

[43] Cross E.J., Koo K.Y., Brownjohn J.M.W., and Worden K. Long-term monitoring and data analysis of the tamar bridge. *Mech. Syst. Signal Pr.*, 35(1–2):16 – 34, 2013.

[44] Moaven B. and Behmanesh I. Effects of changing ambient temperature on finite element model updating of the dowling hall footbridge. *Eng. Struct.*, 43(0):58 – 68, 2012.

[45] Ubertini F., Hong A. L., Betti R., and Materazzi A. L. Estimating aeroelastic effects from full bridge responses by operational modal analysis. *J. Wind Eng. Ind. Aerodyn.*, 99(6):786–797, 2011.

[46] Westgate R.J., Koo K.Y., and Brownjohn J. M. W. Environmental effects on a suspension bridge's dynamic response. In *In Proceedings of the 8th International Conference on Structural Dynamics, EURODYN,(Leuven, Belgium, 4-6 july, 2011)*, pages 1208–1211.

[47] Zhang X. Influence of some factors on the aerodynamic behavior of long-span suspension bridges. *J. Wind Eng. Ind. Aerodyn.*, 95(3):149 – 164, 2007.

[48] Ubertini F., Materazzi A. L., and Comanducci G. Eigenfrequencies of damaged suspension bridges under wind. In *In Proceedings of the 12th Italian conference of Wind Engineering, IN-VENTO, Venice,Italy, 7-10 October, 2012.*

[49] Westgate R., Koo K.-Y., and Brownjohn J. Effect of vehicular loading on suspension bridge dynamic properties. *Struct. and Infr. Eng.*, 11(2):129–144, 2015.

[50] Zhu S., Levinson D., Liu H. X., and Harder K. The traffic and behavioral effects of the i-35w mississippi river bridge collapse. *Transportation research part A: policy and practice*, 44(10):771–784, 2010.

[51] Farrar C. R., Duffey T. A., Doebling S. W., and Nix D. A. A statistical pattern recognition paradigm for vibration-based structural health monitoring. *Structural Health Monitoring*, 2000:764–773, 1999.

[52] Sohn H. and Farrar C. R. A statistical pattern recognition paradigm for vibration-based structural health monitoring. *Smart Engineering System Design, Neural Networks, Fuzzy Logic, Evolutionary Programming, Complex Systems, and Data Mining, St. Louis, MO, USA*, 2000.

[53] Worden K., Sohn H., and Farrar C.R. Novelty detection in a changing environment: regression and interpolation approaches. *J. Sound Vibr.*, 258(4):741 – 761, 2002.

[54] Johnson R. A. and Wichern D.W. *Applied multivariate statistical analysis*, volume 4. Prentice hall Englewood Cliffs, NJ, 1992.

[55] Sohn H., Dzwonczyk M., Straser E. G., Law K.H., Meng T. H., and Kiremidjian A.S. Adaptive modeling of environmental effects in modal parameters for damage detection in civil structures. In *5th Annual International Symposium on Smart Structures and Materials*, pages 127–138. International Society for Optics and Photonics, 1998.

[56] Bodeux J.B. and Golinval J.-C. Application of armav models to the identification and damage detection of mechanical and civil engineering structures. *Smart Mat. Struc.*, 10(3):479, 2001.

[57] Yong L. and Feng G. A novel time-domain auto-regressive model for structural damage diagnosis. *J. Sound Vibr.*, 283(3):1031–1049, 2005.

[58] Posenat D., Kripakaran P., Inaudi D., and Smith I.F.C. Methodologies for model-free data interpretation of civil engineering structures. *Computers & Structures*, 88(7–8):467 – 482, 2010.

[59] Pearson K. On lines and planes of closest fit to systems of points in space. *The London, Edinburgh, and Dublin Philosophical Magazine and Journal of Science*, 2(11):559–572, 1901.

[60] Hotelling H. Analysis of a complex of statistical variables into principal components. *Journal of educational psychology*, 24(6):417, 1933.

[61] Rao C. R. The use and interpretation of principal component analysis in applied research. *Sankhyā: The Indian Journal of Statistics, Series A*, pages 329–358, 1964.

[62] Jeffers J.N.R. Principal component analysis of designed experiment. *Journal of the Royal Statistical Society. Series D (The Statistician)*, 12(3):230–242, 1962.

[63] Jeffers J.N.R. Two case studies in the application of principal component analysis. *Applied Statistics*, pages 225–236, 1967.

[64] Chen H. Principal component analysis with missing data and outliers. *URL: http://www. cmlab. csie. ntu. edu. tw/˜ cyy/learning/papers/PCA_Tutorial. pdf*, 2002.

[65] Cury A. and Crémona C. Assignment of structural behaviours in long-term monitoring: Application to a strengthened railway bridge. *Structural Health Monitoring*, 11(4):422–441, 2012.

[66] Bellino A., Fasana A., Garibaldi L., and Marchesiello S. Pca-based detection of damage in time-varying systems. *Mech. Syst. Signal Proc.*, 24:2250–2260, 2010.

[67] Yan A.M., Kerschen G., De Boe P., and Golinval J.C. Structural damage diagnosis under varying environmental conditions part i: a linear analysis. *Mech. Syst. Signal Pr.*, 19(4):847 – 864, 2005.

[68] Yan A.M., Kerschen G., De Boe P., and Golinval J.C. Structural damage diagnosis under varying environmental conditions part ii: local pca for non-linear cases. *Mech. Syst. Signal Pr.*, 19(4):865 – 880, 2005.

[69] Jolliffe I. T. *Principal component analysis*. Wiley Online Library, 2002.

[70] Kambhatla N. and Leen T. K. Dimension reduction by local principal component analysis. *Neural Computation*, 9(7):1493–1516, 1997.

[71] Hawkins D. M. *Identification of Outliers*. Springer Netherlands, 1980.

[72] Aggarwal C. C. *Outlier analysis*. Springer Science & Business Media, 2013.

[73] Mujica L.E., Rodellar J., Fernandez A., and Guemes A. Q-statistic and t2-statistic pca-based measures for damage assessment in structures. *Structural Health Monitoring*, pages 539–553, 2010.

[74] Ewins D. J. *Modal Testing: Theory, Practice and Application (Mechanical Engineering Research Studies: Engineering Dynamics Series)*. Wiley, 2 edition, 2003.

[75] Cunha A. and Caetano E. Experimental modal analysis of civil engineering structures. *J. Sound Vibr.*, 40(6):12–20, 2006.

[76] Bendat J.S. and Piersol A. G. Engineering applications of correlation and spectral analysis. *New York, Wiley-Interscience, 1980. 315 p.*, 1, 1980.

[77] Brincker R., Zhang L., and Andersen P. Modal identification from ambient responses using frequency domain decomposition. In *Proc. of the 18*'International Modal Analysis Conference (IMAC), San Antonio, Texas*, 2000.

[78] Peeters B. *System Identification and Damage Detection in Civil Engeneering*. PhD thesis, 2000.

[79] Van Overschee P. and B. L. R. De Moor. *Subspace identification for linear systems: theory, implementation, applications*, volume 3. Kluwer academic publishers Dordrecht, 1996.

[80] Ubertini F., Venanzi I., and Comanducci G. Considerations on the implementation and modeling of an active mass driver with electric torsional servomotor. *Mech. Syst. Signal Pr.*, 58–59(0):53 – 69, 2015.

[81] Ubertini F., Gentile C., and Materazzi A. L. Automated modal identification in operational conditions and its application to bridges. *Engineering Structures*, 46(0):264 – 278, 2013.

[82] Ubertini F., Cavalagli N., and Comanducci G. Sensing hardware optimization and automated condition assessment of a monumental masonry. In *1st ECCOMAS Thematic Conference on Uncertainty Quantification in Computational Sciences and Engineering, Crete Island, Greece, 25–27 May 2015*, 2015.

[83] Van Overrschee P. and Moor B. *Subspace identification for linear systems: theory, implementation, applications*. Kluwer Academic Publishers, 1996.

[84] Ilin A. and Raiko T. Practical approaches to principal component analysis in the presence of missing values. *J. Mach. Learn. Res.*, 11:1957–2000, August 2010.

[85] Tipping M. E. and Bishop C. M. Probabilistic principal component analysis. *Journal of the Royal Statistical Society: Series B (Statistical Methodology)*, 61(3), 1999.

[86] Magalhaes F., Cunha A., and Caetano E. Vibration based structural health monitoring of an arch bridge: From automated oma to damage detection. *Mech. Syst. Signal Pr.*, 28:212–228, 2012.

[87] Ubertini F. On damage detection by continuous dynamic monitoring in wind-excited suspension bridges. *Meccanica*, 48(5):1031–1051, 2013.

[88] Ubertini F. Effects of cables damage on vertical and torsional eigenproperties of suspension bridges. *J. Sound Vibr.*, 333(11):2404–2421, 2014.

[89] Lepidi M. and Gattulli V. Static and dynamic response of elastic suspended cables with thermal effects. *Int. J. Solids Struct.*, 49(9):1103 – 1116, 2012.

[90] Luco J. E.and Turmo J. Linear vertical vibrations of suspension bridges: A review of continuum models and some new results. *Soil Dyn Earthq Eng*, 30(9):769 – 781, 2010.

[91] Caracoglia L. Influence of uncertainty in selected aerodynamic and structural parameters on the buffeting response of long-span bridges. *J. Wind Eng. Ind. Aerodyn.*, 96(3):327 – 344, 2008.

[92] Bartoli G. and Mannini C. A simplified approach to bridge deck flutter. *J. Wind Eng. Ind. Aerodyn.*, 96(2):229 – 256, 2008.

[93] Cremona C. A short note on cable fatigue. *In Proc. 5th international symposium on cable dynamics*, 2003.

[94] Carassale L. and Solari G. Wind modes for structural dynamics: a continuous approach. *Probabilistic Eng. Mech.*, 17(2):157 – 166, 2002.

[95] Solari G. and Piccardo G. Probabilistic 3-d turbulence modeling for gust buffeting of structures. *Probabilistic. Eng. Mech.*, 16(1):73 – 86, 2001.

[96] Adão da Fonseca A. The infant dom henrique bridge over the river douro, at porto.

[97] Adão da Fonseca A. and Mato F. M. Infant henrique bridge over the river douro, porto. *Structural engineering international*, 15(2):85–85, 2005.

[98] Adão da Fonseca A. and Bastos R. O. The infante dom henrique bridge over the river doure: construction method, monitoring equipment and structural control.

[99] Adão da Fonseca A., Bastos R. O., and Magalhães F. Ponte infante d. henrique: 10 anos de monitorização do comportamento estrutural da ponte em condições de servço.

[100] Magalhães F., Cunha A., and Caetano E. Dynamic monitoring of a long span arch bridge. *Eng. Struct.*, 30(11):3034 – 3044, 2008.

[101] Magalhães F., Cunha A., and Caetano E. Online automatic identification of the modal parameters of a long span arch bridge. *Mech. Syst. Signal Pr.*, 23(2):316 – 329, 2009.

[102] Magalhães F. and Cunha A. Explaining operational modal analysis with data from an arch bridge. *Mech. Syst. Signal Pr.*, 25(5):1431 – 1450, 2011.

[103] Filipe Magalhães. *Operational modal analysis for testing and monitoring of bridges and special structures*. PhD thesis, Universitade do Porto, Facultade de Engenharia, 2010.

[104] Costa C. and Borri C. Application of indicial functions in bridge deck aeroelasticity. *Wind Eng. Ind. Aerodyn.*, 94(11):859 – 881, 2006.

[105] Chobsilprakob P., Suthasupradit S., and Kim K.D. Aeroelastic analysis of long span bridges via indicial functions considering geometric and material nonlinearity. *Int. J. Steel Struct.*, 11(2):215–226, 2011.

Curriculum Vitae

Gabriele Comanducci was born in Sansepolcro, (Arezzo) Italy, on April 15, 1985. He is engaged with Laura Adami and has one daughter, Ginevra (September 17, 2013).

Education

2004
High School graduated, 100/100 cum laude, Liceo scientifico "Città di Piero" Sansepolcro, Arezzo.

February 2008
Bachelor's in Civil Engineering, cum laude, University of Perugia.
"*Rilievo architettonico edilizio della cappella Luisa Spagnoli in località Santa Lucia a Perugia*".
Supervisor: Prof. Ing. Paolo Belardi. Ass. Supervisor: Ing. Simone Bori e Ing. Valeria Menchetelli.

February 2011
Master of Science in Civil Engineering, cum laude, University of Perugia.
"*Instabilità aeroelastica di impalcati da ponte: metodi di analisi semplificati e ruolo dello smorzamento strutturale*".
Supervisors: Prof. Ing. A. Luigi materazzi, Filippo Ubertini.

Professional Titles

Registered as Professional Engineer (A 3418) in the Association of Engineers of the Province of Perugia, since 2011.

Partecipation in granted research projects

2011-2013
"*Development of active response control systems and techniques for the seismic protection of structures*", University of Perugia, funded by "Fondazione Cassa di Risparmio di Perugia", (Project Code 2010.011.0490), Principal Investigator: A. Luigi Materazzi.

2014-present
"*Structural Monitoring for the protection of the Cultural Heritage: the bell-tower*

of the Basilica of San Pietro in Perugia and the dome of the Basilica of Santa Maria degli Angeli in Assisi", University of Perugia, funded by "Fondazione Cassa di Risparmio di Perugia", (Project Code 2014.0266.021), Principal Investigator: Filippo Ubertini.

Publications

I Ubertini F., Materazzi A.L., Moretti M., Bacchetti M., Venanzi I., Comanducci G..*An Experimental Set-up for Testing Structural Control Strategies Accounting for System Constraints*, EACS 2012, Genova (Italy), June 18-20.

II Ubertini F., Materazzi A.L., Comanducci G..*Eigenfrequencies of Damaged Suspension BridgesUnder Wind*, IN-VENTO 2012, Venezia (Italy), October 7-10.

III Ubertini F., Venanzi I., Comanducci G., Materazzi A.L.. *On the Control Performance of an Active Mass Driven System*, AIMETA 2013, Torino (Italy) September 17-20.

IV Comanducci G., Ubertini F., Venanzi I., Breccolotti M., Materazzi A.L., Garofoli U., Bondi R.. *Un campanile salvato: rilievi dinamici ed identificazione dinamica di un campanile in muratura a seguito di un intervento di miglioramento sismico*, L'ingegnere umbro, 88.

V Ubertini F., Cavalagli N., Comanducci G., Materazzi A.L.. *Campanile di San Pietro: indagini dinamiche e modellazione numerica del campanile della Basilica di San Pietro a Perugia*, L'ingegnere umbro, 89.

VI Comanducci G., Ubertini F., Materazzi A.L..*Early damage detection in wind-excited suspension bridges*, IN-VENTO 2014, Genova (Italy), June 22-25.

VII Venanzi I., Ubertini F., Comanducci G., Materazzi A.L.. *Adaptive control strategies for active mass driver system with physical limitations*, EURODYN 2014, Oporto (Portugal) June 30 - July 2.

VIII Ubertini F., Venanzi I., Comanducci G..*Considerations on the implementation and modeling of an active mass driver with electric torsional servomotor*, Mechanical Systems and Signal Processing, Volumes 58–59, June 2015, Pages 53–69.

IX Comanducci G., Ubertini F., Materazzi A.L..*Structural health monitoring of suspension bridges with features affected by changing wind speed*, Journal of Wind Engineering and Industrial Aerodynamics, accepted for publication.

X Ubertini F., Comanducci G., Laflamme S.. *Deterministic versus non-deterministic approaches for TMD design against bridge flutter*, Computer & structures, under review.

A

APPENDIX

Contents:

A.1 Wind loads

This first Appendix is aimed at producing more details concerning the formulation of the wind loads components acting on the continuum bridge model introduced in the previous Sec. 4.1.

A.1.1 Buffeting loads

Buffeting aerodynamic modal loads in Eqs. (4.7,4.8) are given by

$$\Lambda^{v}_{b,i}(\bar{t}) = 2c_L\alpha^L_b\widetilde{u}^v_i(\bar{t}) + (c_D + c'_L)\alpha^L_b\widetilde{w}^v_i(\bar{t}) \tag{A.1}$$

$$\Lambda^{\theta}_{b,i}(\bar{t}) = 2c_M\alpha^M_b\widetilde{u}^\theta_i(\bar{t}) + c'_M\alpha^M_b\widetilde{w}^\theta_i(\bar{t}) \tag{A.2}$$

where c_L, c_M and c_D are lift, moment and drag aerodynamic coefficients of the deck, respectively, while c'_L and c'_M are derivatives of c_L and c_M with respect to wind angle of attack, evaluated for a nil angle of attack. In Eqs. (A.1,A.2) the following non-dimensional coefficients have been introduced:

$$\alpha^L_b = \frac{\rho_a U^2 B L^2}{32 f_u H_u} \tag{A.3}$$

$$\alpha^M_b = \frac{\rho_a U^2 B^2}{mgb} \tag{A.4}$$

where ρ_a is the air density. Moreover, normalized scalar products between turbulent velocities and eigenfunctions have been introduced in Eq. (A.1,A.2) as

$$\widetilde{u}^r_i(\bar{t}) = \frac{\int_0^1 \overline{u}(\overline{x},\bar{t})\phi^r_i(\overline{x})\mathrm{d}\overline{x}}{\int_0^1 {\phi^r_i}^2\mathrm{d}\overline{x}} \quad r = v,\theta \tag{A.5}$$

$$\widetilde{w}^r_i(\bar{t}) = \frac{\int_0^1 \overline{w}(\overline{x},\bar{t})\phi^r_i(\overline{x})\mathrm{d}\overline{x}}{\int_0^1 {\phi^r_i}^2\mathrm{d}\overline{x}} \quad r = v,\theta \tag{A.6}$$

These quantities are digitally generated under the classical assumption of modeling the turbulent wind field as a multivariate Gaussian stochastic process [94].

A.1.2 Self-excited loads

Self-excited wind loads in Eqs. (4.7,4.8) are modeled through indicial functions [104, 105], written through the widely adopted formula:

$$\Phi_{Rr}(t) = 1 - \sum_{i=1}^{N^{Rr}_\Phi} a^{Rr}_i \cdot \exp\left(- b^{Rr}_i \frac{2U}{B} t \right) \quad R = L, M \quad r = v,\theta \tag{A.7}$$

where parameters a_i^{Rr} and b_i^{Rr} are estimated by fitting measured aeroelastic derivatives and N_Φ^{Rr} represent user-defined numbers to be adopted for achieving a given level of approximation.

Using Eq. (A.7) the self-excited wind loads, in non-dimensional form, Eq. (4.6), can be rewritten as

$$\Lambda_{se,i}^{v}(\bar{t}) = c_L'\left(\alpha_{se}^{Lv}\left(1-\sum_{j=1}^{N_\Phi^{Lv}} a_j^{Lv}\right)\dot{\zeta}_i^{v}(\bar{t}) + \alpha_{se}^{L\theta}\left(1-\sum_{j=1}^{N_\Phi^{L\theta}} a_j^{L\theta}\right)\sum_{k=0}^{\infty}\varphi_{ik}^{v\theta}\zeta_k^{\theta}(\bar{t}) + \right.$$
$$\left. + \sum_{j=1}^{N_\Phi^{Lv}}\left(\alpha_{se}^{Lv} z_{ij}^{Lv}(\bar{t}) + \alpha_{se}^{L\theta}\sum_{k=0}^{\infty}\varphi_{ik}^{v\theta} z_{kj}^{L\theta}(\bar{t})\right)\right) \tag{A.8}$$

$$\Lambda_{se,i}^{\theta}(\bar{t}) = c_M'\left(\alpha_{se}^{M\theta}\left(1-\sum_{j=1}^{N_\Phi^{M\theta}} a_j^{M\theta}\right)\zeta_i{}^{\theta}(\bar{t}) + \alpha_{se}^{Mv}\left(1-\sum_{j=1}^{N_\Phi^{Mv}} a_j^{Mv}\right)\sum_{k=0}^{\infty}\varphi_{ik}^{\theta v}\dot{\zeta}_k^{v}(\bar{t}) + \right.$$
$$\left. + \sum_{j=1}^{N_\Phi^{M\theta}}\left(\alpha_{se}^{M\theta} z_{ij}^{M\theta}(\bar{t}) + \alpha_{se}^{Mv}\sum_{k=0}^{\infty}\varphi_{ik}^{\theta v} z_{kj}^{Mv}(\bar{t})\right)\right) \tag{A.9}$$

where

$$\varphi_{ij}^{rs} = \frac{\int_0^1 \phi_i^r \phi_j^s \mathrm{d}\overline{x}}{\int_0^1 {\phi_i^r}^2 \mathrm{d}\overline{x}} \qquad r,s = v,\theta \tag{A.10}$$

$$\alpha_{se}^{Lv} = \frac{\rho_a U B L}{2\sqrt{2mH_u}} \qquad \alpha_{se}^{L\theta} = \frac{\rho_a mgU^2 BL^4}{128 b f_u H_u^2} \tag{A.11}$$

$$\alpha_{se}^{Mv} = \frac{8\rho_a U B^2 f_u}{mgLb}\sqrt{\frac{2H_u}{m}} \qquad \alpha_{se}^{M\theta} = \frac{\rho_a U^2 B^2 L^2}{4b^2 H_u} \tag{A.12}$$

and

$$z_{ij}^{Rr}(\bar{t}) = \frac{2a_j^{Rr} b_j^{Lv}\overline{U}}{\overline{B}}\int_0^{\bar{t}} \exp\big(-b_j^{Rr}\tfrac{2\overline{U}}{\overline{B}}(\bar{t}-\tau)\big)\dot{\zeta}_i^{r}(\tau)\mathrm{d}\tau \qquad R = L, M \qquad r = v,\theta \tag{A.13}$$

In order to eliminate integral terms from the equations of motion, Eq. (A.13) can be differentiated with respect to $\bar{t}$ making use of Leibnitz's rule, thus yielding the following first order equation:

$$\dot{z}_{ij}^{Rr}(\bar{t}) = \frac{2b_j^{Rr}\overline{U}}{\overline{B}}\big(a_j^{Rr}\dot{\zeta}_i^{r}(\bar{t}) - z_{ij}^{Rr}(\bar{t})\big) \qquad R = L, M \qquad r = v,\theta \tag{A.14}$$

which governs the evolution of variables $z_{ij}^{Rr}(\bar{t})$. Eq. (A.14) shows that $z_{ij}^{Rr}(\bar{t})$ can be interpreted as additional state variables of the system that allow to

reproduce memory terms without the need of computing expensive integrals over time.

Vectors $\mathbf{z}^{Rr}$, in Eq. (4.10), are defined as

$$\mathbf{z}^{Rr}(\bar{t}) = [z_{11}^{Rr}(\bar{t}) \ \dots \ z_{1N^{Rr}}^{Rr}(\bar{t}) \ z_{21}^{Rr}(\bar{t}) \ \dots \ z_{2N^{Rr}}^{Rr}(\bar{t}) \ \dots \ z_{n1}^{Rr}(\bar{t}) \ \dots \ z_{nN^{Rr}}^{Rr}(\bar{t})]^T \tag{A.15}$$

with $R = L, M$ and $r = v, \theta$.

A.2 Structural eigenmodes

The expressions for non-dimensional vertical and torsional natural frequencies and for eigenfunctions of damaged bridge are here reviewed.

Frequencies of antisymmetric vertical modes are

$$\overline{\omega}_n^v = 2\pi n \sqrt{\frac{1+\chi^2}{2} + 4\pi^2 n^2 \mu_h^2} \tag{A.16}$$

where $\mu_h^2 = \frac{E_g J_g}{2H_u L^2}$ is the relative flexural girder rigidity and $\chi^2 = H_d/H_u$ is the tension loss factor, H_d being the static horizontal components of damaged cable tension. Antisymmetric vertical eigenfunctions are:

$$\phi^v{}_n(\overline{x}) = \Phi_n^v \sin(2n\pi\overline{x}) \tag{A.17}$$

where Φ_n^v is a set of amplitude coefficients.

The characteristic equation governing the eigenfrequencies of symmetric vertical modes is the following:

$$\frac{\alpha_2^{v\,2}}{\alpha_1^{v\,2} + \alpha_2^{v\,2}} \frac{\tanh(\alpha_1^v/2)}{\alpha_1^v/2} + \frac{\alpha_1^{v\,2}}{\alpha_1^{v\,2} + \alpha_2^{v\,2}} \frac{\tan(\alpha_2^v/2)}{\alpha_2^v/2} + \frac{2\Gamma}{\Gamma + \kappa^4} \frac{\overline{\omega}^{v\,2}}{\lambda^2} = 1 \tag{A.18}$$

with:

$$\alpha_{1,2}^{v\,2} = \frac{1+\chi^2}{4\mu_h^2} \left(\sqrt{1 + \left(\frac{4\mu_h \overline{\omega}^v}{1+\chi^2} \right)^2} \pm 1 \right) \tag{A.19}$$

where $\lambda_d^{v\,2} = (\Gamma + \kappa^4)\lambda^2/2\Gamma$, $\kappa^2 = f_d/f_u$ is the tension loss factor, $\lambda^2 =$

$\left(\frac{8f_u}{L}\right)^2 \frac{L}{L_{e,u}} \frac{E_c A_c}{H_u}$ is the Irvine's parameter of the main cables and Γ is given by

$$\Gamma = \frac{1-\eta\left(1-\delta\frac{L}{L_e}\right)+\frac{8\kappa^4 f_u^2 \eta\delta}{LL_e}\left(3-12\gamma+\delta^2+12\gamma^2\right)}{(1-\eta)}\frac{L_e}{L_e^u} \tag{A.20}$$

with $L_e = L(1+8(\kappa^2 f_u/L)^2)$. Eigenfunctions of symmetric vertical modes are

$$\phi^v(\overline{x}) = \overline{h}^v \frac{\Gamma+\kappa^4}{2\Gamma}\left(\frac{\lambda}{\overline{\omega}^v}\right)^2\left[1-\left(\frac{\alpha_1^{v\,2}}{\alpha_1^{v\,2}+\alpha_2^{v\,2}}\right)\frac{\cos(\alpha_2^v(\overline{x}-1/2))}{\cos(\alpha_2^v/2)}-\left(\frac{\alpha_2^{v\,2}}{\alpha_1^{v\,2}+\alpha_2^{v\,2}}\right)\frac{\cosh(\alpha_1^v(\overline{x}-1/2)}{\cosh(\alpha_1^v/2)}\right] \tag{A.21}$$

with $\overline{h}^v = \int_0^1 \phi^v(\overline{x})\mathrm{d}\overline{x}$.

Frequencies of antisymmetric torsional modes are

$$\overline{\omega}_n^\theta = \frac{2\pi n}{\varrho_t}\sqrt{\frac{1+\chi^2}{2}+\tau_h^2} \tag{A.22}$$

where $\tau_h^2 = \frac{G_g J_t}{2H_u b^2}$ is the relative torsional girder rigidity. Eigenfunctions of antisymmetric torsional modes are given by expressions analogous to Eq. (A.17).

The characteristic equation governing the eigenfrequencies of symmetric torsional modes is

$$\tan\left(\frac{\alpha^\theta}{2}\right) = \frac{\alpha^\theta}{2} - \frac{2\Gamma}{\Gamma+\kappa^4}\frac{4(1+\tau_h^2)}{\lambda^2}\left(\frac{\alpha^\theta}{2}\right)^3 \tag{A.23}$$

with:

$$\alpha^{\theta\,2} = \frac{\overline{\omega}^{\theta\,2}\varrho_t^2}{\frac{1+\chi^2}{2}+\tau_h^2} \tag{A.24}$$

Symmetric torsional eigenfunctions are

$$\phi^\theta(\overline{x}) = \overline{h}^\theta \frac{\Gamma+\kappa^4}{2\Gamma}\frac{\lambda^2}{\alpha^{\theta\,2}(1+\tau_h^2)}\left(1-\tan\left(\frac{\alpha^\theta}{2}\right)\sin(\alpha^\theta\overline{x})-\cos(\alpha^\theta\overline{x})\right) \tag{A.25}$$

with $\overline{h}^\theta = \int_0^1 \phi^\theta(\overline{x})\mathrm{d}\overline{x}$.

A.3 System matrices

Expressions for the different matrices appearing in Eq. (**??**) are here summarized. Matrices of eigenfrequencies and damping are given by:

$$\boldsymbol{\Omega}^2 = \begin{bmatrix} \boldsymbol{\Omega}^{v\,2} & \mathbf{0} \\ \mathbf{0} & \boldsymbol{\Omega}^{\theta\,2} \end{bmatrix} \quad \boldsymbol{\Xi} = \begin{bmatrix} \boldsymbol{\Xi}^{v} & \mathbf{0} \\ \mathbf{0} & \boldsymbol{\Xi}^{\theta} \end{bmatrix} \quad \Omega^{r\,2}_{ii} = \overline{\omega}^{r\,2}_i \quad \Xi^{r}_{ii} = 2\overline{\xi}^{r}_i \overline{\omega}^{r}_i \quad R = v, \theta \tag{A.26}$$

Aerodynamic damping and stiffness matrices are given by

$$\boldsymbol{\Delta} = \begin{bmatrix} -\boldsymbol{\Delta}^{vv} & \mathbf{0} \\ \boldsymbol{\Delta}^{\theta v} & \mathbf{0} \end{bmatrix} \quad \boldsymbol{\Phi} = \begin{bmatrix} \mathbf{0} & -\boldsymbol{\Phi}^{v\theta} \\ \mathbf{0} & \boldsymbol{\Phi}^{\theta\theta} \end{bmatrix} \tag{A.27}$$

where:

$$\begin{aligned}
\boldsymbol{\Delta}^{vv} &= c'_L \alpha^{Lv}_{se} \left(1 - \sum_{j=1}^{N^{Lv}_{\Phi}} a^{Lv}_j\right) \mathbf{I} \\
\boldsymbol{\Delta}^{\theta v} &= \frac{c'_M \alpha^{Mv}_{se}}{\varrho_t^2} \left(1 - \sum_{j=1}^{N^{Mv}_{\Phi}} a^{Mv}_j\right) \begin{bmatrix} \varphi^{\theta v}_{11} & \varphi^{\theta v}_{12} & \cdots & \varphi^{\theta v}_{1n} \\ \varphi^{\theta v}_{21} & \varphi^{\theta v}_{22} & \cdots & \varphi^{\theta v}_{2n} \\ \vdots & \cdots & \cdots & \vdots \\ \varphi^{\theta v}_{n1} & \cdots & \cdots & \varphi^{\theta v}_{nn} \end{bmatrix}
\end{aligned} \tag{A.28}$$

$$\boldsymbol{\Phi}^{v\theta} = c'_L \alpha^{L\theta}_{se} \left(1 - \sum_{j=1}^{N^{L\theta}_{\Phi}} a^{L\theta}_j\right) \begin{bmatrix} \varphi^{v\theta}_{11} & \varphi^{v\theta}_{12} & \cdots & \varphi^{v\theta}_{1n} \\ \varphi^{v\theta}_{21} & \varphi^{v\theta}_{22} & \cdots & \varphi^{v\theta}_{2n} \\ \vdots & \cdots & \cdots & \vdots \\ \varphi^{v\theta}_{n1} & \cdots & \cdots & \varphi^{v\theta}_{nn} \end{bmatrix} \tag{A.29}$$

$$\boldsymbol{\Phi}^{\theta\theta} = \frac{c'_M \alpha^{M\theta}_{se}}{\varrho_t^2} \left(1 - \sum_{j=1}^{N^{M\theta}_{\Phi}} a^{M\theta}_j\right) \mathbf{I}$$

Coupling matrices between aeroelastic states and structural degrees of freedom

are given by

$$\boldsymbol{\Theta}_{\mathbf{q}} = \begin{bmatrix} \mathbf{0} & \mathbf{0} \\ \mathbf{0} & \boldsymbol{\Theta}^{L\theta} \\ \mathbf{0} & \boldsymbol{\Theta}^{M\theta} \\ \mathbf{0} & \mathbf{0} \end{bmatrix} \quad \boldsymbol{\Theta}_{\dot{\mathbf{q}}} = \begin{bmatrix} \boldsymbol{\Theta}^{Lv} & \mathbf{0} \\ \mathbf{0} & \mathbf{0} \\ \mathbf{0} & \mathbf{0} \\ \boldsymbol{\Theta}^{Mv} & \mathbf{0} \end{bmatrix} \quad \boldsymbol{\Theta}^{Rr} = \begin{bmatrix} \mathbf{t}^{Rr} & \mathbf{0} & \dots & \mathbf{0} \\ \mathbf{0} & \mathbf{t}^{Rr} & & \vdots \\ & & \ddots & \\ \mathbf{0} & & & \mathbf{t}^{Rr} \end{bmatrix} \tag{A.30}$$

with $\mathbf{t}^{Rr} = [2a_1^{Rr}b_1^{Rr}\overline{U}/\overline{B}\ \ 2a_2^{Rr}b_2^{Rr}\overline{U}/\overline{B}\ \ \dots\ \ 2a_{N^{Rr}}^{Rr}b_{N^{Rr}}^{Rr}\overline{U}/\overline{B}]^T$, $R = L, M$, $r = v, \theta$.

Coupling matrix between structural degrees of freedom and aeroelastic states is given by

$$\boldsymbol{\Psi} = \begin{bmatrix} -\boldsymbol{\Psi}^{Lv} & -\boldsymbol{\Psi}^{L\theta} & \mathbf{0} & \mathbf{0} \\ \mathbf{0} & \mathbf{0} & \boldsymbol{\Psi}^{M\theta} & \boldsymbol{\Psi}^{Mv} \end{bmatrix} \tag{A.31}$$

where:

$$\boldsymbol{\Psi}^{Rr} = \psi^{Rr}\boldsymbol{\Psi}_0^{Rr} \quad R = v, \theta \quad r = v, \theta \tag{A.32}$$

with $\psi^{vv} = c'_L\alpha_{se}^{Lv}$, $\psi^{\theta\theta} = c'_M\alpha_{se}^{M\theta}/\varrho_t^2$, $\psi^{v\theta} = c'_L\alpha_{se}^{L\theta}$ and $\psi^{\theta v} = c'_M\alpha_{se}^{Mv}/\varrho_t^2$ and with

$$\boldsymbol{\Psi}_0^{rr} = \begin{bmatrix} \begin{bmatrix} 1 & 1 & \dots & 1 \\ 0 & 0 & \dots & 0 \\ \vdots & \vdots & & \vdots \\ \vdots & \vdots & & \vdots \\ 0 & 0 & \dots & 0 \end{bmatrix} & \begin{bmatrix} 0 & 0 & \dots & 0 \\ 1 & 1 & \dots & 1 \\ 0 & 0 & \dots & 0 \\ \vdots & \vdots & & \vdots \\ 0 & 0 & \dots & 0 \end{bmatrix} & \dots & \begin{bmatrix} 0 & 0 & \dots & 0 \\ \vdots & \vdots & & \vdots \\ \vdots & \vdots & & \vdots \\ 0 & 0 & \dots & 0 \\ 1 & 1 & \dots & 1 \end{bmatrix} \end{bmatrix} \quad r = v, \theta \tag{A.33}$$

$$\boldsymbol{\Psi}_0^{Rr} = \begin{bmatrix} \begin{bmatrix} \varphi_{11}^{Rr} & \varphi_{11}^{Rr} & \dots & \varphi_{11}^{Rr} \\ \varphi_{21}^{Rr} & \varphi_{21}^{Rr} & \dots & \varphi_{21}^{Rr} \\ \vdots & \vdots & & \vdots \\ \varphi_{n1}^{Rr} & \varphi_{n1}^{Rr} & \dots & \varphi_{n1}^{Rr} \end{bmatrix} & \begin{bmatrix} \varphi_{12}^{Rr} & \varphi_{12}^{Rr} & \dots & \varphi_{12}^{Rr} \\ \varphi_{22}^{Rr} & \varphi_{22}^{Rr} & \dots & \varphi_{22}^{Rr} \\ \vdots & \vdots & & \vdots \\ \varphi_{n2}^{Rr} & \varphi_{n2}^{Rr} & \dots & \varphi_{n2}^{Rr} \end{bmatrix} & \dots & \begin{bmatrix} \varphi_{1n}^{Rr} & \varphi_{1n}^{Rr} & \dots & \varphi_{1n}^{Rr} \\ \varphi_{2n}^{Rr} & \varphi_{2n}^{Rr} & \dots & \varphi_{2n}^{Rr} \\ \vdots & \vdots & & \vdots \\ \varphi_{nn}^{Rr} & \varphi_{nn}^{Rr} & \dots & \varphi_{nn}^{Rr} \end{bmatrix} \end{bmatrix} \tag{A.34}$$

Main matrix governing the time evolution of aeroelastic states is given by

$$\boldsymbol{\Pi} = \begin{bmatrix} \boldsymbol{\Pi}^{Lv} & \mathbf{0} & \mathbf{0} & \mathbf{0} \\ \mathbf{0} & \boldsymbol{\Pi}^{L\theta} & \mathbf{0} & \mathbf{0} \\ \mathbf{0} & \mathbf{0} & \boldsymbol{\Pi}^{M\theta} & \mathbf{0} \\ \mathbf{0} & \mathbf{0} & \mathbf{0} & \boldsymbol{\Pi}^{Mv} \end{bmatrix} \quad \boldsymbol{\Pi}^{Rr} = \begin{bmatrix} \mathbf{p}^{Rr} & \mathbf{0} & \dots & \mathbf{0} \\ \mathbf{0} & \mathbf{p}^{Rr} & & \vdots \\ & & \ddots & \\ \mathbf{0} & & & \mathbf{p}^{Rr} \end{bmatrix} \tag{A.35}$$

with

$$\mathbf{p}^{Rr} = \begin{bmatrix} -\frac{2b_1^{Rr}\overline{U}}{\overline{B}} & 0 & \dots & 0 \\ 0 & -\frac{2b_2^{Rr}\overline{U}}{\overline{B}} & & \vdots \\ & & \ddots & \\ 0 & & & -\frac{2b_{N^{Rr}}^{Rr}\overline{U}}{\overline{B}} \end{bmatrix} \quad R = L, M \quad r = v, \theta \quad \text{(A.36)}$$

A.4 Effect of t_{trn} on Linear PCA effectiveness

In Subsec. 5.3.3.1, OR_{dmg} are adopted to verify the real effectiveness in damage detection of Linear PCA. Actually, it has been noticed that the cleansing procedure in this case can not properly remove the environmental and operational conditions that affects the modal properties obtained from real bridge data, being the outliers percentage in the observation period always remarkably higher than the imposed 5%. This fact should be imputed not to a weak effectiveness of the procedure (not only), but especially to anomalous events (wind, traffic, temperature and so on) that produce variations in the considered modal properties during the observation period deeply bigger than those experienced in the training period during which the Upper Control Limit of the control chart is calculated. Such statement may suggest that maybe, in real structures, one year of permanent monitoring could not be sufficient for spanning all the "normal conditions" necessary to properly set the parameters of the statistical techniques enabling damage detection.

In order to understand if the adoption of a longer training period could be useful to the purpose of stabilizing the percentage of outliers in the observation period some additional analysis are performed. More specifically a parametric analysis is carried out with two different values of gr, 8 and 24 respectively, for varying the training period t_{trn} from 75 to 575 days and then calculating the outliers percentage in the consecutive 100 days. The obtained results are presented in Fig. A.1. It clearly appears that in the case of gr= 8 a better convergence is gained and that training periods longer than one year could help to obtain more stable results in damage detection by reducing the number of false positive detections during the observation period. The irregular behavior of the curves for t_{trn} ranging in the interval $[350 - 425]$ is due to the fact that the 100 days in which the outliers are calculated contain a period during which an anomalous behavior of the modal frequencies is registered, anomalous behavior which can observed also in the control charts around day 450. This fact consequently

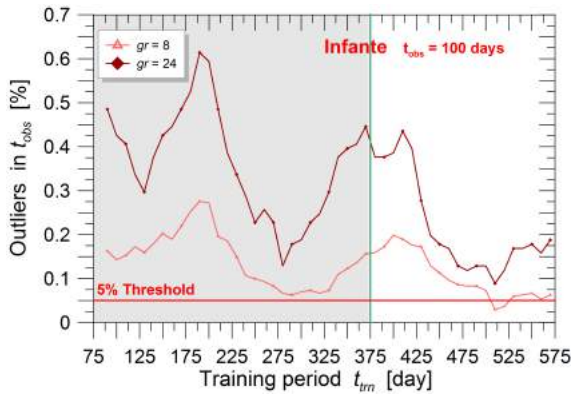

Figure A.1: Outliers percentage for a fixed observation period of 100 days and for varying the length of the training period t_{trn} and the group averaging size

produces the registered unusual increasing of the outliers. For this reason the elimination of such values is suggested once the absence of damage is guaranteed.